DOTTORATO DI RICERCA IN
FISICA E ASTRONOMIA

CICLO XXVI

COORDINATORE Prof. Roberto Livi

THE NONEQUILIBRIUM DISCRETE NONLINEAR SCHRÖDINGER EQUATION

Settore Scientifico Disciplinare FIS/02

Dottorando
Dott. Iubini Stefano

Tutore
Dott. Lepri Stefano

Coordinatore
Prof. Livi Roberto

Anni 2011/2013

Contents

Introduction

The characterization of irreversible processes in many-particle systems is one of the main tasks of nonequilibrium statistical mechanics, as it provides the basis for understanding general problems such as transport phenomena, pattern formation or the dynamics of complex systems. On a phenomenological ground, the assumption of being not too far from global equilibrium leads to postulate a proportionality relation between thermo-mechanical forces and currents. For instance, when considering heat transport in a solid material, such relation is specified by the Fourier law

$$j_Q = -\kappa \nabla T \quad ,$$

through the introduction of a thermal conductivity κ that relates the heat flux $j_Q(\mathbf{x}, t)$ to the gradient of the local temperature $T(\mathbf{x}, t)$. The ultimate goal of a complete theory is to derive macroscopic phenomenological equations like the Fourier law from a statistical-mechanic approach that starts from the fundamental microscopic level. As an example, the knowledge of the statistical measure for general out-of-equilibrium conditions would allow a complete characterization of the macroscopic dynamics, including also the fluctuations of all the relevant observables.

For insulating lattices, where heat transport is due to lattice vibrations, the first attempt to provide microscopic foundations for the Fourier law dates back to Debye, who followed an approach inspired to kinetic theory for deriving an expression of the thermal conductivity in terms of the phonon mean free path and velocity. In 1929, Peierls further extended this idea and showed that anharmonicity plays a fundamental role in guaranteeing energy diffusion, through the so-called Umklapp processes [1]. Since then, the so-called Boltzmann-Peierls theory became a cornerstone in the statistical-mechanic approach to transport phenomena.

These results were also a fundamental starting point for a series of subsequent studies involved in a deeper and deeper understanding of the microscopic mechanisms that characterize irreversible thermodynamics. A remarkable example is offered by the discovery of a breakdown of usual hydrodynamics in simple low-dimensional chains of nonlinear oscillators [2]. In particular, for the class of models with translational invariance, the thermal conductivity was found to diverge in the thermodynamic limit $N \to \infty$ as N^α, where the exponent α is related to the symmetries of the model [2]. However, the discrepancy that still persists between the most advanced theories of anomalous heat conduction (see e.g. [3]) and some recent numerical simulations [4] is

a relevant indicator of the many difficulties that may arise even in apparently simple off-equilibrium setups.

The conceptual gap is even larger when far-from-equilibrium regimes are considered or in the presence coupled transport, i.e. when two or more mutually interacting currents coexist, such as heat and particle ones in thermo-diffusive phenomena. It is also for this reasons that most of the theoretical activity has concentrated in the study of simple processes with purely stochastic dynamics. In fact, despite the lack of accuracy of their microscopic dynamics in describing the evolution of real systems, stochastic systems allow for a easier control of fluctuations [5]. This approach turned out very powerful for the discovery and characterization of nonequilibrium phase transitions [6], including those occurring in exclusion processes [7] and representative e.g. of the various regimes of traffic flows [8].

A particularly notable system in the realm of nonlinear oscillators models is the Discrete NonLinear Schrödinger (DNLS) equation [9, 10] that has important applications in many domains of physics. A classical example is electronic transport in biomolecules [11], while in optics or acoustics it describes the propagation of nonlinear waves in layered photonic or phononic media [12, 13]. With reference to cold atomic gases, the DNLS equation provides an approximate semiclassical description of bosons trapped in periodic optical lattices (for a recent survey see [14] and references therein).

This system is rather interesting since the presence of two conserved quantities (energy and number of particles) naturally requires arguing about coupled transport, in the sense of ordinary linear irreversible thermodynamics mentioned above. In fact, in spite of the many studies of heat conduction in oscillator chains [2, 15, 16, 17], coupled transport processes have been scarcely investigated [18, 19, 20, 21, 22]. Moreover, while DNLS studies have been mostly focused on its dynamical properties such as the emergence of *breather* solutions (i.e. spatially localized and time-periodic excitations) [23, 24], its nonequilibrium properties have not received much attention so far. Actually, the first analysis of the equilibrium properties of the DNLS equation has been presented quite recently in [25], discovering several unusual thermodynamic features such as the existence of a region in the parameters space characterized by the spontaneous formation of breathers and conjectured to correspond to negative temperature states. Although later studies have clarified the entropic mechanisms determining the emergence of breathers [26], it is still unclear which are the relaxation properties of the system in far-from-equilibrium conditions involving breathers.

These are the main reasons that motivated a characterization of the finite-temperature nonequilibrium properties of the DNLS model. The aim of the present dissertation is to tackle this problem by means of analytical and numerical techniques usually employed in statistical mechanics. To be more precise, two main issues are analyzed in detail. The first one concerns the case of an open DNLS chain that steadily interacts with suitable external reservoirs at given temperature and chemical potential. The second topic is related to a statistical characterization of the DNLS microcanonical dynamics in the regime in which breathers dramatically slow down relaxation to equilibrium. The results obtained in both these setups point out the relevance of the DNLS equation

as a reference dynamical model for the study of coupled transport processes in simple nonlinear systems.

In more details, Chapter 1 is devoted to a general presentation of the model, with peculiar attention to the features that are more directly related with the aim of this thesis, while the study of nonequilibrium steady states of a DNLS chain is contained in Chapter 2. In particular, the presence of two coupled currents (of energy and particles) requires a generalization of the phenomenological relation expressed by the Fourier law in order to include also the action of particle gradients. The Onsager transport coefficients [27] are the appropriate tool and their characterization provides interesting details on the irreversible DNLS dynamics. A deeper insight into the nonequilibrium problem is presented in Chapter 3, where the introduction of a specific Langevin dynamics allows to better understand DNLS transport properties, at least in the limit of high particle density, where the model maps into a chain of interacting rotors. In the second part of the thesis we analyze the transient relaxation dynamics occurring when discrete breathers absorb a certain fraction of the available energy of the system. More precisely, in Chapter 4 we show that the microscopic stability of breathers is so strong to produce global metastability and unusual thermodynamic features. The study of a simplified stochastic DNLS model allows to understand the basic ingredients responsible of the slow relaxation. Chapter 5 contains a detailed analysis of its statistical properties, including also a characterization of the peculiar coarsening phenomenon originating from energy localization. Finally, in the Conclusions we briefly summarize the contents of this dissertation, while Appendices A and B are devoted respectively to a presentation of the linear limit of the DNLS equation and a discussion of some numerical methods used in simulations.

The results reported in this dissertation have led to the publication of the following four research articles:

- S. Iubini, S. Lepri, A. Politi, *Nonequilibrium discrete nonlinear Schrödinger equation*, *Physical Review E*, **86** 011108 (2012)

- S. Iubini, R. Franzosi, R. Livi, G.-L. Oppo, and A. Politi, *Discrete breathers and negative temperature states*, *New Journal of Physics*, **15** 023032 (2013)

- S. Iubini, S. Lepri, R. Livi, A. Politi, *Off-equilibrium Langevin dynamics of the discrete nonlinear Schrödinger chain*, *Journal of Statistical Mechanics*, P08017 (2013)

- S. Iubini, A. Politi, P. Politi, *Coarsening dynamics in a simplified DNLS model*, *Journal of Statistical Physics*, (2013), DOI:10.1007/s10955-013-0896-4

Chapter 1

The Discrete Nonlinear Schrödinger equation

The Discrete Nonlinear Schrödinger (DNLS) equation describes a simple model of a lattice of coupled anharmonic oscillators. Its general properties are summarized in Section 1.1 with reference to suitable adimensional units that will be used throughout this thesis. Since the pioneering investigations in the 1970s, the DNLS model has been widely studied, both theoretically and numerically, because of its relevance in several domains of physics. For this reason, Section 1.2 is devoted to a broad-spectrum overview of its applications, including the most significant experimental setups and its relationship with other widespread nonlinear lattice models. Focusing on the topics more directly connected with the aims of this dissertation, in Section 1.3 we review the peculiar features of the class of spatially localized and time-periodic solutions called discrete breathers. As we will see in Chapters 4 and 5, such excitations play a fundamental role in the relaxation properties of the DNLS equation. Furthermore, the study of asymptotic dynamics and irreversible thermodynamics naturally requires to argue about equilibrium statistical mechanics. In this respect, in Section 1.4 we present the main properties of DNLS model in equilibrium at given temperature and chemical potential, as derived in [25].

1.1 General properties

In this Section we present the general properties of the model that has been studied in this thesis. The Hamiltonian function of a one-dimensional DNLS chain on a lattice with N sites can be written as (in suitable adimensional units)

$$H = \sum_{n=1}^{N} \left(|z_n|^4 + z_n^* z_{n+1} + z_n z_{n+1}^* \right) \quad , \tag{1.1}$$

where z_n, iz_n^* are complex, canonical coordinates, and $|z_n|^2$ can be interpreted as the *number of particles*, or, equivalently, the *mass* at site n. The two terms in (1.1) are

commonly called "nonlinear term" and "hopping term" (or "coupling term"). The corresponding Hamiltonian equations of motion, $\dot{z}_n = -\partial H/\partial i z_n^*$, define the DNLS equation and read as

$$i\dot{z}_n = -2|z_n|^2 z_n - z_{n+1} - z_{n-1} \quad . \tag{1.2}$$

For later reference, it is also convenient to introduce the real-valued canonical coordinates

$$p_n = \frac{z_n + z_n^*}{\sqrt{2}}, \qquad q_n = \frac{z_n - z_n^*}{\sqrt{2}i} \quad , \tag{1.3}$$

which allow rewriting the equations of motion (1.2) as

$$\begin{aligned} \dot{p}_n &= -(p_n^2 + q_n^2)q_n - q_{n+1} - q_{n-1} \\ \dot{q}_n &= (p_n^2 + q_n^2)p_n + p_{n+1} + p_{n-1} \quad . \end{aligned} \tag{1.4}$$

An important property of the DNLS dynamics is the presence of a second conserved quantity (besides energy), namely, the total mass

$$A = \sum_{n=1}^{N} |z_n|^2 = \frac{1}{2}\sum_{n=1}^{N}(p_n^2 + q_n^2) \quad , \tag{1.5}$$

The two functions H and A are in involution, i.e. their Poisson brackets $\{A, H\}$ vanish. Their conservation is associated respectively to the invariance of the model (1.2) under temporal shifts and global phase transformations.

With reference to a lattice with periodic boundary conditions, one can prove [25] that the ground state of the Hamiltonian (1.1) for a fixed total mass $A = A_0$ corresponds to a stationary plane-wave solution in the form

$$z_n = \sqrt{\frac{A_0}{N}}\, e^{\,i[\omega t + \pi n]} \quad , \tag{1.6}$$

with a frequency $\omega = 2(A_0/N - 1)$. Upon substituting (1.6) in (1.1) one finds explicitly the ground-state energy

$$H_0 = \frac{A_0^2}{N} - 2A_0 \quad , \tag{1.7}$$

which therefore is a nonlinear function of the total mass A_0.

It is easy to verify that the variable $u_n = z_n \exp(i\pi n)$ satisfies the same equation of z_n, except for the sign of the coupling term. On the other hand, if we define $u_n = z_n^*$, the temporal derivative in (1.2) changes sign. Altogether, by combining these two transformations, one can keep the coupling term unchanged while changing the sign of the nonlinear one. In this thesis we will consider only the case of a positive nonlinear term, i.e. the so-called *focusing* DNLS equation. The *defocusing* regime, corresponding to a negative nonlinear term, can be derived straightforwardly by using the transformations written above. Sometimes the DNLS equation is also written in the more general form

$$i\frac{dz_n}{dt} + \gamma|z_n|^2 z_n + \epsilon(z_{n+1} - 2z_n + z_{n-1}) = 0 \quad . \tag{1.8}$$

For the same reasons, such equation is defined up to transformations that change the sign of the parameters γ and ϵ. Moreover, a rescaling of the coefficient γ (associated to a rescaling of the energy) and the time-dependent transformation $u_n = z_n \exp(-2it\epsilon)$ allow to map Eq. (1.8) to Eq. (1.2).

Although this thesis will exclusively treat the standard DNLS equation with cubic nonlinearity, Eq. (1.2), it is worth recalling that several generalizations of the model have been proposed, especially for characterizing the class of its nonlinear localized modes (discrete breathers). Among the most important, we mention DNLS models with higher-order [28] or saturable [29] nonlinearities and with nonlocal interactions [30].

1.2 History and applications of the DNLS equation

DNLS equations have been broadly used to model numerous phenomena in different fields of physics. One of the main reasons of this relevance is basically related to their capability to effectively describe the typical effects that emerge as a consequence of nonlinearity and discreteness.

Historically, the DNLS equation was introduced in theoretical biophysics to describe the dynamics of the energy transferred to a protein by ATP (*Adenosine triphosphate*) hydrolysis in the framework of Davydov theory [31] (see Fig. 1.1). Its structure rep-

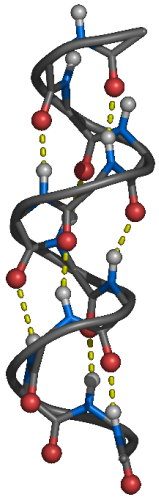

Figure 1.1: Example of an α-helix structure of a protein. Davydov theory describes the interaction between vibrational modes of C=O bonds (Oxygen in red) and hydrogen bonds (dashed yellow lines).

resented a novel feature because, unlike the *continuous* nonlinear Schrödinger equation [11] and the Ablowitz-Ladik equation [32], it is a nonintegrable model. For this reason, a series of systematic studies on its dynamics started with the aim of under-

standing the role of discreteness and nonintegrability in the Davydov equations [33, 34]. In a short time it became clear that the DNLS equation deserved independent interest for the peculiar properties of its periodic and chaotic trajectories [9]. Later on, the DNLS equation became the prototypical model for the study of stationary localized excitations (discrete breathers) in systems of coupled oscillators. In this context, in fact, Aubry and MacKay proved the existence of a one-parameter family of static breathers for the DNLS equation by an analytic continuation from the so-called anticontinuum limit [35, 36]. This theory represented a fruitful connection between the early studies on DNLS systems and the emergent field of breather excitations in nonlinear lattices. The importance of the DNLS equation was also motivated by the strong relationship with the typical models used to describe the dynamics of nonlinear coupled oscillators, such as Klein-Gordon [37] or Fermi-Pasta-Ulam [38] models.

Beyond the growing theoretical interest into studies of the DNLS equation, experimental progress in the field of nonlinear optical waveguide arrays and Bose-Einstein condensation (BEC) in periodic potentials highly contributed to extend the applicability of the model also to realistic setups. In the following we briefly discuss these two classical applications.

The idea of using a DNLS equation to model two optical waveguides interacting through a nonlinear material appeared for the first time in [39]. Later work took inspiration from this suggestion and proposed the DNLS equation to describe discrete self-focusing in arrays of coupled waveguides [40]. The array is comprised of identical equispaced waveguides and it is assumed to be made by a nonlinear Kerr material, i.e. a material whose optical refractive index increases linearly with the intensity of the optical field (see Fig. 1.2). By assuming only nearest-neighbor interactions, it is possible

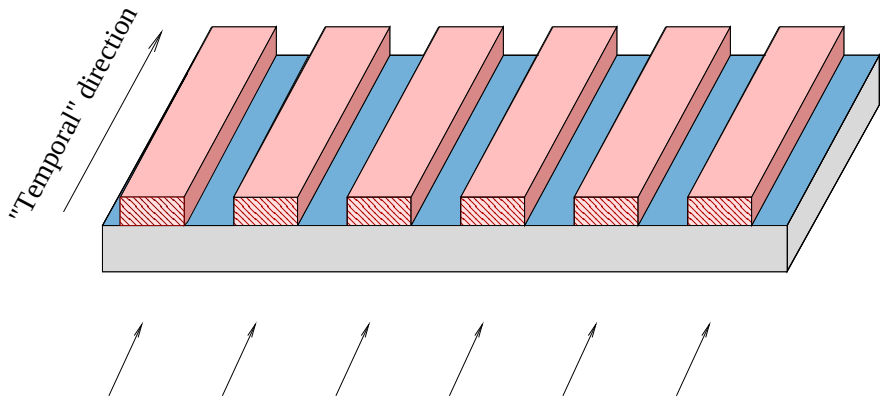

Figure 1.2: Scheme of a waveguide array. Pink regions denote a Kerr material interacting with the neighbours via a tight-binding interaction. The propagation direction of the injected electric field is parallel to the waveguides and corresponds to the temporal evolution of the DNLS equation.

to show that the electric field propagating in the array satisfies a DNLS equation [40]. On the basis of this setup, other works followed proposing the applicability of several properties of the DNLS equation to nonlinear optics. Among them we mention the investigation on collision properties of self-localized states [41] and the use of discreteness and localization to obtain an optical multiport switching between the different channels in the array [42]. Finally, spatially self-localized structures were experimentally observed for the first time in 1998 [43]. Later experimental work showed the existence of mobile breathers and provided a confirmation of the predictions associated to the theory of Peierls-Nabarro barriers [44].

In the context of Bose-Einstein physics, the use of the DNLS dimer was first suggested in [45] to model two coupled BECs in a double-well external potential (trap). With the same approach followed for nonlinear optics, the DNLS model was later proposed [46] for a more complex experimental setup involving BECs trapped in a periodic optical potential generated by counterpropagating laser beams [47]. Basically, the optical potential creates an effective discrete lattice in which the condensates move (see Fig. 1.3). In this context, the DNLS equation corresponds to a superfluid

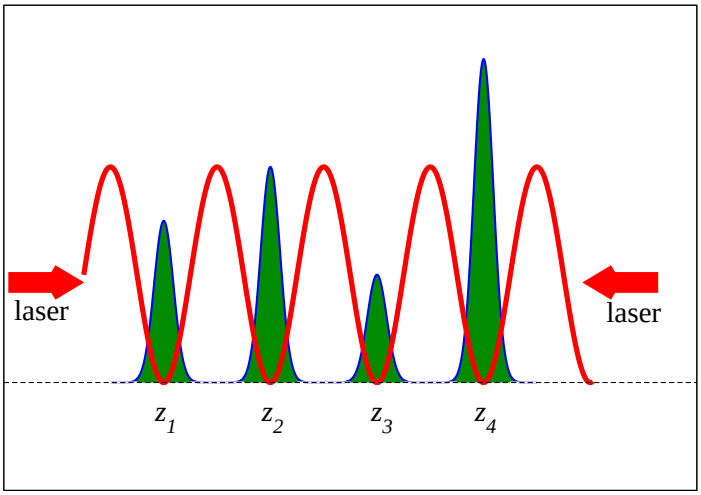

Figure 1.3: Illustration of a BEC loaded in a 1D optical potential (in red). Within the tight-binding approximation [46], z_n denote the wave function of the condensate in the n-th potential well.

limit of the Gross-Pitaevskii equation with periodic external potential [46]. Later experiments confirmed the agreement of the observed parameters with the predictions provided by the DNLS equation [48, 49]. In the last years BEC in optical lattices have become ideal benchmarks to investigate the role of nonlinearity and spatial discreteness in quantum transport phenomena [50, 51]. The refined experimental techniques now available [47, 52, 53, 54, 55] make possible investigations and applications of BEC in quantum coherence, quantum control, quantum information processing and the quantum-classical correspondence [56]. In addition, by virtue of the common de-

scription in terms of DNLS equations, BEC in optical lattices can be considered as the "atomic analogues" of light propagating in waveguide arrays [43].

DNLS equations have also been used to model a variety of other settings, usually as envelope equations for several types of nonlinear lattices (tipically of Klein-Gordon type). Among the most relevant settings we mention electric transmission lines [57] and arrays of micromechanical oscillators [58]. Moreover, in recent studies the DNLS model has been used to describe the violation of reciprocity in wave scattering [59]. Finally, one the most promising applications of the DNLS equation is offered by its connection with the Landau-Lifshitz equation, in the context of ferromagnetic materials [60, 61]. Very recently, in fact, rectification of energy- and spin- currents have been analyzed in a model of a spin nanopillar made by two ferromagnetic layers [62]. More generally, magnetic systems could represent the ideal benchmark to investigate the properties of coupled transport of the DNLS equation in the language of the so called spin-Seebeck effect [63]. In fact, besides the capability of controlling a spin current by means of a thermal gradient, several unusual thermodynamic effects have been found in the nonequilibrium DNLS model. Some of them are described in detail in Chapter 2 and are related to the peculiar dependence of the transport coefficients on the thermodynamic parameters.

1.3 Discrete breathers in nonlinear lattice models

As we will see in detail Chapter 4, the characterization of the nonequilibrium properties of a DNLS equation can be directly related to the presence of breather states that slow down the relaxation towards the equilibrium state. For this reason, we provide in this Section a concise presentation of this class of solutions that are found in generic Hamiltonian nonlinear lattices. Particular emphasis will be addressed to their physical significance.

Discrete breathers are vibrational states sharing the following main features:

1. They are localized in the real space with an amplitude that is exponentially decreasing with respect to the distance from the localization center, see Fig. 1.4.

2. They have an internal degree of freedom oscillating with a frequency ω_b which does not belong to the linear spectrum of excitations (i.e. phonons).

3. They exist as a direct consequence of nonlinearity and spatial discreteness of the model. For example, their localization property is not connected with disorder via the mechanism of Anderson [64] localization[1].

4. They may exist in arbitrary dimensions.

[1]Indeed in random lattices one observes nontrivial phenomena of competition or cooperation between nonlinearity and disorder in generating extended/localized solutions [65, 66, 67], see also [68, 69] for more recent studies having the DNLS equation as a reference model.

5. While they are generic solutions in discrete nonlinear models, they lose physical interest in the continuous limit, as they become nongeneric states.

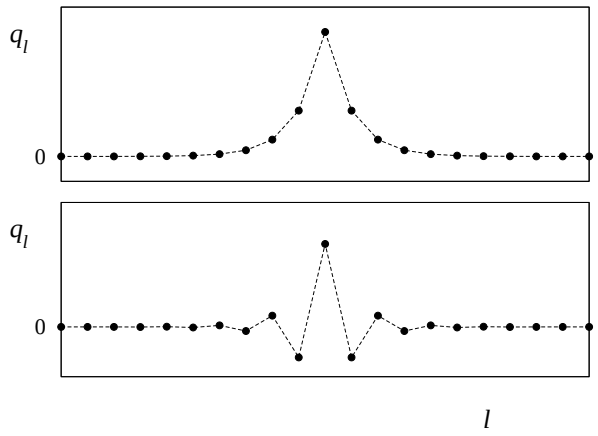

Figure 1.4: In-phase (upper panel) and anti-phase (lower panel) excitations of the lattice field q_l corresponding to a 1D discrete breather.

In order to better clarify the properties above and to put them on a more formal ground, it is worth recalling some fundamental properties of nonlinear lattice Hamiltonian systems. The temporal evolution of a regular lattice in d dimensions is assumed to be ruled by a Hamiltonian function H generating the equations of motion

$$\left\{ \begin{array}{rcl} \dot{p_l} & = & -\frac{\partial H}{\partial q_l} \\ \dot{q_l} & = & \frac{\partial H}{\partial p_l} \end{array} \right. , \tag{1.9}$$

where $p_l(t)$ and $q_l(t)$ are canonical variables and l is an index vector, $l \in \mathbb{Z}^d$. If we study the dynamics of the system for small perturbations of a reference state (for example the ground state), we obtain an eigenvalue problem. Due to translational invariance, the eigenvectors are extended in space (plane waves) and the spectrum of eigenvalues Ω_k is a periodic function in the wavenumber k. In addition, the discreteness of the model makes Ω_k a bounded function, i.e. there exists some Ω_{max} such that $\Omega_k \leq \Omega_{max}\ \forall k$.

A solution of (1.9) is called a static breather solution if it satisfies the localization property (see Fig. 1.4)

$$\lim_{\|l\| \to \infty} q_l = 0 \tag{1.10}$$

and if there exists a frequency $\omega_b = 2\pi/T_b$ such that

$$q_l(t) = q_l(t + T_b)\ ,\ p_l(t) = p_l(t + T_b) \quad . \tag{1.11}$$

A breather solution is called mobile breather if it satisfies (1.10) and (1.11) in an inertial reference system which is moving with some velocity v with respect to the reference of the lattice. Theoretical arguments and numerical observations have also clarified that

mobile breathers typically need a background of extended radiation in order to move [70, 71]. The breather frequency ω_b and all its higher harmonics are also characterized by a non-resonance condition with the linear spectrum

$$n\omega_b \neq \Omega_k \quad \forall n \in \mathbb{N} \text{ and } \forall k \quad . \tag{1.12}$$

From a mathematical point of view, the non-resonance condition is only a necessary condition for the existence of the breather. Physically it corresponds to a stability condition, as it forbids the destruction of the breather by phonon radiation. It is interesting to notice that in spatially continuous models the linear spectrum is unbounded and therefore the condition (1.12) is always violated. Such a property also explains intuitively why breather solutions exist in continuous models only as nongeneric and structurally unstable states, with no physical relevance.

The research field associated with breather solutions was born in 1988 with the publication of a paper by Takeno and Sievers [72], claiming the existence of this class of solutions in classical nonlinear lattices. Starting from this seed, a huge amount of literature has been written on the topic (see e.g. the two reviews [23, 24]). Among the most significant achievements concerning a rigorous formulation of the conditions of existence and stability of breather solutions, we recall the anticontinuum limit theory by Aubry and MacKay [35] and the center manifold theory by James [71]. The stability property is an essential condition for the physical relevance of breather solutions. As an example, breather states are typically attained also starting from slightly perturbed initial conditions (such as Gaussian distributions) and numerically integrating the equations of motion. In particular, the dynamics produces a "distillation" of the breather state from the initial condition, displacing the excess of energy in a delocalized background. The background does not interact with the breather and this ensures the stability of the solution. In some specific cases, the background can satisfy the conditions for the existence of a mobile breather. In these situations one also observes that the localized state acquires a nonzero velocity [70].

Nevertheless, several mechanisms are capable of generating breathers solutions, also starting from nonlocalized initial states. One of the most important is the modulational instability of linearly unstable plane waves. This kind of instability destroys the homogeneous field of the wave and typically produces a series of small amplitude discrete breathers that, on longer timescales, coalesce into a smaller number of higher breathers [73, 74]. Breathers have also been found to emerge upon cooling a *thermalized* lattice at its boundaries by means of a dissipative dynamics [75, 76, 77, 78]. The mechanism originating the spontaneous localization crucially depends on how dissipation acts on phonons of different wavelenghts and it is intimately related to the capability of inducing modulational instability of short wavelenghts while sweeping out long ones [76]. Finally, we recall that in peculiar situations energy localization in breather states can be also an effective mechanism to maximize the total entropy of the system, expecially in the presence of additional dynamical constraints. The thermodynamic role of breather excitations in such kind of systems has been analyzed by Rumpf in a series of papers treating DNLS equations or chains of nonlinear rotors

[60, 26, 79, 80, 81]. This last example represents a particularly important background for this thesis. In fact, in Chapter 4 we will show that for generic initial conditions in the so-called negative temperature region, the evolution of the DNLS equation is towards a multi-breather state. Moreover, in Chapter 5 we will analyze the role of energy localization in the relaxation dynamics of the DNLS system taking into account only entropic effects.

In conclusion of this short review on breather solutions, we remark a significant distinction between discrete breathers and solitonic states that are typically found in nonlinear spatially continuous equations. In fact, while the latters basically do not interact among themselves, the formers usually display inelastic collisions and give rise to a much more complex phenomenology. Up to now a general scattering theory of breather excitations is still far from being formulated. However, several numerical experiments have been performed in different kinds of nonlinear lattices. In this respect, it was found that in breather collisions high-energy breathers systematically grow at expense of smaller ones [82]. For the DNLS equations this type of scenario is described e.g. in [74, 83].

1.4 Statistical mechanics of the DNLS model

The physical relevance of the DNLS equation has justified a study if its thermodynamic properties from the point of view of statistical mechanics. In this section we review the results obtained by Rasmussen et al. [25] who faced this problem for the first time. The phase diagram presented in Fig. 1.5 offers a compact and effective outlook of the overall scenario. It will be a useful tool also for the analysis of the nonequilibrium regimes studied in this thesis.

As a first remark, we recall that the model has a nontrivial additional conserved quantity, the total mass A. The key idea for studying the statistical mechanics of the DNLS chain is to introduce a Gibbsian grandcanonical equilibrium distribution tacking into account also the function A. In particular, one can introduce the partition function Z for a chain with N lattice sites in the form

$$Z = \int \prod_{n=1}^{N} dz_n \, dz_n^* \, \exp\left[-\beta(H - \mu A)\right] \quad , \tag{1.13}$$

where β is the inverse temperature[2] $\beta = 1/T$ and μ is a chemical potential that controls the conservation of A on average. As a consequence, the equilibrium phase-diagram is two-dimensional (see Fig. 1.5), as it involves the energy density $h = \langle H \rangle_g / N$ and the particle density $a = \langle A \rangle_g / N$, where the symbol $\langle \ldots \rangle_g$ denotes the grandcanonical average. There exists a one-to-one correspondence between the thermodynamic variables (a, h) and (β, μ) and the transfer-integral formalism adopted in [25] allows to find it, at least numerically. Two limit cases, however, admit an analytical treatment. The

[2] In this thesis we will always fix the Boltzmann constant $k_B = 1$.

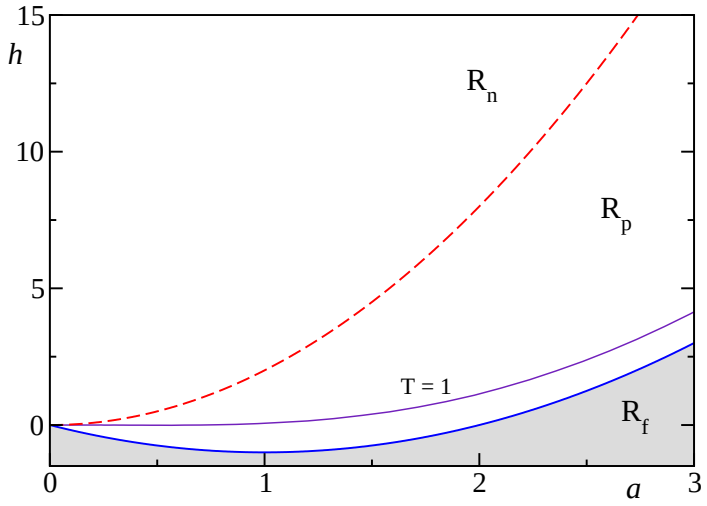

Figure 1.5: Equilibrium phase diagram (a, h) of the DNLS equation. We show the isothermal lines $T = 0$ (solid blue), $T = 1$ (solid purple) and $T = \infty$ (dashed red).

first one corresponds to the ground-state solution (cf. Eq. (1.6))

$$h = a^2 - 2a \tag{1.14}$$

and defines the $T = 0$ line (lower solid line in Fig. 1.5).

The region of states below the ground state is a forbidden region and it is denoted with the symbol $\mathrm{R_f}$. Positive-temperature states lie in the region $\mathrm{R_p}$, in between the ground state and the dashed red line of Fig. 1.5. This curve is defined by

$$h = 2a^2 \quad , \tag{1.15}$$

which corresponds to the infinite-temperature (and $\mu = -\infty$) state, characterized by random phases and an exponential distribution of the amplitudes $|z_n|^2$.

Above the $T = \infty$ line, one finds the region $\mathrm{R_n}$, that was conjectured to contain negative temperature states. In this region, the dynamics of the DNLS equation is characterized by the spontaneous creation of long-lived discrete breathers that are typically superposed to a delocalized background. As we have clarified in Section 1.3, such localized excitations are almost totally decoupled with the background. This is basically the main reason why in $\mathrm{R_n}$ the long-time relaxation properties of the system are completely different from the positive temperature regime, where breathers are absent. A detailed discussion about the role of such peculiar states in slow relaxation phenomena is contained in Chapters 4 and 5.

Negative temperature states have attracted the curiosity of researchers since the pioneering works of Onsager [84] and Ramsey [85]. From a thermodynamic point of view, the presence of negative temperature states implies that the system's entropy S is locally a decreasing function of the total energy E, according to the microcanonical

definition $T^{-1} = \partial S/\partial E$. In nonlinear systems, such condition is often associated to the presence of some fraction of high-energy regular (i.e. non chaotic) degrees of freedom, like discrete breathers for DNLS equations or vortices in turbulent hydrodynamic flows [84]. On the other hand, simpler models which do not support similar excitations usually display uniform negative temperature phases, with no relevant differences with respect to positive temperature states (two examples are offered by the Ising model [85] and by the discrete linear Schrödinger chain described in Appendix A).

By means of statistical arguments, it has been proved that the fate of the DNLS dynamics in $\mathrm{R_n}$ is to concentrate the excess of energy in a *single* macroscopic breather (a sort of black hole), while storing the total mass in an infinite temperature delocalized background [26]. This asymptotic state clearly excludes the existence of negative temperature states for the DNLS model. However, it was also estimated that the convergence towards this state could require astronomical transients [86]. In Chapter 4 we will show that over physically meaningful timescales, the DNLS model relaxes towards long-lasting metastable states with well-defined thermodynamic properties and a negative temperature.

Chapter 2

Nonequilibrium steady states

2.1 Introduction

In this chapter, we study the case of an open DNLS chain that steadily exchanges energy and mass with external reservoirs. The presence of two transported quantities naturally requires to argue about coupled transport, in the sense of ordinary linear irreversible thermodynamics [27].

In order to investigate transport properties, we need to introduce the interaction of the system with external reservoirs that are capable to exchange energy and/or mass. The general setup that will be adopted in this thesis is sketched in Fig. 2.1, where we have drawn a chain of N lattice sites interacting with two different heat baths at its boundaries. Modeling heat baths for the DNLS equation, however, is much

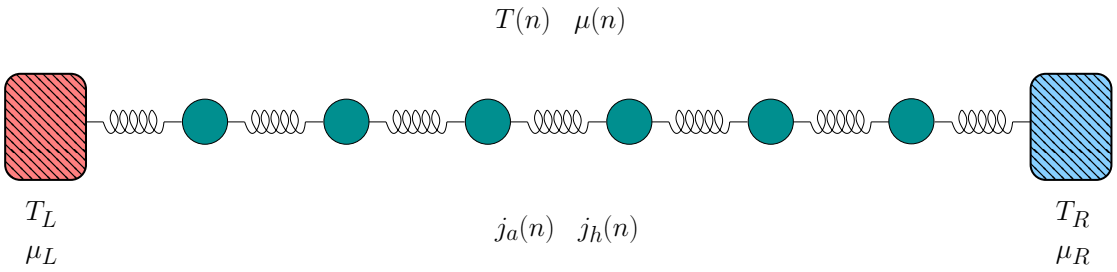

Figure 2.1: A pictorial representation of a DNLS chain with $N = 6$ lattice sites (labeled by n) coupled with two reservoirs operating at different temperatures and chemical potentials. A nonequilibrium steady state is characterized by constant energy and particle fluxes $j_a(n)$, $j_h(n)$ and by stationary profiles of temperature $T(n)$ and chemical potential $\mu(n)$.

less straightforward than for standard oscillator chains, where e.g. simple Langevin thermostats are a typical choice [2, 15]. Indeed, the nonseparable structure of the DNLS Hamiltonian (1.1) requires a non-standard derivation of the corresponding Langevin

equation. A detailed presentation of this approach is provided separately in Chapter 3. Here we define and test a stochastic heat bath based on a Monte-Carlo scheme. This approach allows to define in a simple way different versions of thermostats capable of exchanging energy and/or mass. On the other hand, such definitions are constructed on a phenomenological ground and they lack a direct microscopic derivation starting from first principles.

Another important difference between the DNLS and standard oscillator chains (like the Fermi-Pasta-Ulam or Klein-Gordon models) is that its Hamiltonian is not the sum of kinetic and potential energies. Thus, it is necessary to introduce suitable operative definitions of kinetic temperature T and chemical potential μ, to measure such quantities in actual simulations. In particular, we make use of a general definition of the microcanonical temperature [87] and extend it for the estimate of the chemical potential.

By imposing small T and μ jumps across the chain, we can determine the Onsager coefficients [27], which turn out to be finite in the thermodynamic limit, i.e. both energy and mass conductions are normal processes. From the Onsager coefficients we can thereby determine the "Seebeck coefficient" S [1] which we find to be either positive or negative, depending on the thermodynamic parameters (i.e., mass and energy density). For larger temperature or chemical-potential differences, although one can still invoke the linear response theory, some surprising phenomena emerge. One example is the "anomalous heating" that can be observed when the chain is attached to two thermostats operating at the same temperature: along the chain, T reaches values that are even three times larger than that imposed on the boundaries. This phenomenon can be observed only in the case of coupled transport, since it is due to the variable weight of the non-diagonal terms of the Onsager matrix. It is apparent in the DNLS, because of the strong variability of the Onsager coefficients.

The chapter is organized as follows. In Section 2.2 we define the formalism and the tools necessary to characterize nonequilibrium steady states of the DNLS equation. Section 2.3 is devoted to a discussion of the steady states, both in the case of small and large T, μ differences. In Section 2.4 we provide a pictorial representation of the general transport properties, by reconstructing the zero-flux curves. Finally, the last section is devoted to the conclusions and to a brief summary of the open problems.

2.2 The nonequilibrium setup

In this section we provide a detailed presentation of the nonequilibrium scheme shown in Fig. 2.1. In particular we define the Monte-Carlo heat baths and the relevant quantities that are necessary to characterize nonequilibrium steady states. These include the operative definitions of temperature and chemical potential as well as the definitions

[1] With a slight abuse of terminology, we use the language of thermoelectric phenomena, even though the underlying physical process is thermodiffusion, since particles have no electric charge in the DNLS context.

of energy and mass fluxes. Finally we briefly review the formalism of linear response theory for coupled transport processes.

In this chapter we consider the adimensional DNLS equation Eq. (1.2) with positive quartic term and fixed boundary conditions,

$$i\dot{z}_n = -z_{n+1} - z_{n-1} - 2|z_n|^2 z_n \quad , \qquad z_0 = z_{N+1} = 0 \quad . \tag{2.1}$$

Moreover, we assume that the boundary sites $n = 1$ and $n = N$ are in contact with suitable reservoirs that perturb the total energy H and the total norm [2] A

$$H = \sum_{n=1}^{N} |z_n|^4 + \sum_{n=1}^{N-1} \left(z_n^* z_{n+1} + z_n z_{n+1}^* \right) \qquad A = \sum_{n=1}^{N} 2|z_n|^2 \quad . \tag{2.2}$$

2.2.1 Monte-Carlo heat baths

We aim to characterize the steady states of the chain when put in contact (on the left and right boundaries) with two thermostats at temperature T_L and T_R and chemical potentials μ_L and μ_R, respectively. The implementation of the interactions with a heat bath is often based on heuristics. In particle models, the simpler schemes consist in either adding a Langevin noise, or in assuming random collisions with an equilibrium gas [2, 15]. For the DNLS this is less straightforward: adding white noise and a linear dissipation drives the system to infinite temperature, i.e. to a state in which relative phases are uncorrelated. Actually, a nonlinear damping is needed to sustain a certain degree of phase coherence along the chain. A detailed analysis of the Langevin approach for the DNLS equation is contained in Chapter 3.

In this section we follow a different approach and we define a phenomenological thermostat based on a stochastic Monte-Carlo algorithm. The general scheme of this kind of heat bath involves a stochastic dynamics which perturbs the canonical variables $p_1 \to p_1 + \delta p_1$ and $q_1 \to q_1 + \delta q_1$ [3] at random times, chosen according to a uniform distribution in the interval $[t_{min}, t_{max}]$. The perturbations δp and δq are independent random variables uniformly distributed in the interval $[-R, R]$. Moves are accepted according to the standard Metropolis algorithm, evaluating the cost function $\exp\{-T_L^{-1}(\Delta H - \mu_L \Delta A)\}$ with T_L and μ_L being the temperature and the chemical

[2] The definition adopted here for the total norm A is twice the one presented in Section 1.1. This choice is in fact the most convenient for the setup presented in this chapter, as it allows simpler numerical simulations. The results here reported can be straightforwardly mapped into different normalizations according to the following basic transformations:

$$\begin{aligned} A &\to cA \\ \mu &\to c^{-1}\mu \qquad c \in \mathbb{R}^+ \end{aligned}$$

In particular, the normalization of Section 1.1 corresponds to $c = 1/2$.

[3] For the sake of simplicity we refer to the left boundary, but the same rule refer to the Nth site as well.

potential of the heat bath. This kind of thermostat exchanges both energy and particles. In some cases, however, we need to study the chain behavior in the absence of one of the two fluxes (energy and norm). A simple way to study these setups is to modify the perturbation rule of the thermostat, requiring the exact conservation of the corresponding local density (energy density or norm density). We have thus the following two schemes:

Norm conserving thermostat- The perturbation acts only on the phase ϕ_1 of the complex variable z_1. More precisely we impose $\phi_1 \to \phi_1 + \delta\phi_1 \ \ mod(2\pi)$, where $\delta\phi$ is a random variable, uniformly distributed in the interval $[0, 2\pi]$. This dynamics conserves exactly the local amplitude $|z_1|^2$ and therefore the total norm A.

Energy conserving thermostat- In this case, it is necessary to go through two steps to conserve the energy

$$h_1 = |z_1|^4 + 2|z_1||z_2| \cos(\phi_1 - \phi_2) \quad . \tag{2.3}$$

First, the amplitude $|z_1|$ is randomly perturbed. As a result, both the local amplitude and the local energy change. Then, by inverting, Eq. (2.3), a value of ϕ_1 that restores the initial energy is seeked. If no such solution exists, we go back to the first step and choose a new perturbation for $|z_1|$.

As a first test of the Monte-Carlo dynamics, we verified that $T = const$ and $\mu = const$ lines are correctly reproduced at equilibrium i.e. for $T_L = T_R$ and $\mu_L = \mu_R$, (see, e.g., the open symbols in Fig. 2.2). In particular, the $\mu = 0$ line is in accordance with the curve computed with the transfer integral method (see Fig.1 in Ref. [25]), as well as with the approximate analytical expression given in Ref. [81]. Notice that both set of curves are not monotonous in the (a, h) plane, indicating the presence a nontrivial relation between the energy-norm parametrization and the temperature-chemical potential one.

There is a basic difference between the two types of thermostats. In the general scheme, a steady state is characterized by four parameters T_L, T_R, μ_L, μ_R. On the other hand, for the norm-conserving scheme we only assign T_L, T_R and the norm density a_{tot} of the whole chain. As a consequence, the value of μ on the boundary is not fixed and must be computed from the simulation. If the steady state is unique, the former thermostating scheme must yield the same results, once the chemical potentials are suitably fixed. A numerical test of this equivalence has been performed, by reconstructing some zero-flux profiles with both thermostats. The curves overlap reasonably well, although some small systematic deviations are present. This is because the norm flux is never exactly zero in the non-conservative case (typically of order $\sim 10^{-4}$ in a chain of 1000 sites). In addition, there are slightly different thermal resistance effects in the two schemes. Besides those discrepancies, we conclude that the proposed schemes work equally well for the generation of nonequilibrium steady states.

As usual in nonequilibrium molecular dynamics simulations, some tuning of the bath parameters is required to minimize boundary resistance and decrease the statistical errors, as well as the finite-size effects [2]. For our Monte-Carlo thermostats, we observed that it is necessary to tune the perturbation amplitude R. Typically, there

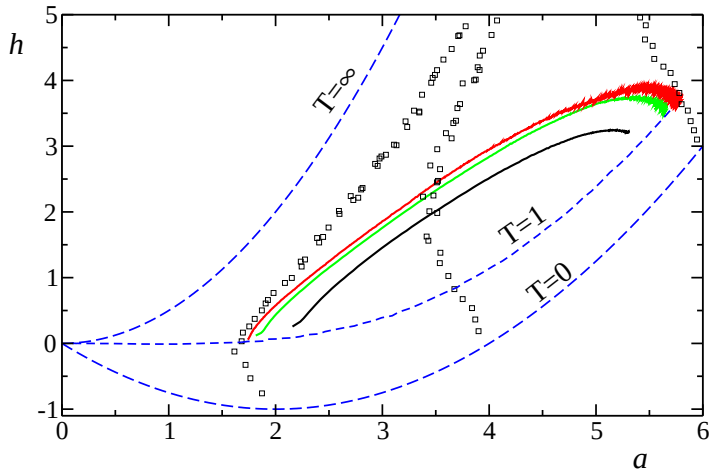

Figure 2.2: Parametric plots of the local norm and energies $[a(y), h(y)]$ for $T_L = T_R = 1$, $\mu_L = 0$, $\mu_R = 2$ and increasing chain lengths $N = 200, 800, 3200$ (solid lines, bottom to top). The three (blue) dashed lines are the isothermal $T = 0$, $T = 1$ and $T = \infty$ respectively. Lines at constant chemical potential (open symbols) $\mu = 0$, $\mu = 1$ and $\mu = 2$ (left to right respectively) are obtained by equilibrium simulations.

is an optimal value of R for which one of the two currents is maximal (keeping the other parameters fixed), but this value may depend on T and μ. Since it would be unpractical to tune the thermostat parameters in each simulation, we decided to fix them in most of the cases. In particular we have chosen $R = 0.5$, $t_{min} = 10^{-2}$ and $t_{max} = 10^{-1}$. Some adjustments have been made only when the fluxes were very small.

2.2.2 Physical observables

In order to characterize the thermodynamic properties of the DNLS, we extend the approach of Ref. [87] to derive suitable operative definitions of the microcanonical temperature T and the chemical potential μ in terms of explicit dynamic observables Θ and $\mathcal{M}$, respectively. The starting point are the usual definitions $T^{-1} = \partial\mathcal{S}/\partial H$, and $\mu/T = -\partial\mathcal{S}/\partial A$, where $\mathcal{S}$ is the thermodynamic entropy. The partial derivatives must be computed taking into account the existence of two conserved quantities (hereafter called C_1 and C_2). Thus,

$$\frac{\partial\mathcal{S}}{\partial C_1} = \left\langle \frac{W\|\vec{\xi}\|}{\vec{\nabla}C_1 \cdot \vec{\xi}}\, \vec{\nabla} \cdot \left(\frac{\vec{\xi}}{\|\vec{\xi}\|W} \right) \right\rangle \tag{2.4}$$

where $\langle\,\rangle$ stands for the microcanonical average,

$$\begin{aligned} \vec{\xi} &= \frac{\vec{\nabla}C_1}{\|\vec{\nabla}C_1\|} - \frac{(\vec{\nabla}C_1\cdot\vec{\nabla}C_2)\vec{\nabla}C_2}{\|\vec{\nabla}C_1\|\|\vec{\nabla}C_2\|^2} \\ W^2 &= \sum_{\substack{j,k=1\\ j<k}}^{2N}\left[\frac{\partial C_1}{\partial x_j}\frac{\partial C_2}{\partial x_k} - \frac{\partial C_1}{\partial x_k}\frac{\partial C_2}{\partial x_j}\right]^2, \end{aligned} \tag{2.5}$$

and $x_{2j} = q_j$, $x_{2j+1} = p_j$. By setting $C_1 = H$ and $C_2 = A$, the above formula defines the microcanonical temperature Θ derived in [87] Moreover, by assuming $C_1 = A$ and $C_2 = H$, Eq. (2.4) defines the expression for the chemical potential observable $\mathcal{M}$. Notice that both expressions are nonlocal. Nevertheless, we have verified that it is sufficient to compute the expressions Θ and $\mathcal{M}$ over as few as 10 sites to obtain, after some time averaging, reliable "local" estimates of both T and μ [4] in the bulk of the DNLS chain.

The expressions for the local energy- and particle-fluxes are derived in the usual way from the continuity equations for norm and energy densities [2], respectively

$$j_a(n) = 2\left(p_{n+1}q_n - p_nq_{n+1}\right) \tag{2.6}$$

$$j_h(n) = -\left(\dot{p}_np_{n-1} + \dot{q}_nq_{n-1}\right) \tag{2.7}$$

The approach to the steady state is controlled by verifying that the (time) average fluxes are constant along the chain ($\overline{j_a(n)} = j_a$ and $\overline{j_h(n)} = j_h$). Moreover it is also checked that j_a and j_h are respectively equal to the average energy and norm exchanged per unit time with the reservoirs.

In the thermodynamic limit (i.e. for sufficiently long chains), the local forces acting on the system are very weak and one can thereby invoke the linear response theory. This means that forces and fluxes are related by the relations [22]

$$\begin{aligned} j_a &= -L_{aa}\frac{d(\beta\mu)}{dy} + L_{ah}\frac{d\beta}{dy} \\ j_h &= -L_{ha}\frac{d(\beta\mu)}{dy} + L_{hh}\frac{d\beta}{dy} \end{aligned} \tag{2.8}$$

where we have introduced the continuous variable $y = n/N$, while β denotes the inverse temperature $1/T$; $\mathbf{L}$ is the symmetric, positive definite, 2×2 Onsager matrix [22]. Notice that the first term in the r.h.s. of the above equations is negative, since the thermodynamic forces are $-\beta\mu$ and μ and that $\det\mathbf{L} = L_{aa}L_{hh} - L_{ha}^2 > 0$.

[4] In general, both Θ and $\mathcal{M}$ contain additional terms $\tilde{\Theta}$ and $\tilde{\mathcal{M}}$ that can, however, be neglected. In the DNLS case, it can be proven that $\tilde{\Theta}\equiv 0$, while simulations indicate that $\tilde{\mathcal{M}}\neq 0$ but also that $\langle\tilde{\mathcal{M}}\rangle = 0$. Indeed, the value of $\mathcal{M}$ computed ignoring $\tilde{\mathcal{M}}$ coincides with the expected value when $\mu_L = \mu_R$, $T_L = T_R$. In any case, even in a nonequilibrium setup, $\mathcal{M}$ must be computed on sufficiently long subchains. This choice is particularly delicate for small nonlinearities and low temperatures. For instance, for $T = 0.5, \mu = -0.5$ subchains of at least $10\div 20$ sites are needed. See also Appendix B.1 for additional details on the numerical calculation of these observables.

The particle (σ) and thermal (κ) conductivity can be expressed expressed in terms of $\mathbf{L}$,

$$\sigma = \beta L_{aa}; \quad \kappa = \beta^2 \frac{\det \mathbf{L}}{L_{aa}} \,. \tag{2.9}$$

Analogously, the Seebeck coefficient S, which corresponds to (minus) the ratio between the chemical-potential gradient and the temperature gradient (in the absence of a mass flux), writes

$$S = \beta \left(\frac{L_{ha}}{L_{aa}} - \mu \right), \tag{2.10}$$

We conclude this subsection, by mentioning another important parameter, the figure of merit

$$ZT = \frac{\sigma S^2 T}{\kappa} = \frac{(L_{ha} - \mu L_{aa})^2}{detL};$$

which determines the efficiency η for the conversion of a heat current into a particle current as [22]

$$\eta = \eta_C \frac{\sqrt{ZT+1} - 1}{\sqrt{ZT+1} + 1}.$$

For large ZT, η approaches the Carnot limit η_C. Understanding the microscopic mechanisms leading to an increase of ZT is currently an active topic of research [88].

2.3 Steady states

2.3.1 Local analysis

In a first series of simulations we have studied the nonequilibrium states in the case of small differences between the two thermostats, verifying that transport is normal, i.e. the Onsager coefficients are finite in the thermodynamic limit. This result is less obvious than one could have imagined and we will clarify it in the following chapter. In any case, for fixed $\Delta T = T_R - T_L$ and $\Delta\mu = \mu_R - \mu_L$, the two fluxes j_a and j_h are inversely proportional to the system size N. At high enough temperatures, the asymptotic scaling sets in already in chains a few hundred sites long (see Fig. 2.3a). Moreover, if ΔT and $\Delta\mu$ are small enough, the profiles of T and μ along the chain are linear as expected.

However, upon decreasing the temperature, the minimal chain length needed to observe a normal transport, becomes very large. As shown in Fig. 2.3b, for the same range of lattice sizes as in panel a, the currents are almost independent on N, as one would expect in the case of ballistic transport. This is because at small temperatures, one can always linearize the equations of motion around the ground state (which depends on the norm density), obtaining a harmonic description and thereby an integrable dynamics.

A plot of the four Onsager coefficients in the (T, μ) plane is reported in Fig. 2.4. Within statistical errors, the off-diagonal terms are always positive in the considered

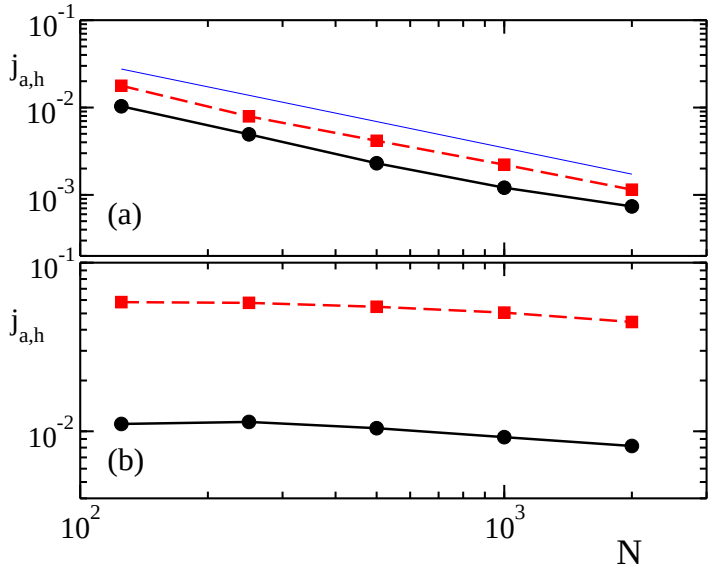

Figure 2.3: (Color onlinel) Average energy current (squares) and norm current (dots) versus chain size N: (a) High-temperature regime $T_L = 2$, $T_R = 4$, $\mu = 0$ and (b) Low-temperature regime $T_L = 0.3$, $T_R = 0.7$, $\mu = 1.5$ The thin (blue) line is the $1/N$ behavior expected for normal transport. Each value is obtained by computing the fluxes on a run of 5×10^6 time units.

range. All coefficients are larger for small T and large μ. This is connected to the scaling behaviour of the linear coefficients in the vicinity of the ground state.

The resulting coefficient S is plotted in Fig. 2.5a, where one can see that there are two regions where the Seebeck coefficient is positive, resp. negative, separated by a curve which, according to Eq. (2.10), is defined by $L_{ha}/L_{aa} = \mu$ (see below). This means that the relative sign of the temperature and chemical-potential gradients is opposite in the two regions (in the presence of a zero norm-flux). This is indeed seen in Fig. 2.5b where the result of two different simulations are plotted in the two regions.

Finally, since the figure of merit ZT roughly follows S, there is only a modest change in the considered parameter ranges. Moreover, for fixed T, ZT decreases upon increasing μ. This is qualitatively in agreement with the general expectation that an increasing strength of interaction (increasing μ means increasing the average norm and thus the nonlinearity) is detrimental for the efficiency.

2.3.2 Global analysis

If the temperature- or the chemical-potential difference is no longer small, the temperature and chemical-potential profiles are expected to have a nonlinear shape. This is because, as we have seen in the previous subsection, the Onsager matrix varies with a and h (or, equivalently, with T and μ).

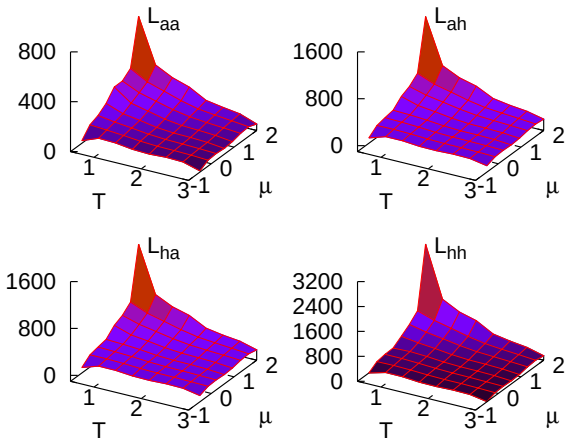

Figure 2.4: Elements of the Onsager matrix $\mathbf{L}$ in the T, μ plane for a chain of length $N = 500$; $\Delta T = 0.1$, $\Delta\mu = 0.05$. Each value is obtained by computing the fluxes on a run of 5×10^6 time units.

A particularly striking example is reported in Fig. 2.6. Both $T(y)$ and $\mu(y)$ profiles do approach the imposed values at the chain edges (up to tiny jumps due to the boundary impedance). However, $T(y)$ exhibits a remarkable non-monotonous profile: although the chain is attached to two heat baths with the same temperature, it is substantially hotter in the middle (up to a factor 3!).

Another way to represent the data is by plotting the local norm and energy densities in the phase plane (a, h). By comparing the results for different chain lengths, we see in Fig. 2.2 that the paths are progressively "pushed" away from the $T = 1$ isothermal and for $N = 3200$ the asymptotic regime is attained.

In order to understand the onset of such anomalous shape, it is convenient to rewrite Eq. (2.8) by referring to T and μ. By introducing vector notations, we can write,

$$\mathbf{J} = \mathbf{A}(\mu, T)\frac{d\mathbf{v}}{dy} \tag{2.11}$$

where $\mathbf{J} = (j_a, j_h)$, $\mathbf{v} = (\mu, T)$, while the matrix $\mathbf{A}$ (which is no longer symmetric) can be expressed in terms of the Onsager matrix and of the fields T and μ in the form $\mathbf{A} = \mathbf{L}\,\mathbf{R}$, where the matrix $\mathbf{R}$ is explicitly

$$\mathbf{R} = \begin{pmatrix} -\frac{1}{T} & \frac{\mu}{T^2} \\ 0 & -\frac{1}{T^2} \end{pmatrix} \quad . \tag{2.12}$$

By now inverting the above equation one obtains

$$\frac{d\mathbf{v}}{dy} = \mathbf{A}^{-1}(\mu, T)\mathbf{J} \tag{2.13}$$

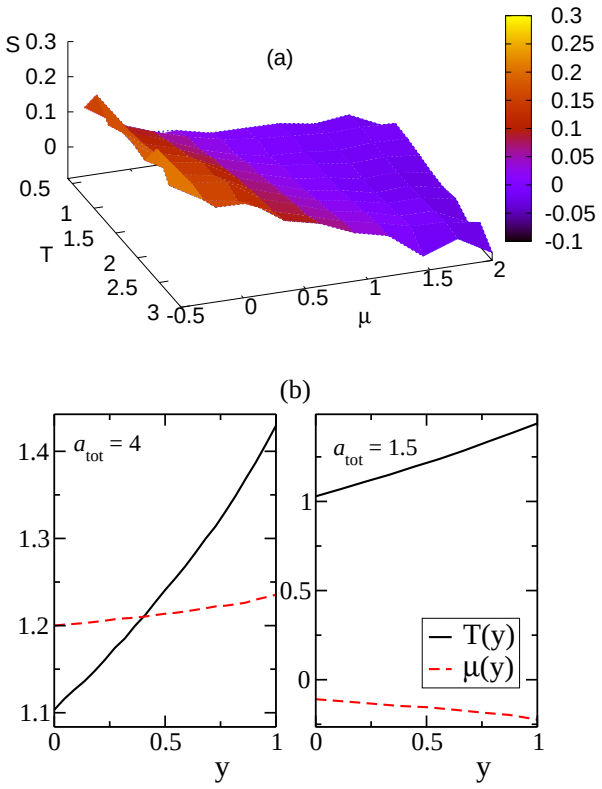

Figure 2.5: (a) Seebeck coefficient S obtained from the data in Fig. 2.4; (b) Temperature and chemical protential profiles for $T_L = 1$, $T_R = 1.5$; simulation with norm-conserving thermostats at two values of the norm density a_{tot} corresponding to values of S with opposite signs.

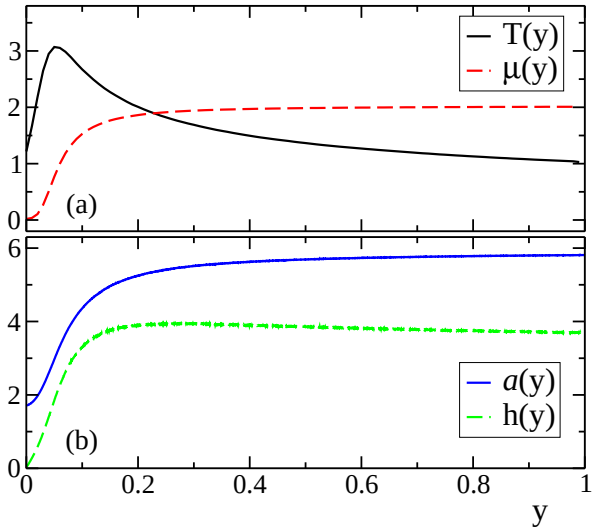

Figure 2.6: (a) Temperature and chemical potential profiles as a function of $y = n/N$ for a chain of $N = 3200$ sites and $T_L = T_R = 1$, $\mu_L = 0$, $\mu_R = 2$. Each point is an average of the appropriate microcanonical expression derived from Eq. (2.4) over a subchain of about 10 sites around n. (b) Norm and energy densities corresponding to the profiles in (a).

where $\mathbf{A}^{-1}$ denotes the inverse of $\mathbf{A}$. This system describes a set of two linear differential equations which are non-autonomous (since the matrix coefficients in general vary with μ and T).

If one assumes to know the "material" properties (i.e. the matrix $\mathbf{A}^{-1}$) and wishes to determine fluxes and profiles, one can proceed by integrating the differential equations, starting from the initial condition $T(0) = T_L$, $\mu(0) = \mu_L$. The *a priori* unknown parameters j_a and j_h can be determined by imposing that the final condition is $T(1) = T_R$ and $\mu(1) = \mu_R$. Alternatively, if the fluxes are known, one can integrate the equations up to any point y_0, and thereby generate the profiles that would be obtained by attaching the right end of the chain to thermal baths with temperature $T_R = T(y_0)$ and chemical potential $\mu_R = \mu(y_0)$.

In order to check the validity of the method, we have also adopted an alternative point of view, by combining the knowledge of the fluxes with simulations of short chains and small gradients to determine the elements of the matrix A in suitably selected points in the (T, μ) plane. In order to estimate the four entries of A, it is necessary to perform two independent simulations for,

$$\begin{cases} T_{L,R} = T \pm \Delta T \\ \mu_{L,R} = \mu \end{cases} \qquad \begin{cases} T_{L,R} = T \\ \mu_{L,R} = \mu \pm \Delta\mu \end{cases}$$

With such information, we have been able to estimate dv_i/dy along the chain (from Eq. (2.13)) and to compare the results with the direct simulations. The results plotted

in Fig. 2.7 demonstrate that the two approaches are in excellent agreement.

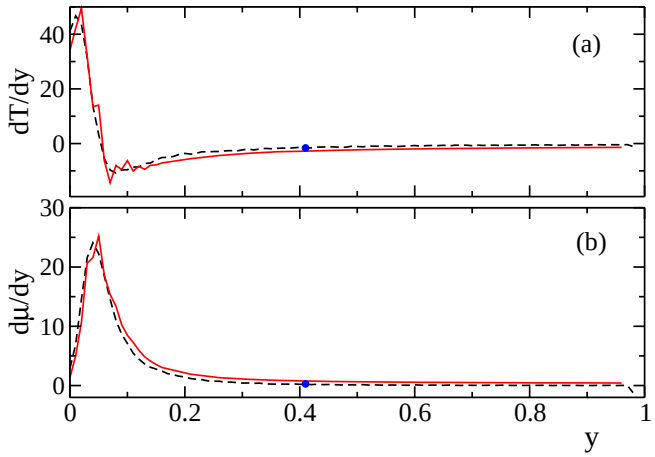

Figure 2.7: Spatial derivatives of T and μ (panels (a) and (b), respectively) computed from the profiles of Fig. 2.6 (black dashed lines) and their reconstruction (red solid lines) by Eq. (2.13) using the linear response coefficients (matrix $\mathbf{A}$). The latter have been calculated on a chain of length $N = 250$. The quality of the reconstruction improves by increasing the lattice size has shown by the blue filled dot which is obtained for $N = 1000$.

2.4 Zero-flux curves

A compact pictorial representation of transport properties is obtained by drawing the lines corresponding to vanishing fluxes j_a and j_h. They can be directly determined by means of the conservative thermostats presented in Section 2.2.1. Some lines are plotted in Fig. 2.8 both in the plane (a, h) and (T, μ). It is worth recall that in the absence of a mutual coupling between the two transport processes (zero off-diagonal elements of the Onsager matrix) such curves would be vertical and horizontal lines in the latter representation. It is instead remarkable to notice that the solid lines, which correspond to $j_h = 0$ are almost vertical for large μ: this means that in spite of a large temperature difference, the energy flux is very small. This is an indirect but strong evidence that the nondiagonal terms are far from negligible.

The condition of a vanishing particle flux $j_a = 0$ defines the Seebeck coefficient which is $S = -d\mu/dT$. Accordingly, the points where the dashed curves are vertical in Fig. 2.8b identify the locus where S changes sign. The $j_h = 0$ curves have no direct interpretation in terms of standard transport coefficients. Finally, if one connects a DNLS chain with any two points in the (μ, T) plane, its profile would correspond to the only path that is characterized by a constant ratio of j_a/j_h.

It is instructive to compare these results with the scenario expected in the "harmonic" limit, where the nonlinear terms in the DNLS are negligible. Here, the dynamics

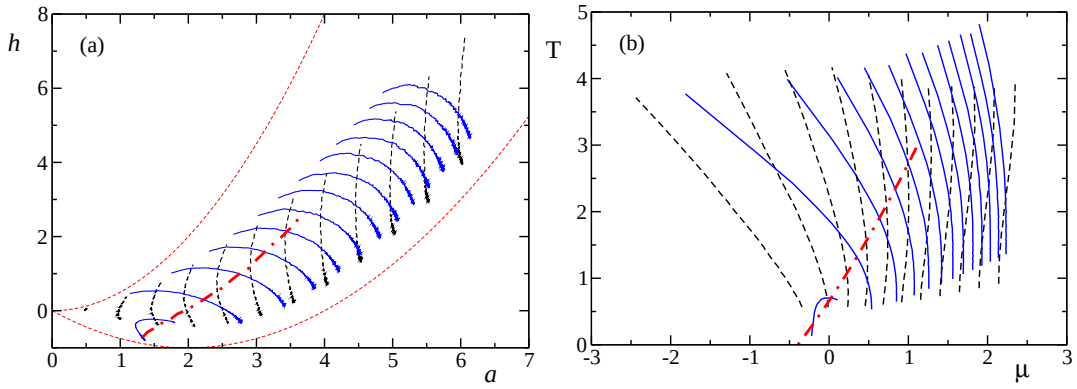

Figure 2.8: Zero-flux curves in the (a, h) and (μ, T) planes (panels (a) and (b), respectively). Black dashed lines correspond to $j_a = 0$ and are obtained with norm-conserving thermostats upon fixing the total norm density a_{tot}, T_L and T_R. Blue solid lines are for $j_h = 0$ using energy-conserving thermostats with fixed total energy density h_{tot}, μ_L/T_L and μ_R/T_R. Simulations are for a chain of length $N = 500$. The thin dashed lines in the upper panel are the $T = 0$ and $T = \infty$ isothermals. The thick dot-dashed lines identify the locus where S changes sign (see text).

is characterized by an ensemble of freely propagating waves and transport is thus ballistic. A direct reconstruction of the zero-flux lines by direct simulations is not very useful, as, in analogy with the known behaviour for the harmonic chain [89], the profiles of T and μ are flat (except for a few sites close to the boundaries). Thus, the curves degenerate to single points and no comparison is possible. We thus resort to a different method of computing transport coefficients for ballistic systems, which is completely analogous to the well-know Landauer theory of electronic transport [90]. Consider an N-site chain in between two leads at different temperatures and chemical potentials (T_L, μ_L), (T_R, μ_R). Since transport is ballistic, energy and norm are carried by N independent phonon modes, whose dispersion law is $\omega(q) = 2\cos q$, q being the wavenumber ($|q| \leq \pi$). Accordingly, the fluxes are N-independent and the ensuing transport coefficients are proportional to N. In this context, the norm and energy fluxes are given (up to some numerical constant) by the formulae

$$\begin{aligned} J_a &= \int_{-2}^{+2} d\omega\, t(\omega)[f_L(\omega) - f_R(\omega)] \\ J_h &= \int_{-2}^{+2} d\omega\, \omega\, t(\omega)\,[f_L(\omega) - f_R(\omega)]\,, \end{aligned}$$

where $t(\omega)$ denotes the transmission coefficient, while $f_{L,R}$ are the equilibrium distribution functions of the reservoirs. If we assume that they are composed of two infinite linear chains (both with the same dispersion), the equipartition principle implies that the distributions are of the Rayleigh-Jeans form (cf. Appendix A), namely

$f_{L,R}(\omega) = f(T_{L,R}, \mu_{L,R}, \omega)$ where

$$f(T, \mu, \omega) = \frac{T}{\omega - 2\mu} \quad ,$$

(the factor 2 stems from the definition of z_n and Eqs. (2.2)) The physical meaning of the formulae is pretty intuitive: they can be derived from suitable generalized Langevin equations following similar steps as for coupled oscillators, see e.g. Ref. [91]. The relevant information is contained in the transmission coefficient, that depends on how the chain is coupled to the external leads. For the Monte-Carlo bath we have used throughout this chapter, the precise form of t is not known. We thus postulate the simplest possible form, namely that, for large N, $t(\omega) = t$ for $|\omega| < 2$ and zero otherwise. For our purposes, we set $t = 1$ in the following, otherwise all the coefficients must be multiplied by t. If we introduce the function

$$\Phi(T, \mu) \equiv \int_{-2}^{+2} d\omega \, f(T, \mu, \omega) = T \ln \left(\frac{\mu - 1}{\mu + 1} \right)$$

which for $\mu < -1$ and $T > 0$ is always positive, we can write,

$$\begin{aligned} J_a &= \Phi(T_L, \mu_L) - \Phi(T_R, \mu_R) \\ J_h &= 4(T_L - T_R) + 2\mu_L \Phi(T_L, \mu_L) - 2\mu_R \Phi(T_R, \mu_R) \, . \end{aligned}$$

By expanding to first order in $\Delta T = (T_L - T_R)$ and $\Delta\mu = (\mu_L - \mu_R)$

$$\begin{aligned} J_a &= M_{00} \Delta T + M_{01} \Delta\mu \\ J_h &= M_{10} \Delta T + M_{11} \Delta\mu \end{aligned} \tag{2.14}$$

where

$$\mathbf{M} = \begin{pmatrix} \frac{\Phi(T,\mu)}{T} & \frac{2T}{\mu^2 - 1} \\ 4 + \frac{2\mu\Phi(T,\mu)}{T} & \frac{4T\mu}{\mu^2 - 1} + 2\Phi(T, \mu) \end{pmatrix} .$$

With the help of the explicit formulae (2.14) we can reconstruct the zero-flux curves as follows. Starting from an initial point (T_{in}, μ_{in}) we compute ΔT and $\Delta\mu$ inverting Eqs. (2.14) setting $J_a = 0, J_h = 1$ and $J_a = 1, J_h = 0$, respectively (the value 1 is arbitrary). We then let $(T_{in}, \mu_{in}) \to (T_{in} + \Delta T, \mu_{in} + \Delta\mu)$ and iterate the procedure until the whole lines are reconstructed.

The results are depicted in Fig. 2.9. The curves for the linear case are defined only in the region $\mu < -1$. The results of the simulations of the DNLS (solid lines) nicely approach the curves of the linear case (dashed lines) upon decreasing μ. The agreement is satisfactory, especially in view of the many *ad hoc* assumptions made in deriving Eqs. (2.14).

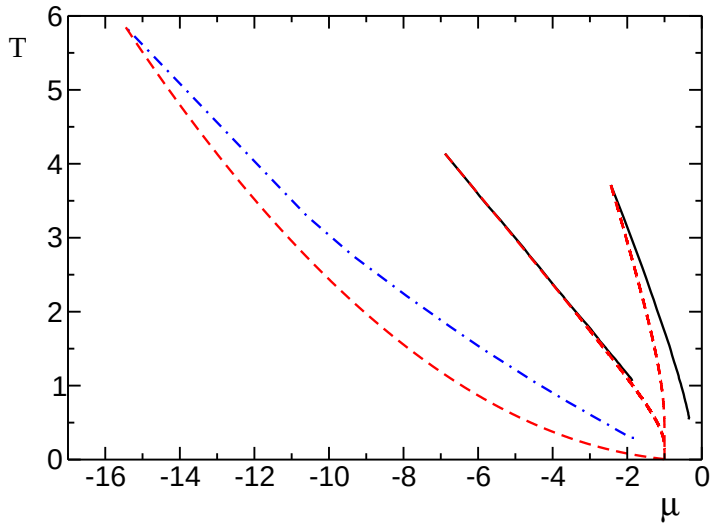

Figure 2.9: Comparison of the zero-flux lines obtained from simulation of the DNLS equations (black solid and blue dot-dashed lines correspond to $j_a = 0$ and $j_h = 0$ respectively). The dashed (red) lines are the zero-flux lines computed by the Landauer formulae as described in the text.

2.5 Discussion

We have presented the first study of stationary thermal transport properties in the DNLS equation. Due to the nonstandard form of its Hamiltonian, several new issues have been brought to the fore dealing with energy transport in oscillator chains. In particular, we have extended the microscopic definition of the temperature to the chemical potential and defined suitable Monte Carlo thermostating schemes to characterize the nonequilibrium steady states of the DNLS model in various regimes. The simulations confirm the expectations that transport is normal (i.e. the Onsager coefficients are finite in the thermodynamic limit), although some almost ballistic transport is found at very low temperature, where the DNLS approaches an almost integrable limit.

Due to the very existence of two naturally coupled transport processes, the nonequilibrium steady state can display nonmonotonous energy and density profiles. To our knowledge, this unusual feature has not been observed so far in any other oscillator or particle model. As seen from Eq. (2.13), it is clear that the temperature profile cannot in general be linear in y, since the elements of $\mathbf{A}^{-1}$ depend on μ and T. In principle, the profiles may have have nontrivial shapes depending on the qualitative behaviour of the solutions of Eq. (2.13). In the DNLS, the phenomenon is particularly pronounced (the temperature inside the chain reaches values that are almost three times larger than those imposed by the thermal baths) because of the strong variability of the Onsager coefficients. It would be interesting to find the physical motivation for this effect to predict and possibly control the conditions for its appearance.

Another novel feature is the fact that the Seebeck coefficient changes sign upon

changing the state parameters e.g. by increasing the interaction strength. The observable consequence of this is that the temperature and chemical potential gradients change their relative signs. Thus, there are situations in which the particle density a may be larger in the colder regions.

The results reported in this chapter have been published in Ref. [92].

Chapter 3

Off-equilibrium Langevin dynamics

3.1 Introduction

The statistical analysis of any system of physical interest requires a proper modelling of the interaction with an external reservoir. The reservoir is expected to exchange energy and particles with the system until a steady state is reached, characterized by the expected temperature and chemical potential. One of the most powerful approaches is based on the introduction of suitable stochastic differential equations such as for the Langevin thermostats that are typically considered in the study of oscillator chains (see, e.g., [2, 15]). In models such as the DNLS equation, this option is less straightforward, because of its non-separable structure. In Chapter 2 we have presented the first study of the nonequilibrium DNLS equation, obtained with the implementation of phenomenological Monte-Carlo thermostats. In this chapter we bridge the gap by augmenting the Hamiltonian equations with a suitable nonlinear damping and a stochastic term. To our knowledge, this is the first such scheme to be proposed in the literature, at least in the present context, although one should mention [93], where the evolution of a DNLS system has been discussed in the presence of small nonlinear damping and a multiplicative noise.

This general Langevin scheme is first used to verify the convergence to equilibrium and then to investigate transport properties in two limit cases, low temperatures and large particle densities, where the DNLS model reduces to a chain of coupled oscillators with internal forces. Such a relationship with translationally invariant models helps to understand that the origin of the normal transport observed in DNLS chains [92] is more subtle than one might have thought. In fact, translationally invariant systems typically exhibit diverging transport coefficients [2]: only in models characterized by phase-like variables (such as the XY model) transport is normal because of the occasional scattering of the phonons with phase-jumps across the energy barriers [2].

Moreover, we find that the chemical potential, which is associated with norm conservation, is equivalent to the rotation frequency of the single rotors and the corresponding force that must be exerted by the external Langevin reservoir for its thermalization is an additional constant torque. Finally, the possibility to map the DNLS equation onto

a standard chain of coupled (phase) oscillators allows deriving a local microscopic definition of the temperature, based on their kinetic energy. This quite interesting since, so far, the only available definition of temperature [14] is both nonlocal and rather convoluted, (see Section 2.2.2) .

The chapter is organized as follows. In Section 3.2 we present the Langevin equations and discuss the equilibrium setup, as well as the case of two external reservoirs at different temperatures and chemical potentials. Section 3.3 contains a microscopic derivation of the generalized Langevin equations. In Section 3.4 we discuss the large mass-density limit, showing that the model can be mapped onto a chain of coupled (nonlinear) rotors. A numerical test of the kinetic definition of the temperature is provided in Section 3.5, while Section 3.6 contains a discussion of the harmonic limit that is attained for low temperatures. Finally, Section 3.7 is devoted to a final discussion of the achievements and to a presentation of future perspectives.

3.2 Langevin thermostats

The equilibrium and nonequilibrium properties of the positive-temperature states have been explored in the previous chapter with the help of Monte–Carlo (MC) thermostats (see Section 2.2.1), under the assumption of the existence of a grand-canonical statistical measure. As a result, it is for instance possible to reconstruct the states characterized by constant chemical potential (see the triangles in Fig. 3.1, which correspond to $\mu = 2$).

In this section we present an alternative approach, based on Langevin thermostats [2]. It allows for a more rigorous mathematical formulation and a more direct physical interpretation. In separable Hamiltonian systems (i.e., those composed of a kinetic and a potential energy) interaction with a Langevin bath simply requires one to modify the momentum equation, by adding a linear dissipation term $-\gamma p_n$, accompanied by a white-noise fluctuation, whose amplitude determines the temperature value. This simple scheme does not work for the DNLS. In fact, one can easily check that in the limit of vanishing fluctuations (which, supposedly correspond to the zero-temperature limit) this dissipative dynamics converges to a fixed point, that does not correspond to the ground state, which, as specified in Section 1.1, is a time-periodic solution.

The problem can be overcome by adopting the following scheme,

$$i\dot{z}_n = (1+i\gamma)\left[-2|z_n|^2 z_n - z_{n+1} - z_{n-1}\right] + i\gamma\mu z_n + \sqrt{\gamma T}\,\xi_n(t) \quad , \tag{3.1}$$

where $\xi_n(t) = \xi'_n + i\xi''_n$ is a complex, Gaussian, white random noise with unit variance and γ is the coupling strength with the bath. In practice, the above equation, which is basically a stochastic, discrete, complex Ginzburg-Landau equation, corresponds to a series of thermostats all operating at temperature T and chemical potential μ, attached to each lattice site. As required for a meaningful reservoir, the dissipative term vanishes along the ground state evolution, $z_n = \sqrt{a}\exp\left[i(\omega t + \pi n)\right]$, where a is the total mass density and $\omega = 2(a-1)$ (see Section 1.1). Notice finally that for vanishing coupling

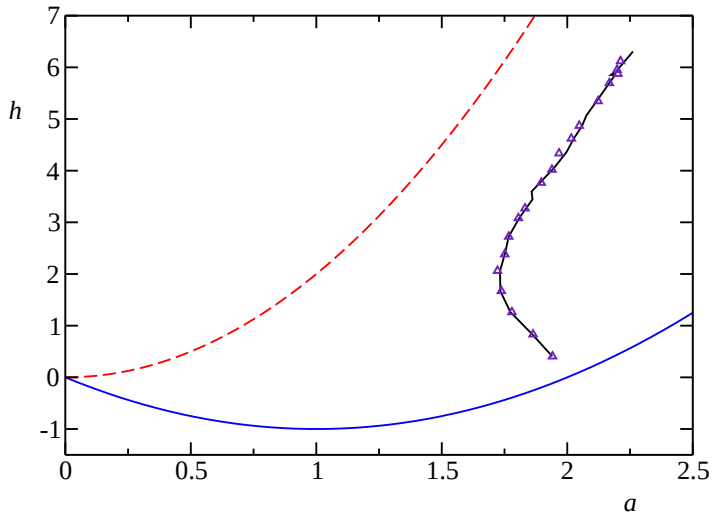

Figure 3.1: Equilibrium phase diagram of the DNLS model in the (a, h) plane (for its derivation see Section 1.4). The positive temperature region lies between the ground state (solid blue line) and the infinite temperature isothermal (dashed red line). The line at constant chemical potential $\mu = 2$ has been obtained, for $0.5 \leq T \leq 10$, making use of the Monte–Carlo stochastic thermostats defined in Section 2.2 (purple triangles) and the Langevin scheme (solid black line).

with the reservoir ($\gamma = 0$), Eq. (3.1) reduces to the unperturbed DNLS equation, Eq. (1.2).

At variance with MC schemes, one can show (with the help of suitable assumptions and approximations) that eq. (3.1) describes the coupling with an ensemble of complex linear oscillators (see the derivation in Section 3.3). Additional physical insight is gained by rewriting Eq. (3.1), in terms of the p_n, q_n variables,

$$\begin{aligned} \dot{p}_n &= -\frac{\partial H}{\partial q_n} - \gamma \frac{\partial H_\mu}{\partial p_n} + \sqrt{2\gamma T}\xi'_n(t) \\ \dot{q}_n &= \frac{\partial H}{\partial p_n} - \gamma \frac{\partial H_\mu}{\partial q_n} + \sqrt{2\gamma T}\xi''_n(t) \quad , \end{aligned} \tag{3.2}$$

where H_μ is the effective Hamiltonian $H_\mu = H - \mu A$. In the absence of thermal noise, the deterministic components of the thermostat, being gradient terms, would drive the system towards a state characterized by a minimal H_μ. The presence of the symplectic forces allows navigating across the microstates characterized by the given H_μ-value. These considerations suggest that this is the proper way to define a dissipation scheme in the DNLS case. Actually, the reason why H_μ is considered instead of H is the presence of two conservation laws: the minimum of the energy depends on the mass density a. In order to ensure the convergence to the proper state, the term $-\mu A$ must be added to the effective Hamiltonian. The additional presence of the fluctuations completes the definition of the generalized Langevin equation, which represents

a proper stochastic reservoir for the DNLS equation with temperature T and chemical potential μ. From (3.2) one can also check that the related Fokker-Planck equation admits as a stationary solution the expected equilibrium grandcanonical distribution $\exp\{-\beta(H-\mu A)\}$, with $\beta = 1/T$ (see Section 3.2.1). This setup can be straightforwardly implemented to investigate non–equilibrium settings, by assuming that the single reservoirs operate at different temperatures/chemical potentials.

In the following we will focus on a typical setup adopted in the study of stationary nonequilibrium regimes: only the first (z_1) and the last (z_N) lattice variables interact with the reservoirs. This means that, assuming fixed boundary conditions (i.e. $z_0 = z_{N+1} = 0$), the evolution on the leftmost site is ruled by the equation

$$\begin{aligned} \dot{p}_1 &= -(p_1^2+q_1^2)q_1 - q_2 - \gamma\left[(p_1^2+q_1^2)p_1 + p_2 - \mu_L p_1\right] + \sqrt{2\gamma T_L}\xi_1' \\ \dot{q}_1 &= (p_1^2+q_1^2)p_1 + p_2 - \gamma\left[(p_1^2+q_1^2)q_1 + q_2 - \mu_L q_1\right] + \sqrt{2\gamma T_L}\xi_1'' \quad , \end{aligned} \tag{3.3}$$

where T_L and μ_L denote the temperature and the chemical potential of the left reservoir, respectively. Analogous equations hold for the right reservoir, which acts on the site $n = N$, where the temperature is T_R, the chemical potential is μ_R, and the coupling strength is set again equal to γ for simplicity. The rest of the chain follows the Hamiltonian evolution (1.2).

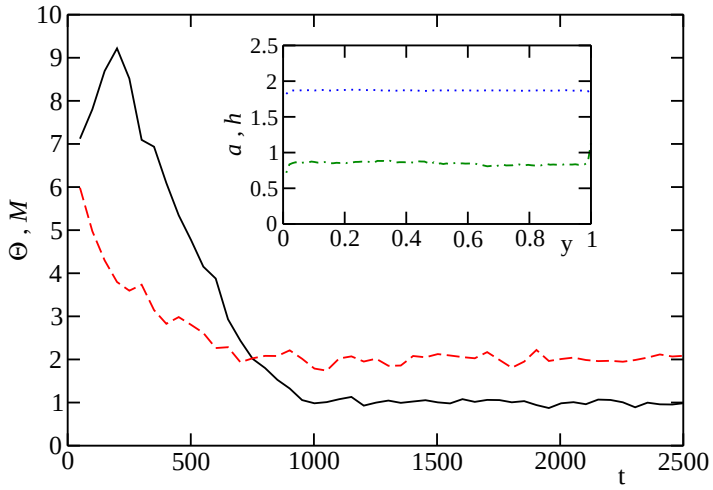

Figure 3.2: Evolution of Θ (black solid line) and $\mathcal{M}$ (red dashed line) in a chain of $N = 100$ sites in contact with two Langevin heat baths with $T_L = T_R = 1$, $\mu_L = \mu_R = 2$. The initial state corresponds to $a = 4$ and $h = 15$. Θ and $\mathcal{M}$ are measured according to Section 2.2.2 and averaged over running windows of 50 time units. In the inset: final spatial profiles of mass (blue dots) and energy (green dot-dashed line) densities as a function of the rescaled site index $y = n/N$.

The simple case of a chain in contact with two reservoirs, operating at the same temperature and chemical potential, allows to test the Langevin scheme (3.3). In Fig. 3.2

we show a typical relaxation process towards an equilibrium state, characterized by the temperature and the chemical potential imposed by the reservoirs. The quantities Θ and $\mathcal{M}$ on the vertical axis denote the dynamical observables of the DNLS chain representing its microcanonical temperature and chemical potential respectively. Such quantities are complicated functions of the canonical variables, see Section 2.2.2 for details. The inset in Fig. 3.2 shows that the asymptotic state reached after the relaxation process is a genuine equilibrium state, corresponding to spatially homogeneous mass and energy densities.

For the sake of completeness, we have also checked the equivalence between the Langevin scheme and the MC reservoirs. As an example, in Fig. 3.1 we show that the isochemical lines $\mu = 2$, obtained with the two approaches, essentially coincide.

We conclude this section by observing that the scheme (3.1) reduces, for $T \to \infty$, to a standard Langevin formulation. Actually, in the large temperature limit, but finite mass- and energy-densities, it turns out that $\mu \to -\infty$ and $\gamma \to 0$. In this limit (3.3) reduces to

$$i\dot{z}_1 = -2|z_1|^2 z_1 - z_2 - i\Gamma z_1 + \sqrt{a_L \Gamma}\,\xi_1 \quad , \tag{3.4}$$

where $\Gamma = -\gamma\mu_L > 0$ and $a_L = -T_L/\mu_L$ are finite quantities. Notice that a_L, which corresponds to the average mass density in the first site, plays the role of an effective temperature.

As a numerical check, we simulated eq. (3.4) with $a_L > a_R$, i.e. in a nonequilibrium setting. Even for relatively short chains, the relation (1.15) is fulfilled at all points of the chain (see Fig. 3.3) meaning that local equilibrium holds. This is further confirmed by the shape of the distribution of the local mass, that is Poissonian, as expected in the $T = \infty$ case [26] (see the inset of Fig. 3.3). Establishement of local equilibrium is not granted a priori, although it is known to generically occur in simulations of chains of nonlinear oscillators, even when transport is anomalous [2]. This is nevertheless a peculiar case, as both temperature and chemical potentials are arbitrarily large. However, it should be remarked that local equilibrium relations can be demonstrated to hold exactly only in very simple cases like for instance the Kipnis-Marchioro-Presutti model [94]. For the present model (but also in other nonlinear chains) it is not at all obvious that energy transfer among oscillators can be even roughly approximated by a Markovian process.

3.2.1 Fokker-Planck formulation

The Fokker-Planck equation is commonly used to describe the evolution of a dynamical system in terms of a probability distribution $\rho(\mathbf{x}, t)$ that represents the probability density for the system to be in the state $\mathbf{x} = (p_1, \ldots, p_N, q_1, \ldots, q_N)$ at time t. In this subsection we focus on the Fokker-Planck equation that corresponds to the Langevin dynamics written in Eq. (3.2). In particular we will prove that one of its stationary solutions is the grand-canonical equilibrium distribution, thus confirming the consistency of our approach.

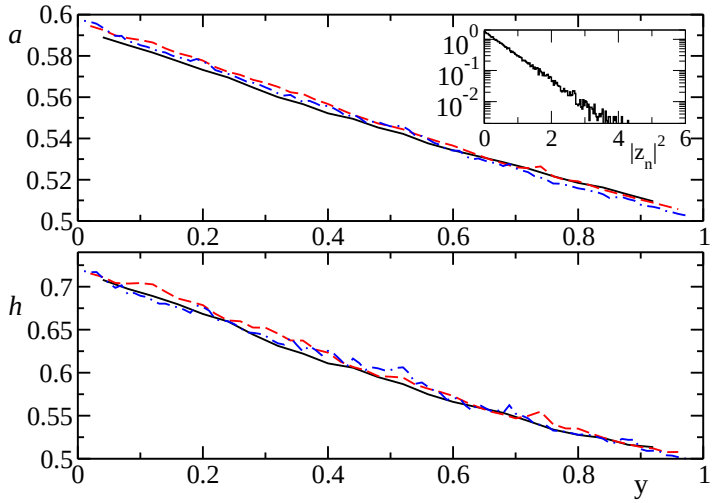

Figure 3.3: Nonequilibrium profiles of mass density (upper panel) and energy density (lower panel) obtained with the infinite temperature Langevin equation (3.4) and parameters $a_L = 0.6$, $a_R = 0.5$, $\Gamma = 1$. Black solid, red dashed and blue dot-dashed lines refer respectively to chain lengths $N = 25, 50, 100$. The profiles are almost linear and $h(y) = 2a^2(y)$ along the chain, confirming that the thermostats act at $T = \infty$. The inset shows that histogram of the local mass $|z_n|^2$ at $n = 20$ is Poissonian, as expected.

Following the derivation contained in [95], we write the Fokker-Planck equation in the form

$$\frac{\partial \rho(\mathbf{x},t)}{\partial t} = -\nabla_{\mathbf{x}} \cdot \mathbf{v}(\mathbf{x})\rho(\mathbf{x},t) + \nabla_{\mathbf{x}} \cdot (\mathbf{B}\,\nabla_{\mathbf{x}}\rho(\mathbf{x},t)) \quad , \tag{3.5}$$

where $\mathbf{v}(\mathbf{x})$ is a vector function of the variables $\mathbf{x}$ and $\mathbf{B}$ is a square matrix. With the assumption of a Markovian friction and Gaussian white noise, $\mathbf{v}(\mathbf{x})$ and $\mathbf{B}$ are directly related to the general form of the Langevin equation

$$\frac{d\mathbf{x}}{dt} = \mathbf{v}(\mathbf{x}) + \mathbf{F}(t) \quad , \tag{3.6}$$

with

$$\langle \mathbf{F}(t)\mathbf{F}(t')\rangle = 2\mathbf{B}\,\delta(t-t') \quad . \tag{3.7}$$

If we now specialize Eq. (3.6) to Eq. (3.2), we find

$$\mathbf{x} = \begin{pmatrix} \mathbf{p} \\ \mathbf{q} \end{pmatrix} \qquad \mathbf{v}(\mathbf{x}) = \begin{pmatrix} -\nabla_{\mathbf{q}} H - \gamma \nabla_{\mathbf{p}} H_\mu \\ \nabla_{\mathbf{p}} H - \gamma \nabla_{\mathbf{q}} H_\mu \end{pmatrix}$$

$$\mathbf{F}(t) = \begin{pmatrix} \sqrt{2\gamma T}\xi' \\ \sqrt{2\gamma T}\xi'' \end{pmatrix} \qquad \mathbf{B} = \gamma T \begin{pmatrix} \mathbf{1} & \mathbf{0} \\ \mathbf{0} & \mathbf{1} \end{pmatrix} \quad ,$$

where $\mathbf{1}$ and $\mathbf{0}$ denote respectively the identity and the null matrix.

As a result, Eq. (3.5) simplifies into

$$\frac{\partial \rho(\mathbf{x},t)}{\partial t} = -\nabla_{\mathbf{x}} \cdot (\mathbf{F}\rho) + \gamma T \, \nabla^2_{\mathbf{x}} \rho \quad . \tag{3.8}$$

We now verify that the grand-canonical distribution $\rho_g = Z \exp(-\beta H_\mu)$, with $Z = \int d\mathbf{x} \exp(-\beta H_\mu)$, is a stationary solution of (3.8), i.e. $\partial \rho_g / \partial t = 0$. In fact, expanding the r.h.s. of Eq. (3.8), we obtain

$$\sum_{n=1}^{N} \left\{ -\frac{\partial}{\partial p_n} \left[\left(-\frac{\partial H}{\partial q_n} - \gamma \frac{\partial H_\mu}{\partial p_n} \right) \rho_g \right] - \frac{\partial}{\partial q_n} \left[\left(\frac{\partial H}{\partial p_n} - \gamma \frac{\partial H_\mu}{\partial q_n} \right) \rho_g \right] + \gamma T \left[\frac{\partial^2}{\partial p_n^2} \rho_g + \frac{\partial^2}{\partial q_n^2} \rho_g \right] \right\}$$

After some algebra, we get

$$\sum_{n=1}^{N} \gamma \left[\rho_g \frac{\partial^2 H_\mu}{\partial x_n^2} + \frac{\partial H_\mu}{\partial x_n} \frac{\partial \rho_g}{\partial x_n} \rho_g + T \frac{\partial^2 \rho_g}{\partial x_n^2} \right] + \mu \rho_g \{A, H\} \quad , \tag{3.9}$$

where $\{A, H\}$ denote the Poisson brackets of the global observables A ad H. As both these functions are conserved quantities of the dynamics, we straightforwardly get $\{A, H\} = 0$. Finally, it is easy to verify that also the quantity proportional to γ in Eq. (3.9) yields zero for our choice of ρ_g.

In conclusion, in this subsection we have provided a description of the DNLS Langevin thermostat in terms of a Fokker-Planck equation, Eq. (3.8), and we have verified that it admits a stationary solution in the form of the Gibbs invariant measure. These results may represent possible starting points for a future analytical treatment of the problem.

3.3 Microscopic derivation of the Langevin equation

In this section we derive Eq. (3.1) by following the system-bath coupling approach [95]. In analogy with what done for harmonic lattices [96], we consider a complex oscillator, described by the dynamical variable z, linearly coupled with a bath of independent, complex harmonic oscillators described by the Hamiltonian

$$H_B = \sum_{\nu} \{ \omega_\nu^a |a_\nu|^2 + \omega_\nu^b |b_\nu|^2 + [K_\nu^* z (a_\nu^* + b_\nu) + c.c.] \} \quad , \tag{3.10}$$

where we have introduced two different species of oscillators, corresponding to the two sets of frequencies ω_ν^a and ω_ν^b, while K_ν are the bath-system coupling constants. Moreover, the variables $(a_\nu, i a_\nu^*)$ and $(b_\nu, i b_\nu^*)$ are independent canonically conjugate coordinates, satisfying the following Poisson brackets

$$\begin{aligned} \{ i a_\nu^*, a_{\nu'} \} = \{ i b_\nu^*, b_{\nu'} \} = \delta_{\nu,\nu'} \\ \{ a_\nu, a_{\nu'} \} = \{ b_\nu, b_{\nu'} \} = \{ a_\nu, b_{\nu'} \} = \{ a_\nu, i b_{\nu'}^* \} = 0 \quad . \end{aligned} \tag{3.11}$$

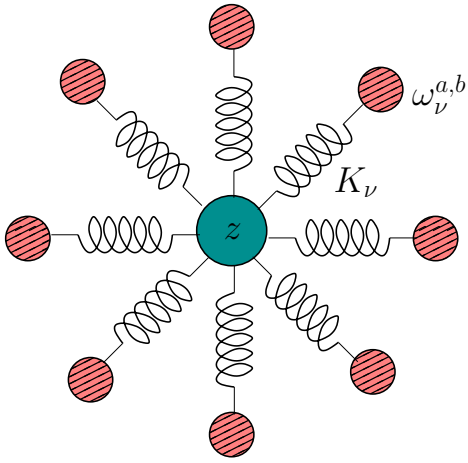

Figure 3.4: Illustration of the bath-system coupling analyzed in this section. The central system (described by the dynamical variable z) is in contact with a set of independent linear oscillators with frequencies $\omega_\nu^{a,b}$. K_ν define the linear coupling constants.

In order to preserve the global symmetry of the system with respect to phase transformations, we impose a second conservation law,

$$A_B = \sum_\nu (|a_\nu|^2 - |b_\nu|^2) \quad . \tag{3.12}$$

The function A_B is the generator of phase transformations of the bath variables. It is easy to verify that the transformation generated by $A_B + |z|^2$,

$$\begin{aligned} a_\nu(s) &= e^{is} a_\nu(0) \\ b_\nu(s) &= e^{-is} b_\nu(0) \\ z(s) &= e^{is} z(0) \quad , \end{aligned}$$

leaves the Hamiltonian H_B invariant. An example of heat bath satisfying these conditions is given by a complex d'Alembert equation, $\Box\phi(x,t) = 0$, for which the quantity A_B represents the total (conserved) charge of the field; see [97] for details. The equations of motion generated by (3.10) are

$$\begin{aligned} i\dot{a}_\nu &= -\omega_\nu^a \, a_\nu - K_\nu^* z \\ i\dot{b}_\nu &= -\omega_\nu^b \, b_\nu - K_\nu z^* \\ i\dot{z} &= f(z) - \sum_\nu K_\nu (a_\nu + b_\nu^*) \quad , \end{aligned}$$

where $f(z)$ accounts for the deterministic part of the evolution of z, not included in

H_B. The first two equations can be formally solved, yielding

$$a_\nu(t) = a_\nu(0)\, e^{i\omega_\nu^a t} + iK_\nu^* \int_0^t e^{i\omega_\nu^a (t-t')} z(t')\, dt'$$
$$b_\nu(t) = b_\nu(0)\, e^{i\omega_\nu^b t} + iK_\nu \int_0^t e^{i\omega_\nu^b (t-t')} z^*(t')\, dt' .$$

By then substituting into the equation for z, we obtain

$$i\dot{z} = f(z) - i \int_0^t G(t-s) z(s) ds + F(t) \quad ,$$

where the noise term $F(t)$ and the dissipation function $G(t)$ are defined as

$$F(t) = -\sum_\nu K_\nu \left[a_\nu(0) e^{\, i\omega_\nu^a t} + b_\nu^*(0)\, e^{-i\omega_\nu^b t} \right] \tag{3.13}$$
$$G(t) = \sum_\nu |K_\nu|^2 \left[e^{i\omega_\nu^a t} - e^{-i\omega_\nu^b t} \right] \quad . \tag{3.14}$$

By now imposing a grandcanonical equilibrium distribution $P \sim \exp[-\beta(H_B - \mu A_B)]$ for the bath of oscillators (cf. Appendix A), where $\beta = 1/T$ is the inverse temperature, we find that the correlation functions of $F(t)$ write

$$\begin{aligned} \langle F(t)F(t') \rangle &= \langle F^*(t)F^*(t') \rangle = 0 \\ \langle F(t)F^*(t') \rangle &= \sum_\nu |K_\nu|^2 \left[e^{i\omega_\nu^a (t-t')} \langle\, |a_\nu(0)|^2 \,\rangle + e^{-i\omega_\nu^b (t-t')} \langle\, |b_\nu(0)|^2 \,\rangle \right] = \\ & \sum_\nu |K_\nu|^2 \left[\frac{e^{i\omega_\nu^a (t-t')}}{\beta(\omega_\nu^a - \mu)} + \frac{e^{-i\omega_\nu^b (t-t')}}{\beta(\omega_\nu^b + \mu)} \right] , \end{aligned} \tag{3.15}$$

where, in order to have positive definite statistical weights, we have also to assume $\omega_\nu^a > \mu$ and $\omega_\nu^b > -\mu$. In the thermodynamic limit the sums over the index ν in (3.14) can be replaced by integrals. Accordingly, we can rewrite Eq. (3.14) in the form

$$G(t) = \int_\mu^{+\infty} d\omega\, G^a(\omega)\, e^{i\omega t} - \int_{-\mu}^{+\infty} d\omega\, G^b(\omega)\, e^{-i\omega t} \quad , \tag{3.16}$$

where $G^{a,b}(\omega) = \rho^{a,b}(\omega)|K(\omega)|^2$ are two positive definite functions and $\rho^{a,b}(\omega)$ the corresponding density of states that we assume to be smooth functions. By following the same approach, Eq. (3.15) writes

$$\langle F(t)F^*(t') \rangle = \int_\mu^{+\infty} d\omega\, \frac{G^a(\omega) e^{i\omega(t-t')}}{\beta(\omega - \mu)} + \int_{-\mu}^{+\infty} d\omega\, \frac{G^b(\omega) e^{-i\omega(t-t')}}{\beta(\omega + \mu)} \quad , \tag{3.17}$$

which is a kind of fluctuation-dissipation theorem [96] where the Bose-Einstein distribution has been replaced by the Rayleigh-Jeans one.

The corresponding generalized Langevin equation is not very practical, since it is non Markovian. We have nevertheless the freedom to choose the coupling and the density of states of the bath. The spectral properties of the process F strongly depend on the behaviour of G close to the ground state and may also display long-range correlations. To understand this point, consider the example in which $G^{a,b}(\omega) = \gamma$. This choice yields a spectral density of $F(t)$ which is logarithmically divergent close to the ground state frequency, thus defining a non-stationary process. The simplest, nonsingular case is obtained by choosing

$$G^a(\omega) = \frac{\gamma}{2\pi}(\omega - \mu), \quad G^b(\omega) = \frac{\gamma}{2\pi}(\omega + \mu) \quad .$$

In this case $F(t)$ becomes a complex white noise

$$\langle F(t)F^*(t')\rangle = \frac{\gamma}{\beta}\delta(t - t') \quad ,$$

while the dissipation function is

$$G(t) = \frac{\gamma}{2\pi}\int_{-\infty}^{+\infty} d\omega\,(\omega - \mu)e^{i\omega t} = -\gamma\left[i\frac{d}{dt}\delta(t) + \mu\delta(t)\right] \quad . \tag{3.18}$$

The full dissipation term is therefore

$$-i\int_0^t G(t - s)z(s)\,ds = -\gamma\dot{z}(t) + i\gamma\mu z(t) \quad , \tag{3.19}$$

and the resulting Langevin equation corresponds to a noisy, driven, complex Ginzburg-Landau equation

$$(i + \gamma)\dot{z} = f(z) + i\gamma\mu z + F(t) \quad . \tag{3.20}$$

In the weak coupling limit ($\gamma \ll 1$), the equation can be further simplified. By multiplying by $(1 + i\gamma)$ and neglecting terms $O(\gamma^{3/2})$, one obtains

$$i\dot{z} = (1 + i\gamma)f(z) + i\gamma\mu z + F(t) \quad , \tag{3.21}$$

which has the same structure as Eq. (3.1).

3.4 The large mass density limit of the DNLS equation

In Section 3.2 we have shown that the Langevin formulation of the DNLS thermodynamics provides a clear physical interpretation of the infinite-temperature limit. On the other hand, in the previous chapter we have shown that the opposite, low-temperature, limit, as well as the case of large mass-densities, is also interesting for its nontrivial transport properties. In this section we show that the Langevin formulation can shed

further light on such regime by revealing a strong relationship with the XY model and thereby bridging a gap between two seemingly different classes of systems.

It is, first of all, convenient to introduce the following change of variables

$$z_n = \sqrt{a}(1+\zeta_n)\exp[i(\omega t + \phi_n + n\pi)] \quad , \tag{3.22}$$

where $\omega = 2(a-1)$. By inserting (3.22) into (1.2), one finds that the new variables ζ_n and ϕ_n obey the dynamical equations

$$\begin{aligned} \dot{\phi_n}(1+\zeta_n) &= 2(1+2a)\zeta_n + 2a(3\zeta_n^2+\zeta_n^3) - (1+\zeta_{n+1})\cos(\phi_{n+1}-\phi_n) \\ &\quad -(1+\zeta_{n-1})\cos(\phi_n-\phi_{n-1}) + 2 \\ \dot{\zeta_n} &= (1+\zeta_{n+1})\sin(\phi_{n+1}-\phi_n) - (1+\zeta_{n-1})\sin(\phi_n-\phi_{n-1}) \quad . \end{aligned} \tag{3.23}$$

In this representation, the ground state (1.6) is simply $\zeta_n = 0$, $\phi_n = 0$. Also, this is the optimal starting point to discuss two limit cases: low-temperatures and large mass-densities. The low-temperature dynamics can be studied by assuming $\zeta_n \ll 1$ and $(\phi_n - \phi_{n-1}) \ll 1$. In Section 3.6, we show that, in this limit, the system is equivalent to a chain of harmonic oscillators with nearest- and next-to-nearest-neighbour interactions. Furthermore, mass conservation of the original model maps into momentum conservation for the oscillators. Such a correspondence is instructive, as it reveals a link with separable models, where a simple local definition of the temperature can be given in terms of the kinetic energy.

The large mass-density regime is studied under the assumption that $a \gg 1$ and $\zeta_n \ll 1$. Here below we show that also in this approximation the Hamiltonian becomes separable. In fact, the dynamical equations (3.23) reduce to leading order to

$$\begin{aligned} \dot{\phi_n} &= \lambda_n \\ \dot{\lambda_n} &= 4a\left[\sin(\phi_{n+1}-\phi_n) - \sin(\phi_n-\phi_{n-1})\right] \quad , \end{aligned} \tag{3.24}$$

where $\lambda_n = 4a\zeta_n$. This system corresponds to a system of coupled rotors, i.e. a classical version of the XY model in one dimension [98, 99, 100, 101]. Its Hamiltonian reads

$$\mathcal{H}_{XY} = \sum_n \frac{\lambda_n^2}{2} - \sum_n 4a\cos(\phi_{n+1}-\phi_n) \quad , \tag{3.25}$$

where λ_n and ϕ_n are a couple of conjugate action-angle variables, the former playing the role of the angular momentum. This analogy was already noticed (for the two-dimensional case) in [102].

At variance with the former case, we have not introduced any smallness hypothesis for $\phi_n - \phi_{n-1}$; as a result, some nonlinear terms are maintained and one can, thereby, explore large temperatures as well. Having assumed that $\zeta_n \ll 1$, this regime can be called *phase* chaos. It is also interesting to observe that in the large mass–density limit the invariance under global phase rotations of the DNLS transforms into the invariance under a translation of the angles ϕ_n. Accordingly, the conservation of the total mass A

transforms into the conservation of the total angular momentum $L = \sum_n \lambda_n$ (this can be easily verified by expanding expression (1.5)). Notice also that the low-temperature limit discussed in Section 3.6 is not fully contained into the large mass-density regime, as it includes the case of relatively small a-values.

Before passing to thermodynamic studies, it is necessary to clarify the range of validity of the XY model as an approximation of the DNLS one. The condition $\zeta_n \ll 1$ implies $\lambda_n \ll a$, i.e. $T \ll a^2$, because on average λ_n^2 is equal to the temperature T. As we are exploring the range of large a-values, one can conclude that, the larger a, the broader the temperature range where the XY model provides an accurate description of the DNLS equation. Before drawing this conclusion, it is, however, necessary to be more careful. In fact, the presence of a finite conductivity in the XY model can be traced back to the existence of (possibly infrequent) jumps of angle-differences across the sinusoidal potential barrier. In the context of Eq. (3.25), the height of this barrier is of the order of a, which is smaller than the maximal acceptable energy a^2 (since $a \ll a^2$, for $a \gg 1$). Accordingly the XY model provides an accurate description also of the barrier jumps and, more than that, the validity of the XY model extends to the high-temperature regime (here "high" means above a) characterized by frequent jumps.

3.4.1 Thermostatted chain

Here, we examine how to describe the bath dynamics within the XY approximation. Let us study the simple setup of a DNLS chain in contact with an external Langevin reservoir at the first site. In the low-temperature limit, i.e. close to the ground state, equation (3.1) specializes to

$$i\dot{z}_1 = -2|z_1|^2 z_1 - z_2 - i\gamma\left[2|z_1|^2 z_1 + z_2 - 2(a-1)z_1 - \delta\mu\, z_1\right] + \sqrt{\gamma T_L}\,\xi_1\,. \tag{3.26}$$

We have consistently assumed the chemical potential to be a perturbation of the ground-state value, i.e. $\mu = \omega + \delta\mu$ with $\delta\mu \ll \omega$. For $a \gg 1$, (3.26) transforms, to leading order in a, into a Langevin equation for the XY model with suitable dissipation and fluctuation terms

$$\begin{aligned} \dot{\phi_1} &= 4a\zeta_1 \\ \dot{\zeta_1} &= \sin(\phi_2 - \phi_1) - \gamma\,(4a\zeta_1 - \delta\mu) + \sqrt{\frac{\gamma T_L}{a}}\,\xi_1 \quad . \end{aligned} \tag{3.27}$$

By then introducing the momenta λ_n, equation (3.24), and the rescaled dissipation parameter $\gamma' = 4a\gamma$, one finally obtains

$$\begin{aligned} \dot{\phi_1} &= \lambda_1 \\ \dot{\lambda_1} &= 4a\sin(\phi_2 - \phi_1) - \gamma'\,(\lambda_1 - \delta\mu) + \sqrt{4\gamma' T_L}\,\xi_1 \quad . \end{aligned} \tag{3.28}$$

These equations describe a rotor chain in contact in the first site with a reservoir at temperature $2T_L$ and constant torque $\gamma'\delta\mu$.

This derivation provides an interesting interpretation of the DNLS chemical potential in the large mass-density limit: at equilibrium (3.28) is expected to sample microstates compatible with the grandcanonical measure $\exp\{-\beta[\mathcal{H}_{XY} - \delta\mu L]\}$, where $L = \sum_n \lambda_n$ is the total angular momentum of the XY chain and $\delta\mu$ can be interpreted as the average angular velocity of the rotors.

3.4.2 Nonequilibrium conditions

The above formulation can be straightforwardly extended to nonequilibrium setups, where $T_R \neq T_L$ and $\mu_R \neq \mu_L$. In this case, it is convenient to perform the XY approximation with respect to a ground state that corresponds to the average chemical potential $(\mu_R + \mu_L)/2$. Accordingly, the resulting XY chain turns out to be forced by *opposite external torques* $\pm\gamma'\delta\mu$, where now $\delta\mu = (\mu_R - \mu_L)/2$.

The observables of major interest in the nonequilibrium context are the fluxes of the conserved quantities. The continuity equations for mass and energy densities of the DNLS model allow determining their explicit expressions

$$j_n^a = i(z_n z_{n-1}^* - z_n^* z_{n-1}) \tag{3.29}$$
$$j_n^h = \dot{z}_n z_{n-1}^* + \dot{z}_n^* z_{n-1} \quad . \tag{3.30}$$

In the large mass-density limit, the leading terms read

$$j_n^a = -2a\sin(\phi_{n+1} - \phi_n) \tag{3.31}$$
$$j_n^h = -2\omega\, a\sin(\phi_{n+1} - \phi_n) - 4a\dot{\phi}_n \sin(\phi_{n+1} - \phi_n) \quad , \tag{3.32}$$

where the variables ζ_n have been expressed in terms of $\dot{\phi}_n$. Notice that the simple symmetric form of the second equation has been obtained by adding to (3.30) the quantity $-a(\dot{\phi}_n - \dot{\phi}_{n-1})\sin(\phi_n - \phi_{n-1})$, whose average is zero in a stationary state. Eq. (3.31) is just the momentum flux of the XY model, i.e. the local force. The term proportional to $\dot{\phi}_n$ in Eq. (3.32) has the typical structure of the energy flux in the XY model: it is nonzero only at finite temperatures. The first term is a coherent contribution that results from the fact that the oscillators rotate with an average common frequency ω: it survives in the zero-temperature limit, when $j_n^h = \mu j_n^a$, so that the heat current $j_n^h - \mu j_n^a = 0$, i.e. there is no heat transport and no entropy production. At low temperatures, Eqs. (3.31, 3.32) describe the Josephson effect, where the chain amounts to a single junction in between two superfluids [103]. The mass current is proportional to the phase gradient and is independent of the system length N, i.e. it provides a ballistic contribution.

3.5 Comparison with numerical simulations

As mentioned above, an important difference between the DNLS equation and oscillator chains (like the Fermi-Pasta-Ulam or Klein-Gordon models) is that its Hamiltonian

is not the sum of kinetic and potential energies. Therefore, it is not obvious how to directly monitor the temperature T and the chemical potential μ in actual simulations. The only general approach we are aware of is based on non-local microcanonical expressions Θ and $\mathcal{M}$ which, unfortunately are rather awkward to compute in practice (see Section 2.2.2 for details). The perturbative analysis of the low-temperature limit and the correspondence with the XY model show that the temperature T and the chemical potential μ can be determined in terms of local variables. This is quite a relevant observation as it may be used to simplify the definition of such thermodynamic quantities. In the following we explore the range of validity of such definitions.

From (3.25) it is straightforward to define a kinetic temperature as the fluctuations of the momentum λ_n with respect to its average value $\langle\lambda_n\rangle$,

$$T_{XY} = \langle\lambda_n^2\rangle - \langle\lambda_n\rangle^2 \quad . \tag{3.33}$$

If we compare the stochastic term in (3.28) with the one imposed by the fluctuation-dissipation theorem and commonly used in the Langevin equation for oscillator models, $\sqrt{2\gamma T}$ (see [2, 15]), we can conclude that our definitions imply $T_{XY} = 2T$ (the factor 2 is just a consequence of the choice of the transformation of variables).

In Fig. 3.5 we compare the general microcanonical definition of temperature for the DNLS model Θ, defined as in Section 2.2.2, with T_{XY} for an equilibrium setting, i.e. external reservoirs at equal temperature and chemical potential; T_{XY} is computed by evaluating, in the same simulation, the average of the ζ_n^2 defined in (3.22). The data clearly show that, by increasing the chemical potential μ (i.e., by increasing a, since $\mu = 2(a-1)$), the range of values in which the two temperatures coincide increases, as expected from the previous considerations. On the other hand, outside the limits of validity of the XY approximation discussed in Section 3.4, Θ and T_{XY} can be strongly different from one another. In such regimes, Θ is the only valid definition of temperature. In the inset of Fig. 3.5 we show that the curves obtained for different values of μ quite well collapse onto each other by rescaling both T_{XY} and Θ by the factor a^{-2}. This implies that the range of validity of the correspondence between these two temperatures increases proportionally to a^2.

Finally, we have tested the validity of the XY approximation in a non-equilibrium stationary regime. In the simplest case one can impose two heat baths at different temperatures, T_R and T_L, and with the same chemical potential μ acting at the chain boundaries. If one chooses the value of μ in such a way that both temperatures are smaller than a^2 (see Fig. 3.5), one obtains temperature profiles very close to each other (data not reported). This scenario is maintained also if a chemical potential gradient is applied, provided both μ_R and μ_L are large enough to make the previous condition hold, while $\delta\mu = (\mu_R - \mu_L)/2$ is smaller than the average chemical potential $(\mu_R + \mu_L)/2$ (see Sections 3.4.1 and 3.4.2). In fact, Fig. 3.6 exhibits a nice agreement between the two temperature profiles. A further test of the validity of XY model is presented in Table 3.1 where the full DNLS fluxes are compared with the ones reconstructed through the XY approximation (see Eqs. (3.31) and (3.32)).

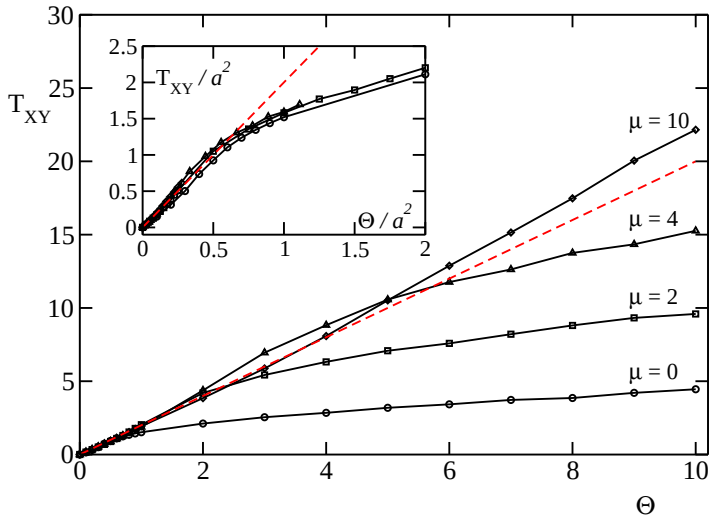

Figure 3.5: Comparison of the XY kinetic temperature T_{XY} with Θ for different values of the chemical potential μ. The dashed line corresponds to $T_{XY} = 2\Theta$, which should hold in the limit of large μ, where the XY approximation is valid. The inset shows the same curves in the rescaled units T_{XY}/a^2 and Θ/a^2. Simulations are performed using Langevin heat baths coupled at the boundaries of a DNLS chain with $N = 50$. T_{XY} and Θ are measured on a subchain of 30 lattice sites.

	DNLS	XY
j^a	-0.234	-0.208
j^h	-1.40	-1.28

Table 3.1: Comparison of the exact DNLS fluxes (first column) and the ones reconstructed by means of eqs. (3.31) and (3.32) (second column) for the nonequilibrium profile described in the caption of Fig. 3.6.

3.6 The low–temperature limit of the DNLS problem

In this section we provide a low–temperature description of the DNLS equation in terms of a harmonic model with separable Hamiltonian. In this limit, the solution of Eq. (3.23) is expected to be close to the homogeneous periodic motion of the ground-state solution (1.6). Thus, we assume $\zeta_n \ll 1$ and $(\phi_n - \phi_{n-1}) \ll 1$ and we expand Eq. (3.23) to linear order. As a result, we obtain

$$\begin{aligned} \dot{\phi}_n &= 4a\zeta_n + 2\zeta_n - \zeta_{n+1} - \zeta_{n-1} \\ \dot{\zeta}_n &= \phi_{n+1} - 2\phi_n + \phi_{n-1} \quad . \end{aligned} \tag{3.34}$$

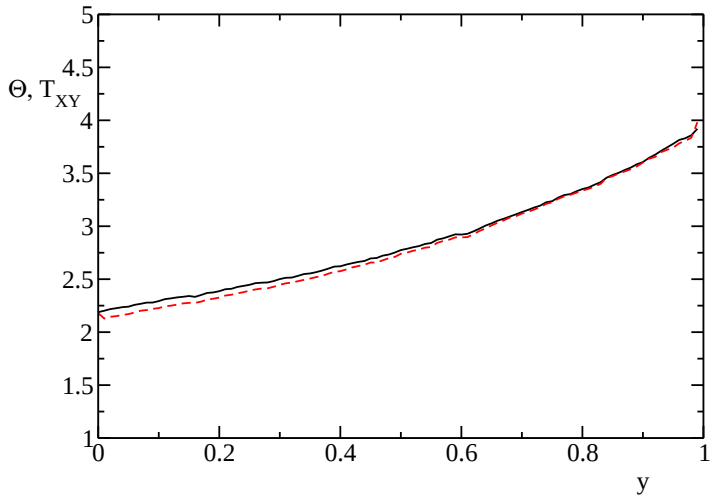

Figure 3.6: Comparison of the XY kinetic temperature profile T_{XY} (red dashed line) with Θ (black solid line) in a nonequilibrium steady state. Simulations are performed using Langevin heat baths with parameters ($T_L = 2$, $\mu_L = 9.6$) and ($T_R = 4$, $\mu_R = 10.4$), coupled to a DNLS chain with $N = 1000$.

If one now introduces the new variable

$$p_n = 4a\zeta_n + 2\zeta_n - \zeta_{n+1} - \zeta_{n-1} \quad . \tag{3.35}$$

the Eqs. (3.34) can be re–written as

$$\begin{aligned} \dot{\phi}_n &= p_n \\ \dot{p}_n &= 4(1+a)(\phi_{n+1} - 2\phi_n + \phi_{n-1}) - \phi_{n+2} + 2\phi_n - \phi_{n-2} \quad . \end{aligned} \tag{3.36}$$

These equations describe the dynamics of a chain of harmonic oscillators with nearest-neighbour and next-to-nearest-neighbour interaction. The corresponding Hamiltonian,

$$\mathcal{H}_h = \sum_n \left[\frac{1}{2} p_n^2 + 2(1+a)(\phi_{n+1} - \phi_n)^2 - \frac{1}{2}(\phi_{n+2} - \phi_n)^2 \right] \quad , \tag{3.37}$$

is, at leading order in p_i and $(\phi_{n+1} - \phi_n)$, fully equivalent to that of the original DNLS equation. Its quadratic structure corresponds to a parabolic approximation around the minimum of the energy. Moreover, the total mass-conservation law of the DNLS maps onto the conservation of the total momentum $P = \sum p_n$. Accordingly, the Hamiltonian (3.37) is translationally invariant. The normal modes, i.e. the plane-wave solutions of Eqs. (3.36), are the discrete analogs of the Bogoliubov modes (non-interacting phonons), in the context of the physics of atomic condensates [103].

Passing to thermodynamics, one interesting implication of the Hamiltonian structure in the low–temperature limit (3.37) is that one can naturally introduce a microscopic definition of temperature in terms of the momentum p_n, i.e.

$$T_h = J\left[\langle p_n^2\rangle - \langle p_n\rangle^2\right] \tag{3.38}$$

where the proportionality constant J is the Jacobian determinant of transformation (3.35), which must be included to allow for a meaningful comparison with the DNLS model (see Appendix B.2 for details). In order to test the definition (3.38), we have measured T_h by numerical simulations of the Langevin scheme defined in Eq. (3.1) and in Fig. 3.7 we have compared it with the temperature of the bath, $T_B \equiv T_L = T_R$, for different values of the mass density, a. As expected, T_h approaches T_B for increasing values of a. In fact, the larger is a, the smaller is the relative amplitude of the fluctuations with respect to the ground state. From this analysis we therefore conclude that the harmonic temperature T_h is a well defined thermodynamic observable in the low–temperature limit. Such a definition is much simpler than the general microcanonical one, Θ, defined in Section 2.2.2.

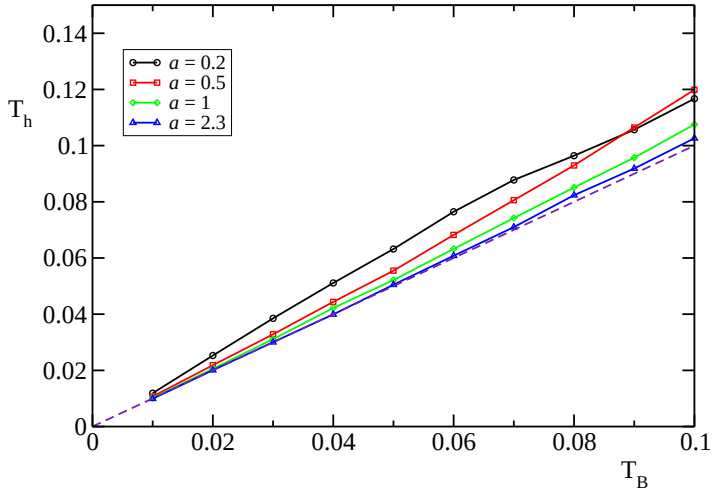

Figure 3.7: Comparison of the harmonic temperature T_h, Eq. (3.38) with the reservoir temperature, T_B. The dashed line correspond to $T_h = T_B$. The Langevin heat baths are coupled at the boundaries of a DNLS chain with $N = 50$. T_h is measured on a subchain of 30 lattice sites to increase the statistics The values of the Jacobian determinant J, which are the product of the eigenvalues of a tridiagonal matrix (see Appendix B.2), have been computed analytically in the $N \to \infty$ limit and are $J = 5.95, 3.73, 2.91, 2.42$ for curves from top to bottom.

For what concerns transport properties, the heat conductivity of the harmonic model (3.37) exhibits a divergence in the thermodynamic limit, as expected for any integrable model (see [89, 2]). Such a conclusion is in contrast with the non-equilibrium numerical studies reported in Chapter 2 that have revealed a finite heat conductivity at finite temperatures. This is clearly a consequence of the presence of nonlinear terms which break the integrability of the dynamics. Their contribution is taken into account in Section 3.4, where we discuss the tight relationship with the one-dimensional XY

model in the limit of large mass densities. In this respect, it is useful to compare the harmonic hamiltonian H_h (3.37) with the one corresponding to the XY model (3.25). The former is valid in the low-temperature regime, while the latter applies for $a \gg 1$ (and $T \ll a^2$). Accordingly, they reduce to one another for small T and large a. In this limit, in fact, the next–to–nearest-neighbour interaction in (3.37) is negligible for $a \gg 1$ and, in the low–temperature limit, one can expand the cosine interaction in (3.25) around zero.

3.7 Discussion

In this chapter we have introduced Langevin heat baths which are able to control both the temperature and the chemical potential in a DNLS model. Numerical simulations indicate that such scheme is simple and practical enough to study finite-temperature DNLS dynamics in both equilibrium and nonequilibrium conditions.

In the large mass-density limit we have approximated the DNLS dynamics in terms of an effective XY model. This allows a clear understanding of the DNLS dynamics, especially in a nonequilibrium setting. We have indeed shown that the effect of thermal baths (which are able to control the chemical potential besides the temperature) acting at the boundaries, is equivalent to an applied torque plus thermal fluctuations. This description allows to give a dynamical interpretation of the chemical potential as well as of the action of thermal baths as means to fix locally the average angular velocities. The corresponding energy flux turns out to be the sum of two different contributions, one due to the phase gradient associated with the torque, the other due to angular-velocity fluctuations. As a consequence, transport in this region has an almost ballistic component, and a diffusive one associated with the XY dynamics which is known to be a normal heat conductor [98, 99]. This accounts for the computations of transport coefficients reported in Chapter 2.

Another remarkable result, is that the relationship with the XY model provides a simple prescription for computing the temperature in the simulations. This last issue is of major importance for non-standard Hamiltonians like the DNLS one, where kinetic and potential energies are not separated. Indeed, the XY approximation allows introducing the simple kinetic expression T_{XY} for the temperature, that can safely approximate the microcanonical one Θ. This is of practical importance, considering that the microscopic definitions of T and μ are pretty much involved for a non separable Hamiltonian, like the DNLS one (Section 2.2.2).

Altogether, starting from the Langevin approach we have achieved a fairly clear physical interpretation of the action of thermal baths as means to fix locally the average angular velocities and kinetic energies of the oscillators. In the framework of the nonequilibrium XY model this means that one can explore more general nonequilibrium states by applying not only temperature but also mechanical (torque) gradients. This possibility has not received much attention in the literature. To our knowledge, only reference [104] treats the joint effect of thermal and mechanical gradients (see also the

nonequilibrium studies in [105] that however refer to the case without external torque and noise).

Some of the numerical results presented above are possible starting points for rigorous investigations. For instance, the evidence of local equilibrium reported in Section 3.2 and the possible approximate description in terms of stochastic models [94] could be a challenging issue for mathematical studies.

Another possible extension of the present work would be to consider the DNLS model on two-dimensional lattices. In this case, the correspondence with the XY model would predict the possibility of observing the transition from normal to anomalous behavior of transport coefficients at the Kosterlitz-Thouless-Berezhinskii transition [106, 107].

The results reported in this chapter have been published in Ref. [108].

Chapter 4

Discrete breathers and metastable states

4.1 Introduction

The analysis provided in Chapters 2 and 3 has unveiled several uncommon features that arise when one considers the setup of a steady nonequilibrium DNLS chain coupled with external reservoirs. Two basic ingredients contribute to make the scenario more complicated than for standard nonlinear oscillator chains, namely the nonseparability of the DNLS Hamiltonian (1.1) and the presence of an additional conservation law in the form of the total mass A.

In this chapter we turn our attention to another well known dynamical property of the DNLS model, that is the capability to develop spatially localized nonlinear excitations, also known as discrete breathers. For long time DNLS equations have represented the ideal benchmark for the dynamic characterization of such peculiar states arising in generic nonlinear lattices (see Section 1.3 for a review of recent and past achievements in this field). On top of that, the intrinsic stability of discrete breathers has motivated a series of studies focused on their role in the coherent transport of energy in more realistic setups (see [14] and references therein).

In the first statistical-mechanics study of the DNLS equation, Rasmussen *et al.* [25] identified a region in the parameter space (Fig. 1.5) that was numerically found to be characterized by the spontaneous creation of discrete breathers, generally superposed to a spatially incoherent phonon background. Such a region is placed above the infinite temperature line and it was conjectured to correspond to a negative temperature (NT) state. From a thermodynamic point of view, the presence of NT states implies that the system's entropy is a decreasing function of the internal energy. In a series of recent papers [26, 79, 80, 81], Rumpf provided a convincing theoretical argument that excludes the physical occurrence of NT equilibrium states in the DNLS model. In particular, he showed that the system eventually reaches a maximum entropy (equilibrium) state formed by a background at infinite temperature superposed to a single breather that collects the "excess" energy. It was also observed that the convergence to

the equilibrium state predicted by Rumpf would need transients lasting over astronomical times [86]. Therefore, the question of characterizing DNLS states over physically accessible time scales remains wide open. Entropy arguments are, in fact, of little help to investigate the convergence to equilibrium in similar regimes.

The occurrence of long transients is not rare in statistical mechanics: it may be due to coarsening, nucleation, the presence of free-energy barriers, or the stability of some dynamical modes. Within the physical setups that are closest to the DNLS model, a nonexponential relaxation was first found in chains of nonlinear oscillators and shown to originate from the presence of long-lived localized solutions [75]. Slow relaxations have been also found in Heisenberg spin chains and traced back to the existence of two conservation laws [60].

In this chapter we show that a broad range of initial conditions (IC) converges towards a well defined thermodynamic state characterized by a negative temperature and a finite density of breathers. Such state does not contradict the theoretical arguments of Rumpf [26, 79], although the dynamical freezing of the high-amplitude breathers slows down the evolution so much as to make the convergence to equilibrium unobservable. Altogether this phenomenon is reminiscent of aging in glasses although a more detailed analysis will be required to frame the analogy on more firm grounds.

In order to clarify such scenario, in the following chapter we will present a stochastic version of the DNLS model that allows to "silence" any dynamical contribution to slow relaxation. This simplified model has allowed us to identify a first source of slowness in a coarsening phenomenon that follows from a sub-diffusive behaviour of the breather amplitudes.

The chapter is organized as follows. In Section 4.2 we provide a thermodynamic characterization of the NT metastable states of the DNLS equation, while, in Section 4.3 we comment on two simple strategies to generate quasi-stationary NT states in the DNLS equation. The methods are based on the introduction of boundary dissipations and the free expansion of wave packets initially at equilibrium at a positive temperature, respectively. Both schemes are far simpler than the thermalization methods recently proposed for BEC trapped in lattices which require non-trivial Mott states followed by sweeps across Feshbach resonances to invert the sign of the atomic interaction [109, 110]. Section 4.4 concludes the chapter with a discussion of the main results and future perspectives.

4.2 Metastable dynamics of an isolated DNLS equation

We start our analysis by studying the long-time evolution of an isolated DNLS chain (with periodic boundary conditions) in the R_n region of the phase diagram of Fig. 1.5. Since the dynamics is microcanonical, this kind of study has required the implementation of a symplectic 4th-order algorithm of Yoshida type [111, 112] that ensured a satisfactory numerical precision in the integration of the equations of motion. Thanks

to this algorithm, we have accurately simulated the dynamics of the model over time scales much longer than in the previous numerical studies.

In order to monitor the convergence towards the equilibrium state it is also necessary to distinguish between breathers and background. This can be done by choosing an amplitude threshold η much larger than the typical background fluctuations but sufficiently smaller than the asymptotic breather amplitude. Taking into account that the background is characterized by Poissonian statistics [26, 79] the previous conditions correspond to the inequality

$$1 \ll \eta/a < \sqrt{N(h/a^2 - 2)} \; . \tag{4.1}$$

In our simulation we have taken $\eta = 10$ that is appropriate even for the smallest system size, $N = 2048$, used in the simulations. Fig. 4.1 presents the space-time evolution for a chain of 4096 sites for $a = 1$ and two different energy densities, namely $h = 2.4$ (panel a) and $h = 2.8$ (panel b). To emphasize the breather dynamics, we plot only the lattice points, where the instantaneous amplitude $a_n = |z_n|^2$ is larger than $\eta = 10$. In Fig. 4.1 one can see that the breathers do not basically move. Moreover, we observe spontaneous birth and death of breathers as in a standard stationary process. This

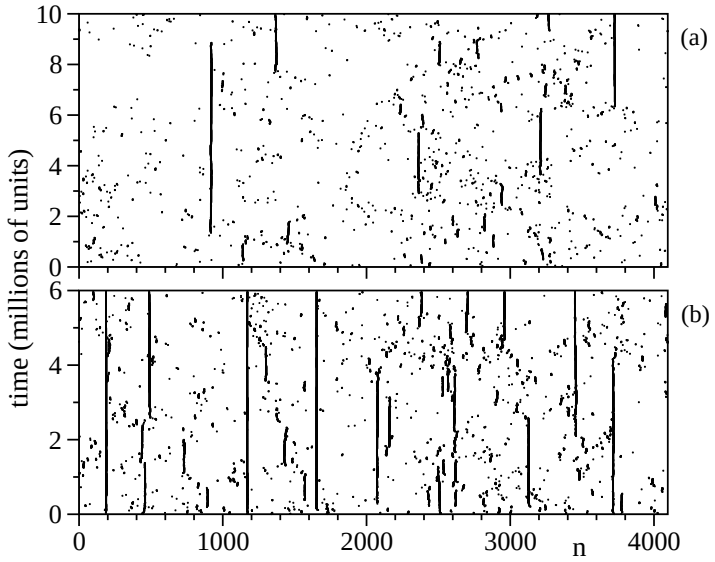

Figure 4.1: Evolution of the local amplitudes in an NT state for $a = 1$ and $h = 2.4$ [panel (a)]; $h = 2.8$ [panel (b)]. Dots correspond to lattice sites n where $a_n > 10$.

is due to the presence of a finite interaction (hopping) energy: the background can store excess energy in the phase differences of neighbouring sites and this implies that breathers can spontaneously nucleate. In order to better investigate the convergence properties of the dynamics, we have built four different sets of ICs, all with the same energy density and number of particle density, but substantially different macroscopic structures (see the caption of Fig. 4.2). First we have monitored the evolution of the density of breathers ρ (identified by setting $\eta = 10$). The average results for $N = 4096$

are plotted in Fig. 4.2a. After a quite long transient of order 10^6, the density appears to converge towards a common finite value, i.e. towards a multi-breather stationary state. Moreover, the dotted line corresponding to a simulation with $N = 2048$ indicates that the asymptotic value of ρ is independent of the system size (and approximately equal to one breather per thousand sites).

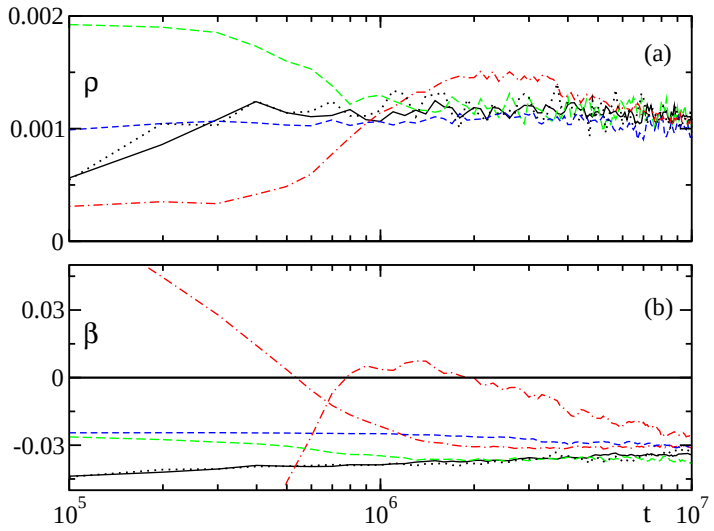

Figure 4.2: Evolution for $a = 1$, $h = 2.4$ of (a) the breather density ρ and (b) the inverse temperature $\beta = 1/T$ starting from different ICs for a chain with $N = 4096$: solid, long–dashed and dashed lines refer to a suitable homogeneous background plus 0, 4 (amplitude 20) and 8 (amplitude 16) breathers, respectively, while the dot-dashed curves refer to half a chain empty. Dotted lines refer to homogeneous ICs and $N = 2048$. Both ρ and β are averaged over a moving window of 10^5 time units. Notice that in panel (b) the two dot–dashed lines correspond to spatial averages in the initially empty and filled sectors of the chain. All data sets have been also averaged over a dozen different realizations of each IC.

We have also monitored the temperature. As we have discussed in Section 2.2, in this model the standard kinetic definition does not apply since the Hamiltonian is not decomposable into kinetic and potential energy. Nevertheless, one can use the microcanonical definition, $T^{-1} = \partial\mathcal{S}/\partial H$, where $\mathcal{S}$ is the thermodynamic entropy and the partial derivative must be computed taking into account the existence of two conserved quantities. This task requires long and careful calculations and gives rise to the nonlocal observable, Θ, already introduced in Section 2.2.2, Eq. (2.4). We have preliminarily verified that such definition works for positive temperatures when applied to the full chain and to short sub chains. This test can be made by comparing the temperature measured in the system with the one *imposed* by an external reservoir (see e.g. Fig. 3.2 for a comparison with the temperature imposed by a Langevin heat bath). Once clarified that Θ provides a correct measure of the DNLS temperature T, we turned our attention to the microcanonical dynamics of the system in the region of

negative temperatures. The results in R_n are plotted in Fig. 4.2b, where one can see that $\beta \equiv 1/T$ converges to a common value for all of the four different classes of ICs (either from above or from below), with negligible finite-size effects (once again the dotted curve refers to a chain of half length, $N = 2048$). Altogether, one can conclude that on the time scales that are numerically accessible (of order 10^7), the dynamics of the DNLS model converges towards a multi-breather state, characterized by a finite density of breathers and a well-defined negative temperature.

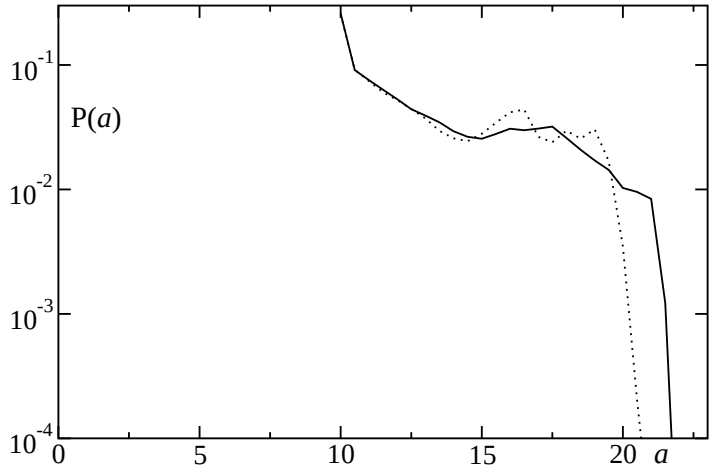

Figure 4.3: Amplitude distribution after a transient of $5 \cdot 10^6$ time units. Data are not collected below the threshold $\eta = 10$. Solid and dotted lines refer to homogeneous ICs in chains with $N = 4096$ and $N = 2048$ respectively . All data sets have been also averaged over a dozen different realizations of each IC.

In practice, the breathers are prevented from becoming "too large". In Fig. 4.3, one can indeed see that the quasi-stationary distribution of breather amplitudes is effectively localized below $a = 22$ and, more importantly, the distribution is basically independent of the system size. This means that there is a dynamical process which "screens" the high amplitude region. One can argue that this dynamical effect is due to the low efficiency of the energy–transfer among breathers interacting through the background, a manifestation of their intrinsic dynamical stability. As a consequence, the evolution is "confined" within a region of the phase space that is characterized by a NT. We still expect a final convergence towards the equilibrium state predicted in [26, 79], but the process occurs on such long (unobservable) time scales [1] to make it unaccessible. It is nevertheless reasonable to speculate that if the IC contains one or more sufficiently-high breathers, the amount of energy that is carried by them is effectively frozen, while the remaining "excess" energy contributes to the convergence towards the quasi-stationary state. In other words, the density ρ of breathers that is generated starting from sufficiently homogeneous states (such as those used in our

[1] In [86] it was already noticed that a single breather state was evolving so slowly as to converge towards the equilibrium state over 10^{70} time units.

simulations) is the maximal density that can be attained for such parameter values. The dependence of the breather density ρ on both energy and particle density is indirectly determined by the effectiveness of the energy transfer mechanisms. One can expect that it increases with h, since the excess energy increases too (see Fig. 4.1), while the dependence on a is less clear, since it affects the interaction strength. Altogether, the scenario is reminiscent of spin-glass dynamics, although a more quantitative analysis in necessary to clarify for example possible aging phenomena.

We finally remark that on a formal ground one could turn the Hamiltonian H defined in (1.1) into $-H$. Since the sign of the hopping term is irrelevant, this amounts to changing the nonlinear interaction term from repulsive to attractive and also $T \to -T$ (see Eq. (2.4)). Accordingly, NT states of H correspond to positive temperature states of $-H$, i.e. the concept of negative temperature is dictated by the physical origin of the mathematical model [2]. However, what makes the issue nontrivial in the DNLS context is that the ground state of $-H$ is, in the thermodynamic limit, a sort of black hole with infinite negative energy. No matter what kind of convention one uses for the sign of H, our simulations show that, in spite of the presence of "black holes" in the phase space, the dynamics relaxes to a metastable state characterized by a finite density of breathers and peculiar thermodynamic properties.

4.3 Generation of NT states

The analysis of the previous section has clearly shown the relaxation of the DNLS dynamics to a NT state following from a set of generic ICs selected in the negative temperature region. More generally, NT states can be attained by suitably evolving homogeneous (i.e. positive temperature) states. Two particularly simple mechanisms here discussed are: (i) a free expansion within a larger lattice; (ii) a localized boundary dissipation with removal of mass (and energy) acting at the extrema of the chain [78].

The free-expansion mechanism is summarized by the dot-dashed lines in Fig. 4.2. In this case, half of the chain has been prepared in a homogeneous thermalized state in $\mathrm{R_p}$, while the other half is initially empty. The values of h and a on the overall chain are chosen in $\mathrm{R_n}$. By averaging over a dozen initial conditions, we observe that the inverse temperature β converges to a common negative value in both halves of the chain, while the average breather density ρ relaxes to the same value ($\mathcal{O}(10^{-3})$) originated from different classes of initial conditions in $\mathrm{R_n}$. In either BEC in optical lattices, or arrays of optical waveguides, this procedure amounts to preparing a standard equilibrium state at $T > 0$ and leaving it to spread in sufficiently larger lattice structures. This method is much simpler than the experimental schemes described in [109], although relatively large system sizes (e.g., $N \sim \mathcal{O}(10^3)$ for the parameter values in Fig. 4.2a) might be necessary to observe the spontaneous formation of breathers.

An alternative procedure for observing NT states starting from an IC at positive

[2] Recent experiments with NT Bose-Einstein condensates in optical lattices are based on this idea [113].

temperature is to use losses at the ends of the lattice [78, 14]. Average trajectories resulting from the presence of a boundary dissipation in chains of different, but limited, sizes is shown in Fig. 4.4. The smoothness of these lines indicates that this process is quite regular and effective. This notwithstanding, we have observed that fluctuations may drive some of the trajectories to an empty state, although this event becomes more and more rare for increasing values of the chain size and the initial energy density. In an experimental setup the feasibility of such a mechanism depends mainly on the possibility of controlling the dissipation procedure.

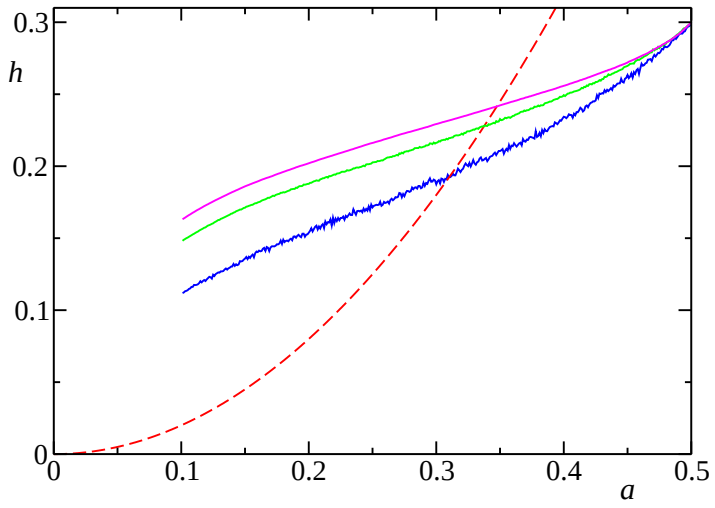

Figure 4.4: (Color online) Average trajectories (over an ensemble of 500 realizations) in the phase diagram (a, h) in the presence of boundary dissipation for different chain sizes: $N = 400, 200$ and 100 from top to bottom. The dashed line corresponds to $T = \infty$.

After reaching the region R_n in the phase diagram (a, h) we have turned the localized dissipations off and proceeded to measure the microcanonical temperature. For the three simulations reported in Fig. 4.4 for $N = 400, 200$ and 100, we have measured temperatures of $-3.4\ 10^{-2}$, $-2.2\ 10^{-2}$ and $-9.9\ 10^{-2}$, respectively. This demonstrates that the long-lived NT states described here can be experimentally accessible in set-ups containing a relatively small number of lattice sites. Although the expression of the microcanonic temperature is complicated (see Eq. (2.4)), NT can be measured once the amplitudes and phases of the lattice BEC [114, 115] or of the waveguide array have been recovered.

When considering relatively small numbers of lattice sites, the absolute value of the final temperature depends on the size of the sample. This is demonstrated, for example, by the fact that in Fig. 4.4 the final temperature for the simulations with $N = 400$ is more negative than that with $N = 200$, while one would have expected the opposite when considering the final values of the energy densities. Although finite size effects lead to larger fluctuations in the evaluation of the absolute value of the final temperature, the important message here is that the negative character of T should be

measurable at the end of out-of-equilibrium processes performed on lattices of relatively small size, thus paving the way for the observation of NT states experimentally.

As a final remark, we observe that much attention has been devoted in the literature to the study of the formation of an intrinsically localized state (ILS) both theoretically [46] and experimentally [43, 116]. The ILS is obtained from an initial Gaussian wave-packet that typically evolves to a single breather state, by releasing part of the initial energy to the lattice in the form of a radiation-like background [14]. In the light of our results, this scenario can be viewed as a first preliminary evidence of the existence of the region at negative temperature, R_n, in the thermodynamic diagram of Fig. 1.5. As a matter of fact, one can observe the formation of an ILS only if the initial Gaussian wave-packet is in R_n. If the initial wave-packet starts in R_p, relaxation to a positive-temperature state is observed. The ILS is a close approximation of the equilibrium state in R_n predicted by Rumpf [80], i.e. a background at infinite temperature supporting the excess energy into a single breather. In this respect, the measurement of the phase distribution in the background is a promising tool to infer the temperature in experimental setups: it will useful to explore to what extent the idea can be turned into a quantitative protocol.

4.4 Discussion

Extremely long-lived states at negative temperature corresponding to a quasi-stationary density of breathers have been identified in the numerical simulations of the DNLS equation. The asymptotic convergence to the single-breather equilibrium state occurs on quite long (and practically unattainable) time scales. The reason why breathers play an important role in the attainment of NT states is the existence of a second conservation law which favours energy concentration, while limiting its global entropic cost. We do not expect similar scenarios to occur in lattices where breathers appear in models with a single conservation law (see e.g. [117]). It might, nevertheless, be instructive to investigate the local temperature dynamics in the vicinity of the breathers, even in such cases.

From a theoretical point of view, we envisage a quantitative theory that relates the slow time scales to the breather amplitudes, their stationary density and the system size so as to establish possible connections with, e.g., aging phenomena. This is, however, a pretty ambitious program. In fact, it is very hard to invoke analytical arguments capable of describing accurately this kind of slow relaxation phenomenon. A possible strategy for shedding some light on this issue is to reduce progressively the complexity of the problem by studying simple toy models that display the essential phenomenology. In this respect, in the following chapter we will gain further insights in the nature of the NT quasi-stationary states by studying a simplified stochastic DNLS model that produces a sub-diffusive dynamics of the breather amplitudes.

The results reported in this chapter also indicate the possibility of observing NT states experimentally, in BEC and optical waveguides, as a result of quasi-stationary

states yielding peculiar nonequilibrium thermodynamic properties. We have suggested two possible scenarios where quasi-stationary NT states can be realized: free expansion of a positive temperature state in a larger lattice and the utilization of boundary dissipations. Initial Gaussian wave-packets leading to single breather ILS may also be used for the realization of maximum entropy states although the measurement of the phase distribution is required in order to establish the infinite temperature nature of the background.

As a final remark, it would be worth clarifying to what extent the scenario described here survives when passing to continuous models, although computationally heavy simulations are required before drawing reliable conclusions. Finally, let us note, *en passant*, that a richer scenario would presumably arise in higher-dimensional setups, due to the existence of a finite activation energy thresholds for the discrete breathers (see the recent review [118]).

The results reported in this chapter have been published in Ref. [119].

Chapter 5

Coarsening and localization in a simplified DNLS model

5.1 Introduction

The DNLS model (1.2) is known to be characterized by a so-called negative temperature region, where localized solutions (discrete breathers) spontaneously arise and survive for long times (see Sections 1.3 and 1.4). On the basis of entropic arguments (Section 4.1) the system is expected to converge towards a state characterized by a single breather sitting on a homogeneous background at infinite temperature. Nevertheless, the numerical study reported in Chapter 4 has challenged such a conclusion, since the process turns out to be both extremely slow and accompanied by the continuous birth and death of breathers.

A clarification of the asymptotic regime in the original DNLS model is a rather ambitious task, because of both its nonlinear character and the weak coupling between breathers and background. In order to overcome such difficulties, in this chapter we introduce a purely stochastic Microcanonical Monte Carlo (MMC) model with the goal of exploring the role of entropy contributions not only in the identification of the asymptotic state, but also for the characterization of the convergence process. Analogously to the DNLS equation, the MMC model is characterized by two conservation laws (energy and norm) and by a local evolution rule. More precisely, such constraints are representative of the original DNLS dynamics in the high-norm density limit, where the interaction energy between neighbouring sites is negligible. Furthermore, we show that the MMC dynamics is characterized by a coarsening process during which the localized solutions progressively disappear, while their typical height increases. Although the purely stochastic character of the MMC model is rather distant from the genuine deterministic DNLS dynamics, its study can help to clarify the kind of constraints that are expected to emerge during the convergence to the asymptotic state.

Coarsening is a fairly common feature of out-of-equilibrium systems, either relaxing towards equilibrium [120] or kept well far from equilibrium [121]. It corresponds to a growth of the typical length scale λ of the system, which usually increases with a

power law, $\lambda(t) \approx t^{\gamma}$, which defines the coarsening exponent γ. According to the value of γ, different universality classes can be defined, which depend, first of all, on conservation laws. Two exponents, $\gamma = 1/2$ and $\gamma = 1/3$, are specially widespread. They correspond to diffusive processes with ($\gamma = 1/3$) and without ($\gamma = 1/2$) the conservation of the order parameter. The simplest models displaying such coarsening behaviour are the so-called models A and B of dynamics [122], which represent, for example, the relaxation to equilibrium of a deeply quenched Ising model, when the magnetization is not conserved (model A) or is conserved (model B) by dynamics. The latter case, because of the equivalence between Ising and lattice gas model, makes the exponent $\gamma = 1/3$ of special relevance for condensation processes and for large classes of nonequilibrium statistical mechanics models [123].

The MMC model is still too complicated to be able to predict the universality class it belongs to. In fact, it is not even possible to anticipate its qualitative dynamics: the fact it produces coarsening is not trivial at all. Once noticed that simulations do show coarsening, it is natural to expect an exponent γ strictly smaller than $1/2$, because conservation laws always slow down coarsening. In fact, we will find $\gamma = 1/3$, a very common value for systems where the order parameter is conserved. However, our model has two conserved quantities and cannot be mapped to any known model. Therefore, this is not a standard result. Rather, it highlights certain properties which might be common to more complicated systems.

The chapter is organized as follows. In Section 5.2, we introduce the model and show some general properties of its evolution, when the initial condition is chosen within the negative temperature region. In Section 5.3 we illustrate the coarsening process for generic initial conditions, with particular reference to the scaling behavior of the number of surviving breathers. The following two sections are devoted to a discussion of two regimes: the fast relaxation which drives the background towards an infinite-temperature state (Section 5.4), the slow relaxation that is responsible for the coarsening process (Section 5.5). Such studies help to identify the reason for the increasing slowness of the coarsening, that is then better clarified in Section 5.6, thanks to an analogy with a suitable exclusion process. By combining the various elements, a justification for the exponent $\gamma = 1/3$ is given. Finally, in Section 5.7, we summarize the main results and mention the still open problems.

5.2 The model

In this section we define the stochastic DNLS model and discuss some general properties of its dynamical behavior.

The purpose of the stochastic model is to single out the role of entropic constraints in the convergence towards the equilibrium state of the full DNLS equation. A particularly simple regime in which this task can be fruitfully accomplished is identified in the large energy- and particle-densities limit. In this parameter region, in fact, the contribution of the hopping term to the Hamiltonian (1.1) is negligible and the local phases of the

variables z_n do not play any role. As a consequence, the system is characterized only by the local particle numbers $a_n = |z_n|^2$. With this idea in mind, we introduce our simplified model by defining a set of positive amplitudes a_n a regular lattice of length N, where periodic boundary conditions are assumed. Two quantities are conserved during the evolution, namely the total mass

$$A = \sum_{n=1}^{N} a_n, \tag{5.1}$$

and the total energy

$$H = \sum_{n=1}^{N} a_n^2; \tag{5.2}$$

which correspond to norm and energy in the DNLS equation in the large norm-density limit (cf. Eqs. (1.1) and (1.5)). Despite its simplicity, the model keeps all the essential features of the original problem. In particular it is possible to prove that, within the negative temperature region, the equilibrium state is still characterized by a single breather superposed to an infinite-temperature background [80]. In the absence of an interaction energy, we have investigated the convergence to the equilibrium state by introducing a MMC method with a local stochastic rule that allows us to move on the hyper-surface characterized by a fixed energy and particle number. In this way, the evolution mimics the deterministic microcanonical dynamics and identifies the role of entropic forces.

The MMC dynamics is defined as follows. Given a generic configuration at time t, a triplet $(n-1, n, n+1)$ of consecutive sites is randomly selected and updated so as to ensure that the mass and energy are locally (and thereby globally) conserved,

$$a_{n-1}(t+1) + a_n(t+1) + a_{n+1}(t+1) = a_{n-1}(t) + a_n(t) + a_{n+1}(t) \tag{5.3a}$$

$$a_{n-1}^2(t+1) + a_n^2(t+1) + a_{n+1}^2(t+1) = a_{n-1}^2(t) + a_n^2(t) + a_{n+1}^2(t). \tag{5.3b}$$

These two laws are basically equivalent to the conservation of momentum and energy in a chain of oscillators (once a_n is interpreted as the oscillator velocity) and one might thus expect similar diffusion phenomena. Here there is, however, an additional constraint: all a_n must be positive. Therefore, the legal configurations, that are located along the circle identified as the intersection between a plane and a sphere (the above two conditions), may be further confined to three separate arcs. This happens when the maximal amplitude $\overline{a}$ (within the triplet) is sufficiently larger than the other two amplitudes (see Fig. 5.1). If, for simplicity, $\underline{a}$ is the (equal) amplitude of the two other sites, it is easy to check that a "three-arcs" solution appears when $\overline{a} > 4\underline{a}$.

Whenever this is the case, the definition of the model is completed by specifying that we restrict the choice to the same arc of the initial condition. This choice is motivated by the will to reproduce as closely as possible the original DNLS dynamics. In fact, the most important instances of three-arcs solutions are "breathers", i.e. isolated sites

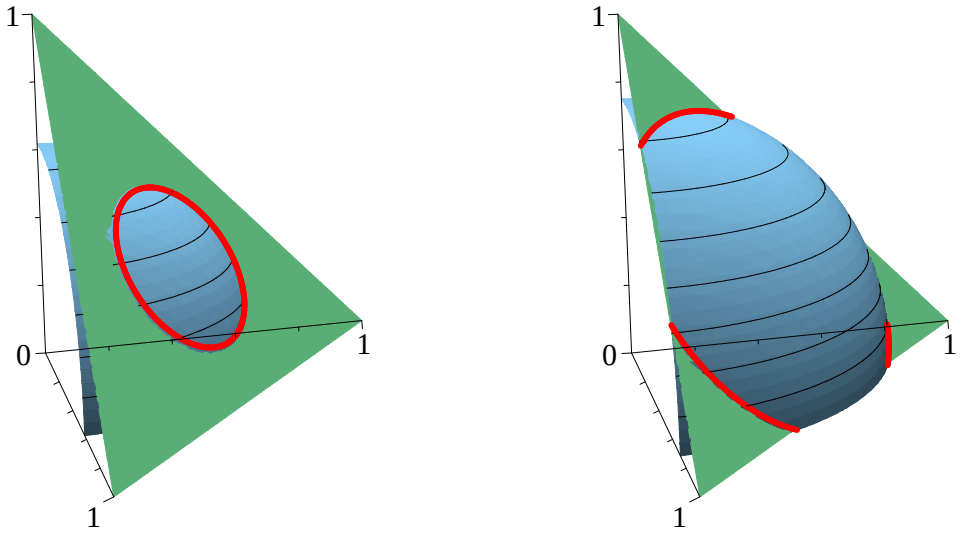

Figure 5.1: Accessible MMC states (red thick line) as intersection between the plane $a_{n-1} + a_n + a_{n+1} = 1$ and a sphere with square radius 0.4 (left panel) and 0.58 (right panel).

with an anomalously large amplitude. Such breathers, once generated, do not appear to diffuse in the DNLS model: this property is ensured in the MMC setup by forbidding the change of arc, which would correspond to a shift of one or even two sites of the breather itself.[1]

In order to identify the breathers, it is necessary to introduce an absolute threshold η to distinguish them from the background. Depending whether $a_n > \eta$ ($a_n < \eta$) a site is classified as a breather (background) and its amplitude denoted with b_n (g_n). A typical example of the MMC evolution is shown in Fig. 5.2 (see the next section for a more accurate discussion, where we show also that the threshold value η is irrelevant in so far as it is large enough).

Let us now introduce the average and the variance of the two phases as,

$$\begin{aligned} b &= \langle b_n \rangle \qquad & \sigma_b^2 &= \langle (b_n - b)^2 \rangle \\ g &= \langle g_n \rangle \qquad & \sigma_g^2 &= \langle (g_n - g)^2 \rangle \end{aligned} \tag{5.4}$$

where $\langle \dots \rangle$ is the spatial average, taken over all sites of the same family.

Imposing the conservation of A and H, we obtain the *exact* relations,

$$A = (N - L)g + Lb \tag{5.5}$$

$$H = (N - L)(g^2 + \sigma_g^2) + L(b^2 + \sigma_b^2) \tag{5.6}$$

where L denotes the number of breathers. By defining the average amplitude and

[1] We have implemented two additional rules which allow for breather diffusion, but the coarsening exponent does not change (see later Fig. 5.4).

energy per site,

$$a = \frac{A}{N}, \qquad h = \frac{H}{N}, \tag{5.7}$$

we obtain

$$a = (1-\rho)\, g + b\rho \tag{5.8}$$
$$h = (1-\rho)\,(g^2+\sigma_g^2) + \rho(b^2+\sigma_b^2) \tag{5.9}$$

where $\rho = L/N$ is the breather density (in the following, the average distance $\lambda = \rho^{-1}$ will also be used). In the limit $\rho \ll 1$,

$$g = a - b\rho \tag{5.10}$$
$$h = a^2 - 2ab\rho + b^2\rho + \sigma_g^2 + \sigma_b^2\rho \tag{5.11}$$

where we have also used the information (obtained from numerics, see next section) that $b \gg g$, because b increases in time while g saturates.

Since the entire dynamics is invariant under a change of a scale, it is convenient to rescale the amplitude to its average value a. This is perfectly equivalent to assuming that $a = 1$ (as we do from now on). As a result,

$$\rho = \frac{h - 1 - \sigma_g^2}{-2b + b^2 + \sigma_b^2}\,. \tag{5.12}$$

In Ref. [80], on the basis of purely entropic arguments, it has been found that for $h < 2$ all breathers eventually disappear, otherwise one survives (for $h > 2$), accompanied by an infinite-temperature background, characterized by a Poissonian distribution of the amplitudes. Let us see, how such predictions manifest themselves in the current setup.

From Eq. (5.10), for small densities, $g = 1$ and $b \simeq (h - 1 - \sigma_g^2)\sqrt{\lambda}$ (recall that now $a = 1$). Therefore, the background has a finite amplitude, while the breather amplitude scales as the square root of breather average distance. It is worth noting that $g \leq 1$ and asymptotically $g \to 1$. Therefore, for $\rho \ll 1$, since an infinite-temperature background corresponds to $\sigma_g^2 = g^2$, the request of a positive ρ in Eq. (5.12) corresponds to $h > 2$, the condition already derived in [80].

5.3 Phenomenology

In this section we illustrate the evolution, showing that it corresponds to a coarsening process. We have worked with two classes of initial conditions: (i) a fraction f of equal-height breathers sitting on a homogeneous background characterized by a uniform amplitude distribution within an interval of width δa (ICa); (ii) a homogeneous distribution of amplitudes characterized by the superposition of two exponential functions (ICb). We have verified that they give equivalent results, for the same value of h (that is systematically chosen to be larger than the critical value 2).

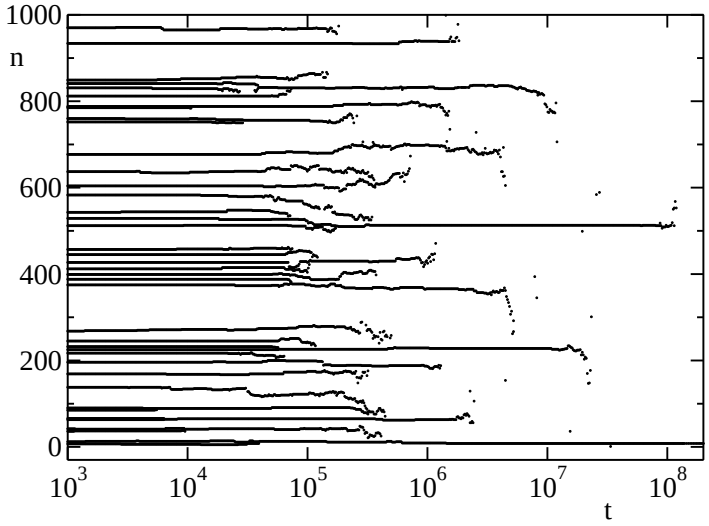

Figure 5.2: Evolution of the local amplitude in a chain with $N = 1000$ and $h = 7.45$. Breathers are identified by dots and correspond to the sites n where $a_n > \eta$, with $\eta = 12.5$. The initial condition is of type ICa with parameters $f = 0.05$ and $\delta a = 0.95$.

In Fig. 5.2 we plot breathers positions as a function of time t, where the time is measured in numbers of Monte Carlo moves divided by the system size (N). The figure clearly shows the basic, qualitative features of dynamics: (i) breathers do not typically move, but may diffuse just before disappearing under the threshold η (i.e. when their amplitude becomes sufficiently small); (ii) since the distinction breathers/background creates an artificial discontinuity, a breather may disappear and then reappear for a short time; (iii) the density of breathers decreases in time (coarsening process), because breathers gradually disappear. This process occurs when a breather goes below the threshold η.

The first quantitative analysis of the coarsening process is done by comparing direct simulations with Eqs. (5.10) and (5.12), see Fig. 5.3. The constraints derived from the conservation of total energy and amplitude are found to be in good agreement with numerics even in the region of small λ. Fig. 5.3 clearly shows that the coarsening process (i.e. the growth of λ) is directly related to an increase of the average amplitude of the breathers, while the amplitude of the background remains finite. The same behavior occurs also for the variances σ_b^2 and σ_g^2.

The next important quantitative aspect of dynamics concerns the coarsening law, i.e. the time dependence of the distance between breathers, $\lambda(t)$, see Fig. 5.4. After an initial transient, λ is found to grow in time as $\lambda(t) \sim t^n$ with a coarsening exponent $\gamma = 1/3$ that is independent of the system size (in fact the whole curve is independent of N, if N is large). Moreover, such asymptotic behavior is largely independent of the details adopted to select a point in the available phase space. We have indeed considered two variations of the standard MMC algorithm (S). The first variant (C1) consists in selecting randomly a point either on the full circle or in the *union* of the three

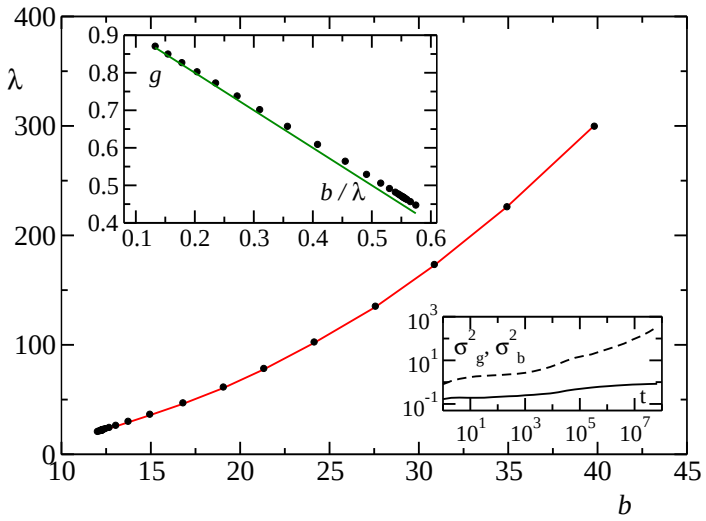

Figure 5.3: Kinematics of the simplified DNLS model. Black dots refer to direct simulations of a chain of $N = 6400$ lattice sites, $h = 7.23$ and $\eta = 8.45$ (initial condition of type ICa with parameters $f = 0.05$ and $\delta a = 0.86$). The solid red line is obtained according to Eq. (5.12). *Upper inset:* comparison of Eq. (5.10) (solid green line) with simulations (black dots). Bottom-right points deviate from the expected trend as a consequence of a contribution of terms $\mathcal{O}(\lambda^{-1})$ in the early stages of coarsening. *Lower inset:* temporal evolution of the variances σ_g^2, σ_b^2. Asymptotically σ_g^2 (black solid line) converges to a finite value corresponding to the condition of infinite temperature background, while σ_b^2 (black dashed line) increases as a consequence of the coarsening process.

disconnected arcs. The second variant (C2) consists in partitioning the circle solutions in three symmetric arcs and selecting a point of the same arc as the initial configuration (also when the full circle would be available). Altogether, the three algorithms (S, C1, C2) can be classified according to their symmetry with respect to cyclic permutations of the triplet (partial, full, absent, respectively). It is quite remarkable to notice that the scaling behavior remains unchanged even when the breathers are allowed to diffuse in real space (setup C1). This is because the coarsening does *not* proceed via coalescence (or annihilation) of the breathers: such a process is inconsistent with the simultaneous conservation of energy and mass.

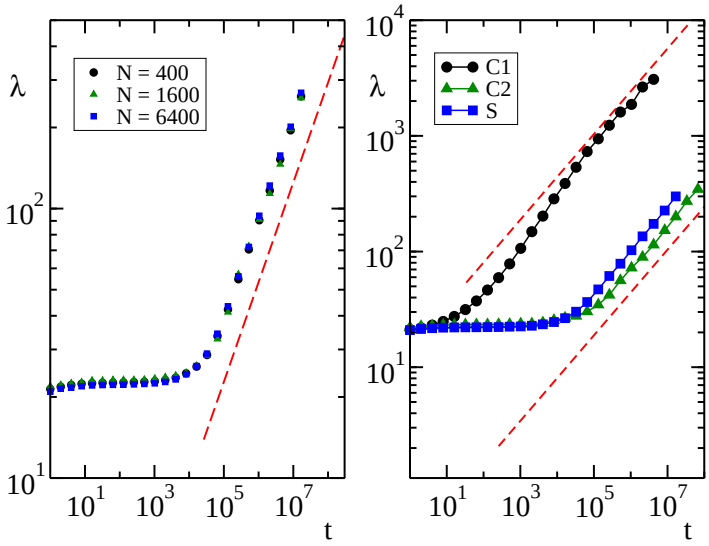

Figure 5.4: *Left panel:* Average distance λ versus time t for three different system sizes $N = 400, 1600, 6400$. *Right panel:* Comparison of three different microscopic dynamics for a chain of $N = 6400$ lattice sites. Simulation parameters are the same of Fig. 5.3.

Dynamics, however, allows the exchange of matter between neighboring (and next neighboring) sites. In particular, breathers exchange matter with the underlying "sea", which acts as a mediator, so that breathers can effectively transfer matter between them. As a consequence of that, the breather amplitude fluctuates in time and it may go below threshold, and eventually be absorbed by the background. The key point of this evolution is the presence of a fast convergence towards local equilibrium, where the background temperature becomes infinite as shown in the next section. If two or more breathers are present, they interact via the background (Section 5.5) which allows them to exchange matter and acquire a finite life time which is the ultimate reason for the coarsening process, that will be studied in detail in Section 5.6.

Now let us analyze more precisely the exchange of matter between a (large) breather and the surrounding background. This study will allow to understand that the "quantum" of transferred matter decreases with increasing breather amplitude. In order to understand the dynamics in the presence of a large breather, let us consider a

triplet of consecutive sites and denote with a, ya and za, the corresponding amplitudes in decreasing order from the largest to the smallest one, so that $1 > y > z$. If[2] $1 + y^2 + z^2 > 2(y + z + yz)$ the possible solution belongs to 3 distinct arcs. This is indeed the case when a breather is contained in the triplet since ya and za are both much smaller than a, i.e. $y, z \ll 1$. Under this assumption ($y, z \ll 1$), it can be easily shown that the rotation angle θ belongs to the interval $[-\sqrt{3}y, +\sqrt{3}z]$ and the new amplitude values are

$$\begin{aligned} a' &= \left[1 + \frac{\theta}{\sqrt{3}}(z - y) - \frac{\theta^2}{3}\right] a \\ y' &= y + \frac{\theta}{\sqrt{3}}(1 - z) + \frac{\theta^2}{6} \\ z' &= z - \frac{\theta}{\sqrt{3}}(1 - y) + \frac{\theta^2}{6} \end{aligned} \tag{5.13}$$

The largest variations are the opposite contributions $\pm\theta/\sqrt{3}$ which affect y and z, respectively. As a result, the process corresponds, to leading order, to a transfer of matter between two low-amplitude sites. This means that the breather is, in a first approximation, transparent to a propagation of matter. In order to quantify the interaction of the breather with the background, we have to consider the second order terms. Although the mass exchange is negligible (of order $1/a$), the energy exchange is finite, no matter how big is a.

Therefore, we can conclude that it is neither the position nor the mass of the breather which performs a random motion, but rather its energy. This is preliminarily confirmed by introducing a representation where the total energy H_n from site 1 to site n,

$$H_n = \sum_{j=1}^{n} a_j^2 \quad , \tag{5.14}$$

is plotted for all $n \leq N$ versus time. The wide white regions visible in Fig. 5.5 record the presence of breathers, while the dark areas correspond to sequences of background sites. The dark areas coalesce, until the entire "space" is split into a single black region (the homogeneous background) and a single white region (one breather). The random fluctuations of the white areas signal the exchange of energy between neighboring breathers.

5.4 Fast relaxation

In this section we discuss the relaxation to equilibrium of a single breather sitting on top of a generic background. We analyze the process starting from an initial condition that is as far as possible from the asymptotic state, i.e. from the highest possible breather

[2]This expression generalizes the condition $y, z < \frac{1}{4}$ for $y = z$, mentioned below Eqs. (5.3).

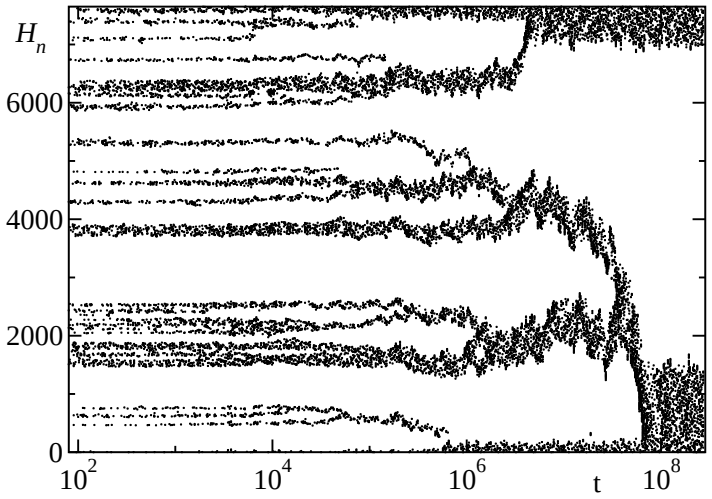

Figure 5.5: Energy diffusion for a chain of 1000 sites and $h = 6.75$. The initial condition is of type ICb with exponential rates 1.725 and 0.138. Black dots represent the values of H_n (defined in Eq. (5.14)) for all n from 1 to $N = 1000$.

amplitude b, compatible with the given energy and mass densities. This condition (IC1 for later reference) is achieved by selecting a constant background (i.e. zero-temperature) with amplitude g such that $b^2+(N-1)g^2 = hN$ and with $(N-1)g+b = N$. In the large N limit, $g = 1$ and $b = \sqrt{(h-1)N}$.

As soon as the system is let free to evolve, an energy-transfer $\Delta H(t) = \langle b^2(0)-b^2(t)\rangle$ and a mass-transfer $\Delta A(t) = \langle b(0) - b(t)\rangle$ set in, which contribute to decrease the breather amplitude. Since b is and remains on the order of $\sqrt{N}$, the energy $\Delta H(t)$ is an extensive quantity (and one should more properly look at the intensive observable $\Delta h(t) = \Delta H(t)/N$), while $\Delta A(t)$ is subextensive, so that the density of mass in the background is substantially unchanged. In practice, the transferred energy contributes to increase background fluctuations. Accordingly, one can equivalently monitor either $\Delta h(t)$ or the fluctuations σ_g^2. In Fig. 5.6 we plot the evolution of $\Delta h(t)$ for various system sizes and fixed h. A nice data collapse is observed after introducing the scaling function

$$\Delta H = NG(t/N^2), \tag{5.15}$$

where $G(x) \approx \sqrt{x}$ for $x \ll 1$ and $G(x) \approx 1$ for $x \gg 1$. In practice, up until times on the order of N^2, the energy transfer follows a diffusive law $\Delta H = \sqrt{t}$ with a diffusion coefficient that is independent of N. It is reasonable to conjecture that the energy absorption by the background is limited by the diffusion over the background itself (this question will be discussed again in a later section to justify the overall scaling behavior of the coarsening process). The diffusion stops when the background reaches the maximally entropic state, i.e. infinite temperature.

It is convenient to approach the problem also in a different way by determining the first passage times for the rescaled breather energy $\varepsilon = b^2/N$. In practice, we fix a series of equispaced thresholds ε_j ($\delta\varepsilon = \varepsilon_{j+1} - \varepsilon_j$) and determine the first time

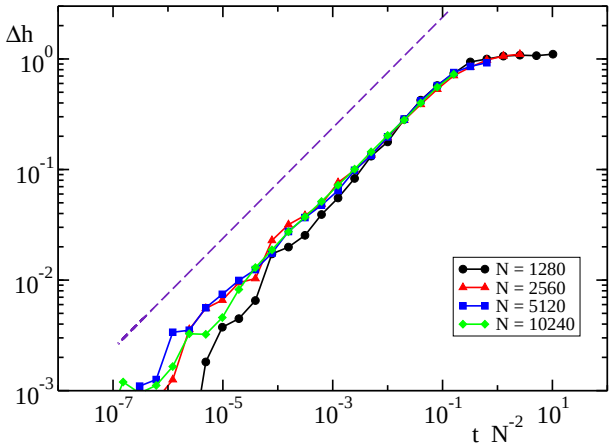

Figure 5.6: Scaling properties of the energy loss $\Delta h(t)$ of a single breather relaxing on initially flat background for different system sizes N. The purple dashed line indicates a slope 1/2. Simulations are performed selecting initial conditions of type IC1 with $b = 2\sqrt{N}$ (that corresponds to a total energy density $h = 5$).

t_j the energy crosses the jth threshold. Such times are then averaged over different realizations (see the angular brackets) to determine the effective force that drives the energy transfer process,

$$F_j = \frac{\delta\varepsilon}{\langle t_{j+1} - t_j \rangle} \quad . \tag{5.16}$$

The results are plotted in Fig. 5.7 (upper panel), where the origin of the x axis is now chosen at the equilibrium value and the force is scaled by a factor N^2, consistently with Eq. (5.15). As a further check of consistency with the previous observation, notice that the force field behaves, for ε approaching the state of maximal energy ε_0 (equal to 1 for the simulations reported in Figs. 5.7), as

$$F(\varepsilon)N^2 \approx \frac{1}{\varepsilon_0 - \varepsilon} \tag{5.17}$$

which both tells us that in ε_0 there exists a barrier that cannot be overcome, and is consistent with the evolution of the breather energy. In fact, in the continuum limit a solution of the deterministic dynamical equation $\dot{\varepsilon} = F(\varepsilon)$ is

$$(\varepsilon_0 - \varepsilon) \approx \frac{\sqrt{t}}{N} \tag{5.18}$$

(see the dashed line in Fig. 5.6). Therefore, we see that the pseudo-diffusive law can be interpreted as the result of a divergence of the effective force.

We conclude this analysis by commenting about the amplitude of the stochastic fluctuations that are plotted in the lower panel of Fig. 5.7. The diffusive force σ is measured as the standard deviation of the first passage times. We see that σ vanishes for $\varepsilon = \varepsilon_0$ where fluctuations can, indeed, only decrease the breather amplitude and

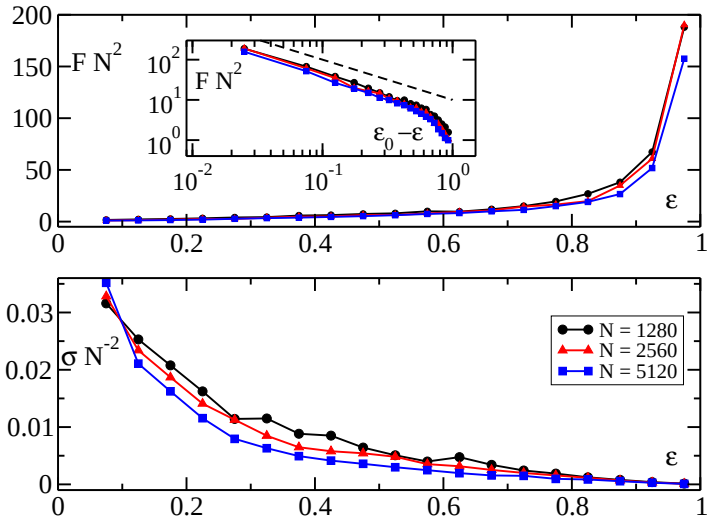

Figure 5.7: *Upper panel:* Effective force $F(\varepsilon)$ calculated via first passage times for three different sizes N. The zero of the horizontal axis corresponds to the equilibrium energy. The same quantity $F(\varepsilon)$ is shown in the inset in terms of $(\varepsilon_0 - \varepsilon)$, where $\varepsilon_0 = 1$ is the initial energy. The dashed line refers to a power law $1/(\varepsilon - \varepsilon_0)$. *Lower panel:* Standard deviation of the first passage times σ. F and σ have been calculated on a sample of 100 independent initial conditions with the same parameters of Fig. 5.6 and $\delta\varepsilon = 0.05$.

progressively increases until the fixed point is reached and we also see that their amplitude scales as N^2. Altogether, this "fast" relaxation process lasts a time of order N^2.

Notice that one could have equivalently described the scenario by monitoring the average fluctuations σ_g^2 of the background. In such a case, we would have observed that the variance of the background amplitude increases as in a diffusion process, converging to a final state in which the interface is made of random and independent heights.

5.5 Slow relaxation and coarsening

In the previous section we have studied how a single breather relaxes towards the equilibrium state, where it has the optimal amplitude. In the presence of two (or more) breathers, the relaxation proceeds into two steps, see Fig. 5.8. First, the background converges towards the infinite-temperature state on a time scale that is analogous to that one studied in the previous section with reference to a single breather. Then, a slow random exchange of energy between the breathers starts, mediated by the background. The energy of each breather performs a random walk with the constraint that the total breather energy is approximately constant. The process proceeds until the energy of a breather becomes so low that it is adsorbed by the background, and its energy has been transferred to the other breather(s). In this section we provide a characterization

of such a slow dynamics by studying a simple setup that involves only two breathers. Finally, a straightforward generalization allows to explain the coarsening exponent $\gamma = 1/3$.

In order to cut away the transient dynamics corresponding to the relaxation of the background, the initial condition (IC2 for later reference) is now fixed by: (i) generating an infinite-temperature background, where the amplitudes a_n are i.i.d. variables, distributed according to the Poisson distribution $P(a_n) \propto \exp(-a_n/g)$ [80]; (ii) adding two equidistant breathers with amplitude $b_1, b_2 \gg g$ in a lattice of size N with periodic boundary conditions. If $N \gg 1$, the total mass is almost entirely contained in the background. Accordingly, mass conservation implies that the energy contained in the background is nearly conserved (provided that the background is at infinite temperature) and the energy contained in the two breathers conserved as well.

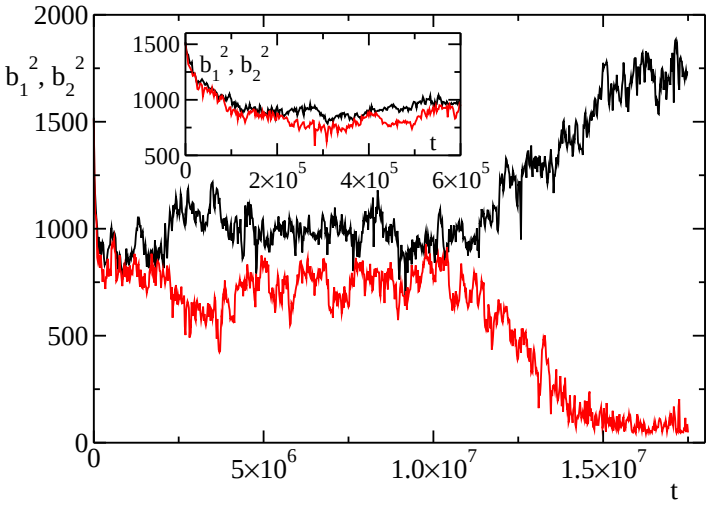

Figure 5.8: Example of two breathers (with energies $b_1^2(t)$ and $b_2^2(t)$) relaxing in a chain with $N = 1280$. The initial condition is characterized by a flat background and two equidistant breathers with amplitude $b_1(0) = b_2(0) = 40$. The first part of the evolution (see the inset) corresponds to a an energy transfer from both the breathers to the background. Once the background has reached the infinite temperature point (for $t \gtrsim 5 \times 10^5$), the breathers start to exchange energy among themselves until one of them is completely blown out.

The first important property to point out is that the process of energy exchange between the two breathers is independent of their amplitude. More precisely, in Fig. 5.9 we report the probability distribution $P_2(\Delta H)$ of the energy transfer between two breathers after a time $t = 2^{19}$, with $\Delta H = [b_1^2(0) - b_1^2(t)]$. The distribution is very well fitted by a Gaussian function with zero average and appears unaffected by the choice of the initial configuration $[b_1(0), b_2(0)]$. We can therefore conclude that such a process is determined only by the properties of the stationary background in between the two breathers. From Fig. 5.9 it is also clear that the only relevant information concerns the time evolution of the variance $\sigma_2^2(t)$ of the distribution. According to stationarity,

we can compute $\sigma_2^2(t)$ in terms of time averages, instead of averages over independent initial conditions. In formulae,

$$\sigma_2^2(t) \equiv \left\langle \left[b_1^2(0) - b_1^2(t) \right]^2 \right\rangle = \overline{\left[b_1^2(t+t_0) - b_1^2(t_0) \right]^2}\,, \tag{5.19}$$

where the overbar denotes the average over time t_0 and $\langle \cdots \rangle$ denotes average over different initial conditions. Finally notice that stationarity holds as long as both breathers are present on the chain. In the following of this section we will always explore this regime.

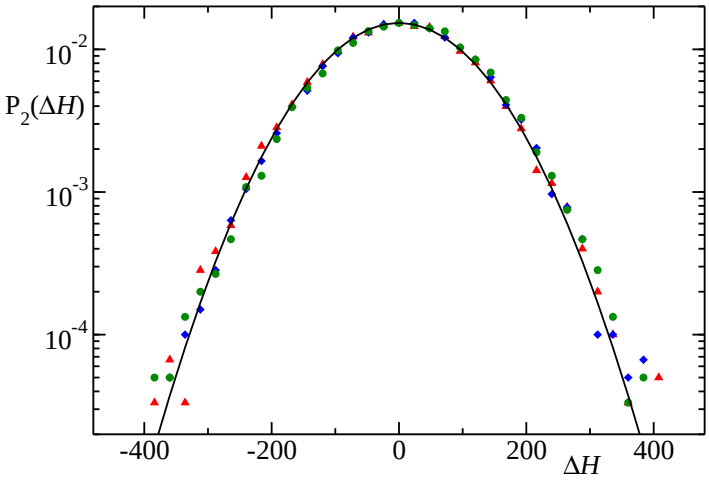

Figure 5.9: Probability distribution of the energy transfer ΔH of the first breather after a time $t = 2^{19}$ in a two-breather setup with initial conditions of type IC2. Three different configurations of initial breather amplitudes have been considered: $[b_1(0) = b_2(0) = b]$ (red triangles), $[b_1(0) = b_2(0) = b\sqrt{2}]$ (blue diamonds) and $[b_1(0) = b\sqrt{2}, b_2(0) = b]$ (green circles), with $b = 100$. The black solid line refers to a Gaussian fit. Each data set is obtained from a sample of 10000 independent realizations of the MMC dynamics on a chain with $N = 640$.

In order to perform a quantitative analysis of $\sigma_2^2(t)$, we have averaged the energy fluctuations of a sample of S independent trajectories[3] for different lattice sizes N. Upon increasing N, we keep fixed the parameters b_1, b_2 and g characterizing the initial condition IC2, so that the only change involves the distance between the two breathers.

The results reported in Fig. 5.10 show a growth in time of the energy fluctuations. In particular, for large enough times, $\sigma_2^2(t)$ has a linear profile, thus indicating the existence of a diffusive law. The associated diffusion constant is however inversely proportional to the system size N (and therefore also to the spatial separation of the breathers, equal to $N/2$). As a consequence, the larger the chain is, the slower the energy diffusion process is. A data collapse is finally obtained by rescaling energy and time respectively by N and N^2.

[3]The average over independent trajectories is a practical numeric tool for improving the statistics for large times t.

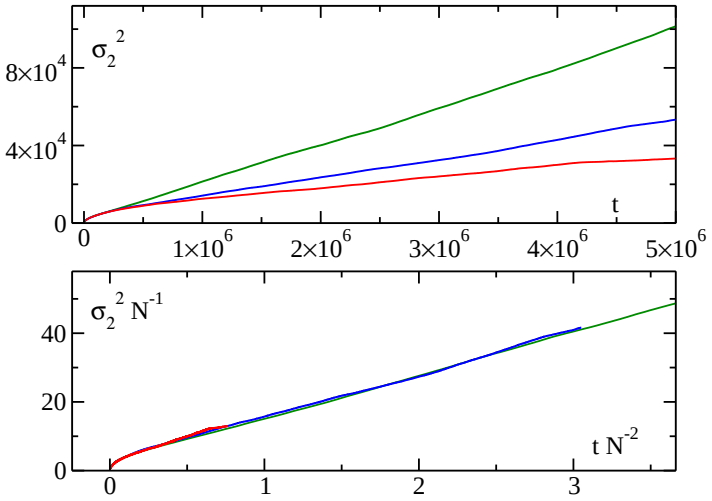

Figure 5.10: *Upper panel:* Time evolution of the energy fluctuations σ_2^2 of two breathers sitting on an infinite temperature background. Lines from top to bottom refer to lattice sizes $N = 640, 1280, 2560$, respectively. Data are obtained from a set of $S = 10$ samples evolved for 3.4×10^7 time units, starting from an initial condition of type IC2 with two breathers of amplitude $b = 100$. Running averages are performed monitoring time differences from $dt = 10^3$ to $dt = 5 \times 10^6$ time units. *Lower panel:* Data collapse on the universal function $f_2(x)$ after the rescaling $t \to t/N^2 = x$ and $\sigma_2^2 \to \sigma_2^2/N$.

A more general description of the overall scenario can be obtained by comparing the results of Fig. 5.10 with the same kind of simulations performed with only one breather in the chain, i.e. in a equilibrium regime. Energy fluctuations, denoted with $\sigma_1^2(t)$, are now expected to be *finite* for large enough times, with the characteristic scaling $\mathcal{O}(N)$ with the system size. Fig. 5.11 points out the equivalence of the dynamic behavior in presence of one *and* two breathers for small times. In this regime, in fact, a breather cannot know about the existence of some other breather in the chain and behaves as if it were at equilibrium (local equilibrium). Only after a characteristic time $t_c \sim N^2$ a "bifurcation" occurs, separating the linear growth of fluctuations in presence of two breathers from the saturation required by (global) equilibrium in presence of only one breather.

The results plotted in Fig.s 5.10 and 5.11 can be summarized by the following scaling relations for the variances σ_1^2, σ_2^2 of the energy of a single breather when the system is made up of one and two breathers, respectively:

$$\sigma_i^2 = N f_i \left(\frac{t}{N^2} \right) \tag{5.20}$$

where $f_1(x) \approx f_2(x) \approx \sqrt{x}$ for $x \ll 1$, while at large $x \gg 1$, $f_1(x) \approx 1$ and $f_2(x) \approx x$. In particular, $\sigma_2^2 \approx t/N$ at large times, which gives a first explanation of the coarsening exponent $\gamma = 1/3$. In fact, during the coarsening process the energy of the breather scales as N, where N is now the distance between breathers. Therefore, the time to

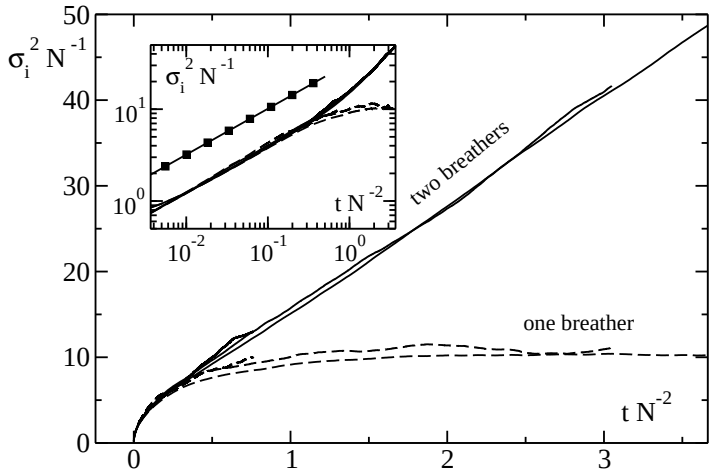

Figure 5.11: Comparison of the universal functions $f_1(x)$ and $f_2(x)$ in presence of one breather (dashed lines) and two breathers (solid lines), respectively. The functions $f_i(x)$ are extracted by means of the rescaling $t \to t/N^2 = x$ and $\sigma_i^2 \to \sigma_i^2/N$ for three different sizes $N = 640, 1280, 2560$. Simulations are performed using the same parameters specified for Fig. 5.10. The inset shows the behavior of $f_i(x)$ for small x. The square-solid line is a power law with exponent $1/2$.

allow a breather to disappear corresponds to $\sigma_2^2 \sim N^2$, i.e. $t/N \sim N^2$, and finally $N \sim t^{1/3}$.

5.6 Comparison with a Partial Exclusion Process

In the previous sections we have provided a characterization of the simplified DNLS stochastic model in the presence of localized excitations. The very existence of such localized states has been related to the simultaneous conservation of energy and mass. If, for example, we suppressed one conservation law, we would recover a standard diffusion process, always relaxing to an homogeneous state, with no room for breathers. On the other hand, the stochastic process generated by the MMC rule turns out to be nontrivial even at a microscopic level, since the available phase space depends nonlinearly on the local amplitudes. From a macroscopic point of view, this property leads to a nonlinear Fokker-Planck equation. The question is therefore if it is possible to further simplify the DNLS model, keeping all the essential features of its dynamics. This possibility might allow to obtain a more rigorous explanation of the coarsening exponent $\gamma = 1/3$.

In this section we show that a simple partial exclusive process (PEP) can reproduce the coarsening observed in the DNLS context. The continuous variable a_n is replaced by a discrete, integer amplitude u_n which represents the number of particles on site n. The evolution rule is purely stochastic: once an ordered pair of neighbouring sites (n, m) $(m = n \pm 1)$ has been randomly selected, the transformation $(u_n, u_m) \to (u_n - 1, u_m + 1)$

is made if and only if $u_n > 0$ and $u_m \neq 1$. In practice, one can divide the lattice into two parts: (i) breather-sites ($u_n > 1$) which can freely exchange particles with the surrounding environment; (ii) background ($u_n = 0, 1$) which behaves as in a standard exclusion process. As soon as any given height u_n decreases down to 1, the breather is irreversibly absorbed by the background. Therefore, we can expect this model to exhibit a coarsening dynamics, which will be compared to the dynamics of the simplified DNLS model.

In the previous sections it proved useful to study the relaxation of two-breather states towards a final configuration characterized by a single breather. We are now going to do the same for the PEP model: see Fig. 5.12, where a configuration with two breathers is sketched.

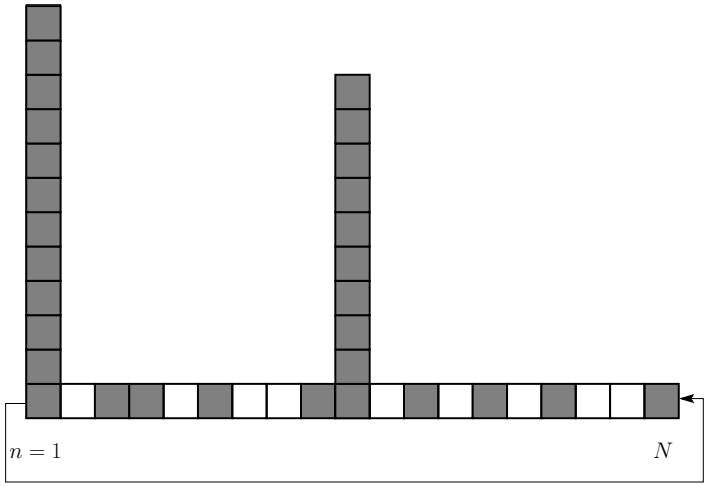

Figure 5.12: The simplified model: two columns of bricks (grey squares) interact exchanging particles through a channel modeled by a simple exclusion process (PEP) with periodic boundary conditions. Each site of the channel can sustain no more than one particle at a time. Particles evolve according to a standard diffusion algorithm endowed with the exclusion rule.

We start by investigating the transport properties of the background field in both models with the help of the power spectrum of the long-wavelength Fourier modes. In order to study qualitatively similar dynamic regimes, we have chosen two initial conditions with the same density of particles, in a condition of maximum entropy, i.e. infinite temperature. In the MMC model, this requirement amounts to a Poissonian initial distribution of the amplitudes [80] with average g, while for the PEP model the same regime corresponds to an average occupation number $\tilde{\rho} = 0.5$. Accordingly, we have chosen $g = \tilde{\rho} = 0.5$. The results are plotted in Fig. 5.13: as expected the power spectrum of the PEP model is well fitted by a Lorentzian distribution, a clear evidence of diffusion. A diffusive behavior in the MMC model is not so straightforward, as its microscopic rule is much more complicated than a standard diffusion algorithm, but this is what we find also in this case. Moreover, the power spectra of the two models

nicely overlap in a wide region of the Fourier space and prove the validity of the PEP model as an effective reduction of the MMC algorithm. On the other hand, the slight gap in the low frequency region suggests a different behavior of the (static) diffusion constants associated to the two dynamics.

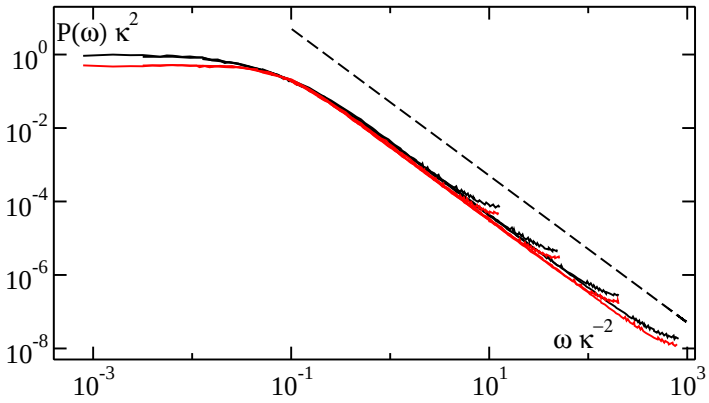

Figure 5.13: Power spectra $P(\omega)\kappa^2$ versus $\omega\kappa^{-2}$ of the MMC dynamics (black solid line) and the PEP model (red solid line) for low-κ Fourier modes, with $\kappa = 2\pi m/N$ and $m = \{1, 2, 4, 8\}$. Data refer to MMC (PEP) chains with $N = 256$ lattice sites in an infinite temperature state with average occupation number $g = 0.5$ ($\tilde{\rho} = 0.5$). The black dashed line is a power law with exponent -2.

Having ascertained that perturbations propagate across the background diffusively in both models, we analyze the dynamics in the presence of breathers. In the PEP model, we proceed by determining the mean lifetime τ of a couple of columns separated by two channels of length $N/2$ (N being the total size of the system). The quantity τ is defined as the average time that is necessary for one of the two columns to be destroyed (i.e. to reach a unitary height), supposing that the columns have initial heights $u_0 = kN$, where k is a positive constant. Fig. 5.14 clearly shows that τ scales with the system size as a power law, $\tau \sim N^3$. This scaling law is the same as for the original MMC model and it is responsible for the characteristic coarsening process of the breathers with an exponent $\gamma = 1/3$.

Let us now evaluate the coarsening time for the PEP model and compare it with numerical results shown in Fig. 5.14. If $u_0 = kN$ is the initial breather height, the typical time τ for the disappearance of one breather is given by the relation $u_0^2 = \tau/\Delta t$, where Δt is the typical time for exchanging one particle between the two breathers. If the system were composed by the two neighboring breathers only, $\Delta t = 1$, but in our case, once the "emitting" breather has been chosen, the exchange becomes effective only if the move (breather)$\rightarrow$(neighbouring site) is allowed and if the diffused particle reaches the other breather before being re-absorbed by the emitting breather. The move (breather)$\rightarrow$(neighbouring site) occurs with probability 1/2. which is the average occupancy of background sites. The diffusion to the other breather occurs with probability $2/N$ [124], where $N/2$ is the distance between breathers. Therefore

$\Delta t = N$ and

$$(kN)^2 = \frac{\tau}{N} \tag{5.21}$$

so that

$$\tau = k^2 N^3 \tag{5.22}$$

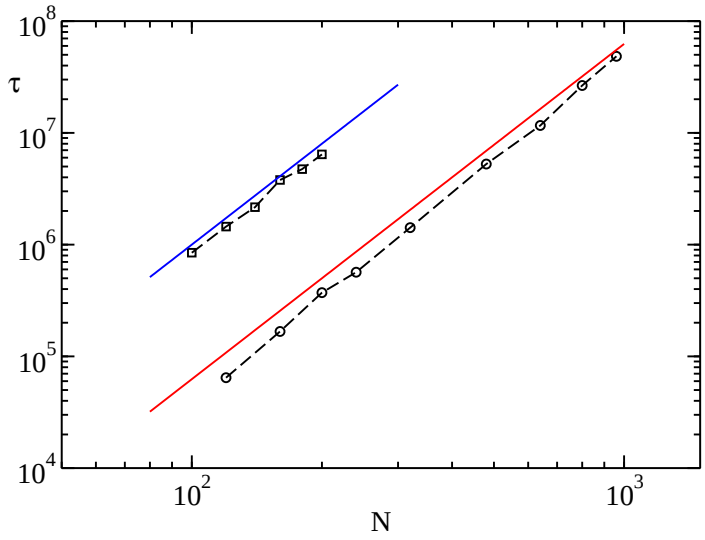

Figure 5.14: Average lifetime τ of a couple of columns exchanging particles through a PEP channel with length $N/2$. The columns have equal initial height u_0 linearly increasing with the system size N as $u_0 = kN$. Simulations have been performed choosing $k = 1$ (open squares) and $k = 1/4$ (open circles). The initial configuration of the channel corresponds to an infinite temperature state with average occupation number $\tilde{\rho} = 1/2$. Solid lines are defined by the equation $\tau = k^2 N^3$ with $k = 1$ for the upper blue line and $k = 1/4$ for the lower red one.

5.7 Discussion

In this chapter we have thoroughly studied a microcanonical Monte Carlo model which approximately reproduces the evolution of a DNLS equation for large mass densities ($a \gg 1$). In the so-called negative temperature region (which corresponds to an energy density $h > 2a^2$), we observe the spontaneous formation of breathers (see Figs. 5.2 and 5.5).

Our studies reveal that, in agreement with the entropic arguments put forward in Ref. [79] (see also Section 4.1), the system converges towards a stationary state composed of a single breather in equilibrium with an infinite temperature background. The evolution is characterized by two time scales. Over "fast" times (on the order N^2), the background equilibrates at infinite temperature, while a population of breathers forms

to store the "excess" energy that cannot be contained in the background. This phenomenon can be attributed to the existence of two positive-defined conserved quantities (energy and mass) which scale with a different power of the local variable (quadratic and linear, respectively): as a result, breathers can contain extensive amounts of energy, while marginally contributing to the mass which is, instead, essentially stored in the background. This regime has been investigated in the simplest possible setup: a single breather sitting on a flat background. The data in Figs. 5.6 and 5.7 clearly show the presence of a time scale N^2.

On a longer time scale N^3, the evolution is characterized by a coarsening process, characterized by an exchange of energy among the breathers, until they progressively disappear, leaving just one alive. Coarsening occurs on a purely stochastic basis, because a breather may lose some of its energy, which diffuses along the background possibly reaching a neighboring breather. Accordingly, the breather height fluctuates and, when a breather goes below threshold, it is "adsorbed" by the infinite temperature background and it cannot appear again. The coarsening exponent $\gamma = 1/3$ (see Fig. 5.4) is a consequence of three facts. First, conservation of mass and energy implies that the breather energy (not breather height, i.e. mass) performs a random walk. Second, conservation of mass and energy implies that the energy of a breather scales as the distance λ between breathers. Third and finally, the elementary time scale for exchanging mass between breathers is set by the inverse of the probability that a "quantum" of mass released by a breather is able to attain the neighboring breather instead that going back. This probability scales as $1/\lambda$.

In order to give a more firm basis to the derivation of $\gamma = 1/3$, the furtherly simplified PEP model has been introduced and analyzed. Such a model shows remarkable similarities with the original DNLS dynamics: (i) the condensation onto a single site appears above a critical value (defined by the mass density $\tilde{\rho} = 0.5$ in the PEP model and by the energy density $h = 2$ in the simplified DNLS); the same scaling exponent is found in the two models. It is, however, necessary to recall a crucial difference: the presence of two rather than just a single conservation law in the simplified DNLS model. The very same difference exists with other models where a similar scenario can be found: the Kinetic Ising Model with conserved magnetization [125] and a class of zero-range processes [126].

Finally, going back to the original DNLS model, it is worth recalling two major simplifications introduced in this paper: (i) the interaction energy between neighbouring sites has been neglected (the MMC model indeed corresponds to the high mass-density limit of the DNLS equation); (ii) dynamical effects are disregarded (the model is purely stochastic). The first limitation could be removed by reintroducing the interaction term in the original Hamiltonian. As a result, one would be, however, forced to account also for the phase dynamics (absent in the MMC model) with the related difficulty (impossibility) of deriving explicit microcanonical transformations. This is, nevertheless, a route that would be worth to explore, especially to check the robustness of the coarsening process herein investigated.

As for possible dynamical effects, one cannot exclude that the dynamical arrest of the coarsening observed in Chapter 4 is partly due to the weak coupling of the rapidly rotating breathers with the background which makes energy and mass exchanges even slower than in our stochastic process.

The results concerning the evidence of coarsening in the MMC model and its significance for the DNLS dynamics have been published in Ref. [119]. The detailed analysis contained in this chapter has been published in Ref. [127].

Conclusions and perspectives

In this dissertation we analyzed the out-of-equilibrium properties of the Discrete Nonlinear Schrödinger (DNLS) equation, focusing on two different aspects of this general subject. The first topic concerns the irreversible thermodynamics of a DNLS chain that steadily exchanges energy and mass with external reservoirs at finite temperature. The second one is related to the macroscopic characterization of the slow relaxation dynamics in the presence of discrete breathers weakly interacting with a thermal background.

The response of a macroscopic system to an external perturbation and its relaxation from nonequilibrium to equilibrium states are two classical problems in nonequilibrium statistical mechanics [27]. The motivations that led to investigate them in DNLS equations started from the increasing interest that has been addressed to these models for their capability of describing several phenomena in different fields of nonlinear physics. In this respect, while a vast literature has been devoted to strictly dynamical problems, much less is known about finite-temperature properties. On the other hand, the continuous refinement of experimental techniques has recently allowed observations of the DNLS dynamics also for timescales that are much longer than the intrinsic scales of the dynamics [113, 54]. Such asymptotic regimes naturally require a statistical-mechanical treatment, corresponding to a coarse graining procedure from the microscopic dynamics to the macroscopic level.

The strategy we have adopted for the characterization of an open nonequilibrium DNLS amounts to connecting the boundaries of the system to suitable models of external reservoirs of energy and mass. This setup is particularly versatile and allows to investigate both equilibrium properties (when the parameters of the external heat baths are equal) and nonequilibrium ones (in the presence of thermodynamic forces). In the latter case, the existence of two independent conserved quantities of the DNLS dynamics naturally places the problem in the context of coupled transport processes. However, the symmetries of the model and the nonseparability of its Hamiltonian brought out several new issues concerning energy transport and thermalization in oscillator chains. In particular, we have specifically defined and tested suitable models of reservoir, both via phenomenological Monte-Carlo dynamics and by Langevin equations. The latter strategy is definitely the most promising one, as it allows also for a rigorous analytical treatment of the thermostatted system by means of a Fokker-Planck equation. In addition, standard thermodynamic observables like the temperature and the chemical potential need a careful microcanonical derivation based on the results of

Ref. [87].

Our results indicate that stationary thermal transport in the DNLS equation is normal, i.e. the transport coefficients are finite in the thermodynamic limit, according to Fourier/Fick laws. This property is not straightforward in the context of heat transport in low-dimensional systems [2], where the heat conductivity can diverge as a power law of the system size, with an exponent that depends on the symmetries of the model. Thermodiffusive effects can be characterized in terms of a Seebeck coefficient that depends on the thermodynamic parameters. In particular, upon increasing the nonlinearity of the system, such quantity changes sign. Consistently, also the thermal and chemical gradients are found to change their relative signs when the transport of mass is absent. In more general transport conditions, when both energy and mass fluxes are present, the Onsager coefficients define the linear relationships between thermodynamic forces and fluxes. When the boundary temperature or chemical-potential differences are no longer small, nonmonotonic stationary temperature profiles can be observed, with peak temperatures three times larger than the ones imposed on the boundaries. This phenomenon can be observed only in the presence of coupled transport and basically corresponds to an out-of-equilibrium conversion of almost coherent degrees of freedom into thermal fluctuations, analogous to the Joule effect.

The above phenomenology is definitely independent on the dynamical model adopted for the heat bath. However, Langevin heat baths offer a deeper insight into nonequilibrium stationary states of the DNLS equation. In this respect, the limit of large mass densities is particularly interesting, as it allows to map the DNLS setup onto that of a chain of nonlinearly coupled rotors with external torques and thermal noise. Such relationship with a translationally invariant model clarifies that the origin of normal transport observed in the DNLS chain is more subtle than one could have imagined. In fact, nonlinear chains with translationally invariant interaction typically exhibit diverging transport coefficients [2]. Only in models with phase-like displacements, like the rotor chain, transport is normal because of the occasional phase jumps across the potential barrier that produce an effective phonon scattering and prevent anomalous diffusion [98]. Altogether, the Langevin approach provides a clear physical interpretation of the action of the external reservoirs as means to locally fix the average angular velocities and the kinetic fluctuations of the oscillators. To our knowledge, such general nonequilibrium framework involving the action of both thermal and mechanical gradients has not received much attention in the literature of nonlinear dynamical systems (one of the few examples is contained in Ref. [104]). As a future study it will be interesting to establish possible connections between our thermodynamic approach and universal concepts such as chaos and synchronization [128, 129]. In this respect, it may be also speculated that their competition in extended systems could give rise to different nontrivial transport regimes, possibly separated by nonequilibrium dynamical phase-transitions [130].

The second part of the dissertation was devoted to the characterization of the DNLS model in the phase displaying nonlinear localized excitations (discrete breathers). The reason why breathers play an important role in this phase is the existence of a second

conservation law (the total mass) which favours energy concentration, while limiting its entropic cost [60]. The motivations of this study were to clarify the nature of the long-time macroscopic dynamics, bridging the gap between purely entropic arguments [26] and the peculiar dynamic features of breather degrees of freedom [23]. In fact, on the one hand, energy localization into larger and larger discrete breathers represents an effective mechanism for the system to increase its total entropy [26]; on the other hand, the intrinsic stability of high-energy discrete breathers makes such excitations almost locally decoupled with the rest of the chain. Therefore the asymptotic convergence to the expected maximum entropy (equilibrium) state is not obvious a priori. In particular, it was observed that it would need transients lasting over astronomical times [86].

The approach followed in this thesis consisted in studying the DNLS dynamics from a statistical point of view and over long, but physically accessible timescales. Our results indicate that the system relaxes to a metastable state characterized by a negative temperature and a finite density of breathers. In particular, breathers are prevented from becoming too large as a consequence of a dynamical screening of the high amplitude region. Therefore, the evolution of the system is confined in a reduced region of the available phase space. The existence of a thermodynamic behaviour in such reduced component is nontrivial at all and it is reminiscent of spin-glass dynamics [131]. In this respect a more quantitative analysis will be necessary in future studies to shed some light into possible aging phenomena arising in the presence of breather excitations. One of the most interesting aspects of the overall scenario is that the related mechanism of ergodicity breaking would be induced by dynamical (and not only entropic) barriers [132]. To our knowledge, such peculiar property is quite rare in statistical mechanics [132]. Finally, we showed that quasi-stationary negative temperature states can be accessed starting from generic initial conditions by means of simple nonequilibrium transient processes, namely free expansions or boundary dissipations. These results indicate also the possibility to observe the above phenomenology in experiments involving the typical setups described by the DNLS equation, like Bose-Einstein condensates in optical lattices [46] and optical waveguides arrays [40].

An interesting question that naturally arises from the above results is whether a modification of the dynamic properties of the breather excitations is sufficient to produce a different scenario. In this respect, further insights in the nature of the DNLS quasi-stationary states have been provided via Microcanonical Monte Carlo (MMC) simulations in the so-called weak-coupling limit. This limit basically corresponds to neglecting the phase dynamics of the system and to exploring the only role of entropy contributions to the relaxation dynamics. In such conditions we found that relaxation to equilibrium is indeed observable and it is achieved via a coarsening dynamics of breathers. Specifically, we found that the average density of breathers decreases in time as a power-law with exponent 1/3. Although the purely stochastic character of the MMC dynamics is quite distant from the DNLS dynamics, its study can help to identify the primary constraints that are expected to exist in the convergence to the asymptotic state. As an example, the MMC model allowed to single out a "fast"

relaxation timescale, consisting in a direct exchange of energy between breathers and background, from a "slow" one, resulting from an effective breather-breather interaction mediated by the background. Moreover, the reduction of the MMC dynamics into a suitable Partial Exclusion Process provided a clear explanation of the origin of the subdiffusive coarsening exponent.

Altogether, the study of stochastic nonequilibrium processes mimicking the full DNLS dynamics revealed that a slow relaxation dynamics appears (in the form of coarsening) even at the simplest level, as a consequence of the fundamental symmetries of the problem. The presence of a coarsening dynamics in these simplified models is not trivial at all, as they are rather different from the standard reference models of coarsening [120]. Such peculiarity deserves by itself future deeper insights. In addition, going back to the original DNLS equation, it will be interesting to clarify the reason why the coarsening process appears to be much slower and possibly stop, giving rise to the quasi-equilibrium states commented above. In this respect, a promising approach amounts to consider a *noisy* DNLS equation, i.e. a standard DNLS dynamics in the presence of external stochastic noise. In fact, it is known that in one spatial dimension external noise can be a relevant parameter of the coarsening problem, as it can induce coarsening even when the deterministic dynamics would block it [120]. This approach could represent also a valid starting point to investigate the role of dimensionality in the localization dynamics.

As a concluding remark, we point out that the results and methods described in this thesis open also several possibilities for the study of more general nonequilibrium setups. A remarkable example consists in an open DNLS chain that is steadily kept out-of-equilibrium between the two regions at positive and negative temperature. Besides being an interesting *trait d'union* between the two themes analyzed in this thesis, such a setup carries several new aspects on the behaviour of nonequilibrium systems. Preliminary results [133] indicate that the presence of breathers is capable to deeply modify the transport properties of the system. In fact, depending on the weight of nonlinearity, one observes a transition from a normal conducting regime to a quasi-insulating phase dominated by breathers. The possible critical nature of this phenomenon is a challenging open question that will deserve future studies.

Appendix A

The low-mass limit of the DNLS equation

In this Appendix we review the main properties of the DNLS model in the limit of vanishing nonlinearity, i.e. for low mass densities (cf. e.g. Ref. [26]). Although this limit misses many interesting features of the original DNLS equation, it is however of relevant practical importance, as it defines a simple integrable system sharing the same symmetries of the nonlinear model.

The Hamiltonian H_l of the discrete linear Schrödinger (DLS) equation writes

$$H_l = \sum_{n=1}^{N} \left(z_n^* z_{n+1} + z_n z_{n+1}^* \right) \quad , \tag{A.1}$$

whith the same definition of total mass given in Eq. (1.5). The Hamiltonian H_l can be diagonalized by means of a discrete Fourier transform

$$a_k = \frac{1}{\sqrt{N}} \sum_{n=1}^{N} e^{-\frac{2\pi i}{N} kn} z_n \qquad k = 1, \ldots, N \quad , \tag{A.2}$$

leading to

$$H_l = \sum_{k=1}^{N} |a_k|^2 \omega_k \quad , \tag{A.3}$$

where $\omega_k = 2\cos(2\pi k/N)$ is the energy spectrum of the system and $|a_k|^2$ represents the amplitude of the k-th mode, with the property $\sum_{k=1}^{N} |a_k|^2 = A$.

The partition function

$$Z = \int \prod_{k=1}^{N} da_k \, da_k^* \, e^{-\beta(H - \mu A)} \tag{A.4}$$

can be now calculated in terms of complex Gaussian integrals and rewrites

$$Z = \prod_{k=1}^{N} \frac{2\pi}{\beta(\omega_k - \mu)} \quad . \tag{A.5}$$

As a result, we can explicitly write the free energy F, the mass density $a = \langle A \rangle / N$ and the energy density $h_l = \langle H_l \rangle / N$ as follows

$$\begin{aligned} F &= -\frac{1}{\beta} \ln Z = \sum_{k=1}^{N} \ln \left[\frac{2\pi}{\beta(\omega_k - \mu)} \right] \\ a &= \sum_{k=1}^{N} f(\beta, \omega_k, \mu) \\ h_l &= \frac{1}{\beta} + \mu \sum_{k=1}^{N} f(\beta, \omega_k, \mu) \quad , \end{aligned} \tag{A.6}$$

where $f(\beta, \omega_k, \mu) = [\beta(\omega_k - \mu)]^{-1}$ is the average occupation number of the state k. By then substituting the explicit form of the energy spectrum $\omega_k = 2\cos(2\pi k/N)$, in the $N \to \infty$ limit we obtain

$$a = -\frac{1}{\beta\sqrt{\mu^2 - 4}} \tag{A.7}$$

$$h_l = \frac{1}{\beta} + \mu a \quad . \tag{A.8}$$

The above equations are well defined for $|\mu| > 2$ and allow to construct the complete equilibrium phase diagram of the linear model, see Fig. A.1. The accessible states are in between the ground state $h_l = -2a$ ($\beta = +\infty$) and the maximum energy state $h_l = 2a$ ($\beta = -\infty$). The horizontal axis $h_l = 0$ ($\beta = 0$) separates positive temperature states from negative temperature ones.

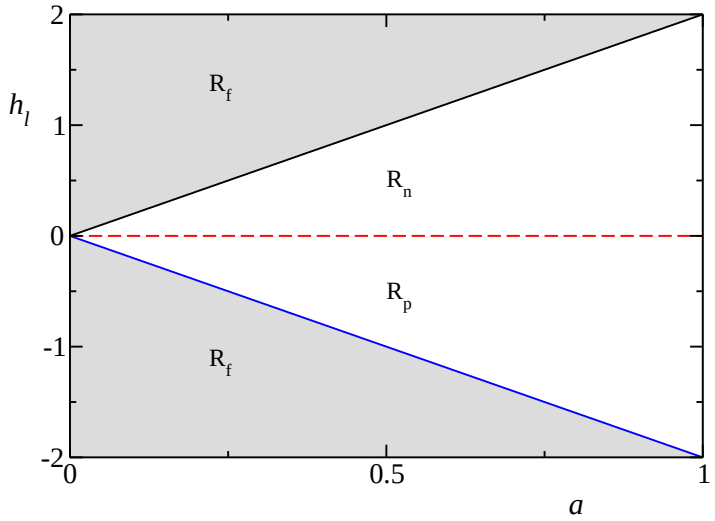

Figure A.1: Equilibrium phase diagram (a, h_l) of the DLS equation. We show the isothermal lines $\beta = +\infty$ (solid blue), $\beta = 0$ (dashed red) and $\beta = -\infty$ (solid black). The region R_p, R_n and R_f are defined as in Section 1.4.

Appendix B

Numerical methods

B.1 Evaluation of Θ and $\mathcal{M}$ in numerical simulations

The explicit numerical evaluation of the microcanonical observables Θ and $\mathcal{M}$ defined in Section 2.2.2 for a generic DNLS chain with N lattice sites is particularly awkward. In particular, the main difficulty concerns the evaluation of the term

$$\vec{\nabla} \cdot \left(\frac{\vec{\xi}}{\|\vec{\xi}\| W} \right) \quad , \tag{B.1}$$

that contains a nontrivial combination of partial second derivatives of the functions H and A. In this respect, we have developed a "numerical" approach to this problem by approximating the directional derivatives in Eq. (B.1) with finite difference quotients. In order to better clarify this point, we rewrite Eq. (2.4) in the form

$$\frac{\partial \mathcal{S}}{\partial C_1} = \left\langle h \sum_{i=1}^{2N} \frac{\partial g_i}{\partial x_i} \right\rangle \quad , \tag{B.2}$$

where

$$h = \frac{W\|\vec{\xi}\|}{\vec{\nabla} C_1 \cdot \vec{\xi}} \qquad\qquad g_i = \left(\frac{\xi_i}{\|\vec{\xi}\| W} \right) \quad . \tag{B.3}$$

By definition, upon introducing an infinitesimal perturbation ϵ_i in the i-th direction with respect to a reference state $\vec{x}_0 \in \mathbb{R}^{2N}$,

$$\left. \frac{\partial g_i}{\partial x_i} \right|_{\vec{x}_0} = \lim_{\|\vec{\epsilon}_i\| \to 0} \frac{g_i(\vec{x}_0 + \vec{\epsilon}_i) - g_i(\vec{x}_0)}{\|\vec{\epsilon}_i\|} \qquad \vec{\epsilon}_i = \begin{pmatrix} 0 \\ \vdots \\ \epsilon \\ \vdots \\ 0 \end{pmatrix} \leftarrow i \quad . \tag{B.4}$$

Finally, for a small, but *finite* perturbation, one can write

$$\left.\frac{\partial g_i}{\partial x_i}\right|_{\vec{x}_0} \approx \frac{g_i(\vec{x}_0+\vec{\epsilon}_i)-g_i(\vec{x}_0)}{\|\vec{\epsilon}_i\|} \qquad \|\vec{\epsilon}_i\| \ll 1 \quad . \tag{B.5}$$

For the numerical simulations performed in this thesis, we have chosen a precision $\|\vec{\epsilon}_i\| = 10^{-9}$. This simple trick allows one to compute the observables Θ and $\mathcal{M}$ with excellent degree of precision and in terms of the only first derivatives of H and A, that are easily evaluable analytically.

B.2 The harmonic temperature T_H

In this section we derive the explicit expression for the coefficient J in Eq. (3.38), which is necessary in order to obtain a quantitative comparison between the temperature of the DNLS model and the one associated to the chain of harmonic oscillators (3.37). The Jacobian factor J arises in Eq. (3.38) because we compute the harmonic temperature T_h on the dynamics of the DNLS model.

Let us call $(W_1 \circ W_2)$ the transformation that allows to switch from the original DNLS variables (a_n, ϕ_n) to the ones of the harmonic model, with W_1 and W_2 defined as follows (cf. Eq.s (3.22) and (3.35))

$$\begin{aligned} \zeta_n &= \frac{a_j}{2a} \qquad (W_1) \\ p_n &= 4a\zeta_n + 2\zeta_n - \zeta_{n-1} - \zeta_{n+1} \qquad (W_2) \quad , \end{aligned}$$

where in W_1 we made use of the property $\zeta_n \ll 1$. The factor J is therefore defined by

$$J^N = det(W_2 \circ W_1) = det(W_2) \cdot det(W_1) = \frac{det(W_2)}{(2a)^N} \quad .$$

In order to compute $det(W_2)$, we notice that W_2 can be decomposed as

$$W_2 = 4a\mathbf{1} + \nabla_d^2 \quad ,$$

where $\mathbf{1}$ is the identity matrix and ∇_d^2 is the discrete Laplace operator, defined by $\nabla_d^2 \zeta_n = 2\zeta_n - \zeta_{n-1} - \zeta_{n+1}$. If we now consider a problem with Dirichlet boundary conditions, we can explicitly write the complete set of eigenvalues $\{w_2^{(k)}\}$ of W_2 in the form (cf. e.g. [134])

$$w_2^{(k)} = 4a + 4\sin^2\left[\frac{\pi k}{2(N+1)}\right] \qquad k = 1, \ldots, N \quad .$$

Upon introducing the function $f = \ln\left[det(W_2)\right]$ with the property [1]

$$f = \ln \prod_k w_2^{(k)} = \sum_k \ln\left[w_2^{(k)}\right] \quad ,$$

[1] Notice that f is a well defined real-valued function because all the eigenvalues $\{w_2^{(k)}\}$ are strictly positive.

we can write

$$f = \frac{2(N+1)}{\pi} \int_0^{\pi/2} \ln\left[4a + 4\sin^2(x)\right]\, dx \quad ,$$

and finally get $det(W_2) = \exp(f)$. In the limit $N \to \infty$ the role of the boundary conditions is negligible and the final expression for J is

$$J(a) = \frac{\exp\left\{\frac{2}{\pi}\int_0^{\pi/2} \ln\left[4a + 4\sin^2(x)\right]\, dx\right\}}{2a} \quad . \tag{B.6}$$

Notice that in the limit $a \to \infty$ $J(a)$ approaches the asymptotic value $J = 2$. This is the reason why we obtain the relation $T_{XY} = 2T$ for the large mass limit discussed in Section 3.5.

Bibliography

[1] R. E. Peierls. *Quantum theory of solids*. Oxford University Press, 1955.

[2] S. Lepri, R. Livi, and A. Politi. Thermal conduction in classical low-dimensional lattices. *Phys. Rep.*, 377:1, 2003.

[3] H. van Beijeren. Exact Results for Anomalous Transport in One-Dimensional Hamiltonian Systems. *Phys. Rev. Lett.*, 108:180601, 2012.

[4] D. Xiong, J. Wang, Y. Zhang, and H. Zhao. Nonuniversal heat conduction of one-dimensional lattices. *Phys. Rev. E*, 85:020102, Feb 2012.

[5] L. Bertini, A. De Sole, D. Gabrielli, G. Jona-Lasinio, and C. Landim. Stochastic interacting particle systems out of equilibrium. *Journal of Statistical Mechanics: Theory and Experiment*, 2007(07):P07014, 2007.

[6] J. Marro and R. Dickman. *Nonequilibrium phase transitions in lattice models*. Cambridge University Press, 2005.

[7] G. Schütz and E. Domany. Phase transitions in an exactly soluble one-dimensional exclusion process. *Journal of statistical physics*, 72(1-2):277–296, 1993.

[8] D. Helbing. Traffic and related self-driven many-particle systems. *Rev. Mod. Phys.*, 73:1067–1141, Dec 2001.

[9] J. Eilbeck, P. Lomdahl, and A. Scott. The discrete self-trapping equation. *Physica D*, 16:318–338, 1985.

[10] P. G. Kevrekidis. *The Discrete Nonlinear Schrdinger Equation*. Springer Verlag, Berlin, 2009.

[11] A. Scott. *Nonlinear science. Emergence and dynamics of coherent structures*. Oxford University Press, Oxford, 2003.

[12] A. M. Kosevich and M. A. Mamalui. Linear and nonlinear vibrations and waves in optical or acoustic superlattices (photonic or phonon crystals). *J. Exp. Theor. Phys.*, 95(4):777, 2002.

[13] G. Tsironis and D. Hennig. Wave transmission in nonlinear lattices. *Phys. Rep.*, 307(5-6):333–432, 1999.

[14] R. Franzosi, R. Livi, G. Oppo, and A. Politi. Discrete breathers in Bose–Einstein condensates. *Nonlinearity*, 24:R89, 2011.

[15] A. Dhar. Heat Transport in low-dimensional systems. *Adv. Phys.*, 57:457–537, 2008.

[16] L. Delfini, S. Lepri, R. Livi, and A. Politi. Anomalous kinetics and transport from 1D self-consistent mode-coupling theory. *J. Stat. Mech.: Theory and Experiment*, page P02007, 2007.

[17] G. Basile, C. Bernardin, and S. Olla. Momentum conserving model with anomalous thermal conductivity in low dimensional systems. *Phys. Rev. Lett.*, 96:204303, 2006.

[18] M. Gillan and R. Holloway. Transport in the Frenkel-Kontorova model 3: thermal-conductivity. *J. Phys. C*, 18(30):5705–5720, 1985.

[19] C. Mejia-Monasterio, H. Larralde, and F. Leyvraz. Coupled normal heat and matter transport in a simple model system. *Phys. Rev. Lett.*, 86(24):5417–5420, 2001.

[20] H. Larralde, F. Leyvraz, and C. Meja-Monasterio. Transport Properties of a Modified Lorentz Gas. *J. Stat. Phys.*, 113:197–231, 2003.

[21] G. Casati, L. Wang, and T. Prosen. A one-dimensional hard-point gas and thermoelectric efficiency. *J. Stat. Mech.: Theory and Experiment*, (03):L03004, 2009.

[22] K. Saito, G. Benenti, and G. Casati. A microscopic mechanism for increasing thermoelectric efficiency. *Chem. Phys.*, 375:508–513, 2010.

[23] S. Flach and C. Willis. Discrete breathers. *Physics Reports*, 295(5):181–264, 1998.

[24] S. Flach and A. V. Gorbach. Discrete breathers – Advances in theory and applications. *Physics Reports*, 467(1):1–116, 2008.

[25] K. Rasmussen, T. Cretegny, P. Kevrekidis, and N. Grønbech-Jensen. Statistical mechanics of a discrete nonlinear system. *Phys. Rev. Lett.*, 84(17):3740–3743, 2000.

[26] B. Rumpf. Simple statistical explanation for the localization of energy in nonlinear lattices with two conserved quantities. *Phys. Rev. E*, 69:016618, 2004.

[27] N. Hashitsume, M. Toda, R. Kubo, and N. Saitō. *Statistical physics II: nonequilibrium statistical mechanics*, volume 30. Springer, 1992.

[28] M. I. Weinstein. Excitation thresholds for nonlinear localized modes on lattices. *Nonlinearity*, 12(3):673, 1999.

[29] A. Khare, K. Ø. Rasmussen, M. R. Samuelsen, and A. Saxena. Exact solutions of the saturable discrete nonlinear Schrödinger equation. *Journal of Physics A: Mathematical and General*, 38(4):807, 2005.

[30] P. Kevrekidis, B. Malomed, A. Saxena, A. Bishop, and D. Frantzeskakis. Higher-order lattice diffraction: solitons in the discrete NLS equation with next-nearest-neighbor interactions. *Physica D: Nonlinear Phenomena*, 183(1):87–101, 2003.

[31] A. Davydov. Solitons in Molecular Systems. *J. Theor. Biol*, 38:559, 1973.

[32] M. Ablowitz and J. Ladik. A nonlinear difference scheme and inverse scattering. *Stud. Appl. Math*, 55(3):213–229, 1976.

[33] A. Scott and L. Macneil. Binding energy versus nonlinearity for a small stationary soliton. *Physics Letters A*, 98(3):87–88, 1983.

[34] J. Eilbeck, P. Lomdahl, and A. Scott. Soliton structure in crystalline acetanilide. *Physical review. B, Condensed matter*, 30(8):4703–4712, 1984.

[35] R. MacKay and S. Aubry. Proof of existence of breathers for time-reversible or Hamiltonian networks of weakly coupled oscillators. *Nonlinearity*, 7:1623–1643, 1994.

[36] S. Aubry. Breathers in nonlinear lattices: existence, linear stability and quantization. *Physica D: Nonlinear Phenomena*, 103(1):201–250, 1997.

[37] A. Morgante, M. Johansson, G. Kopidakis, and S. Aubry. Standing wave instabilities in a chain of nonlinear coupled oscillators. *Physica D: Nonlinear Phenomena*, 162(1-2):53–94, 2002.

[38] G. Berman and A. Kolovskii. The limit of stochasticity for a one-dimensional chain of interacting oscillators. *Zh. Eksp. Teor. Fiz*, 87:1938, 1984.

[39] S. Jensen. The nonlinear coherent coupler. *Quantum Electronics, IEEE Journal of*, 18(10):1580–1583, 1982.

[40] D. Christodoulides and R. Joseph. Discrete self-focusing in nonlinear arrays of coupled waveguides. *Optics letters*, 13(9):794–796, 1988.

[41] A. Aceves, C. De Angelis, T. Peschel, R. Muschall, F. Lederer, S. Trillo, and S. Wabnitz. Discrete self-trapping, soliton interactions, and beam steering in nonlinear waveguide arrays. *Physical Review E*, 53:1172–1189, 1996.

[42] O. Bang and P. D. Miller. Exploiting discreteness for switching in waveguide arrays. *Optics letters*, 21(15):1105–1107, 1996.

[43] H. Eisenberg, Y. Silberberg, R. Morandotti, A. Boyd, J. Aitchison, et al. Discrete spatial optical solitons in waveguide arrays. *Physical Review Letters*, 81(16):3383–3386, 1998.

[44] R. Morandotti, U. Peschel, J. Aitchison, H. Eisenberg, and Y. Silberberg. Experimental observation of linear and nonlinear optical Bloch oscillations. *Physical Review Letters*, 83(23):4756–4759, 1999.

[45] A. Smerzi, S. Fantoni, S. Giovanazzi, and S. Shenoy. Quantum coherent atomic tunneling between two trapped Bose-Einstein condensates. *Physical Review Letters*, 79(25):4950, 1997.

[46] A. Trombettoni and A. Smerzi. Discrete solitons and breathers with dilute Bose-Einstein condensates. *Physical Review Letters*, 86(11):2353, 2001.

[47] B. Anderson and M. A. Kasevich. Macroscopic quantum interference from atomic tunnel arrays. *Science*, 282(5394):1686–1689, 1998.

[48] F. Cataliotti, S. Burger, C. Fort, P. Maddaloni, F. Minardi, A. Trombettoni, A. Smerzi, and M. Inguscio. Josephson junction arrays with Bose-Einstein condensates. *Science*, 293(5531):843–846, 2001.

[49] F. Cataliotti, L. Fallani, F. Ferlaino, C. Fort, P. Maddaloni, and M. Inguscio. Superfluid current disruption in a chain of weakly coupled Bose–Einstein condensates. *New Journal of Physics*, 5(1):71, 2003.

[50] O. Mandel, M. Greiner, A. Widera, T. Rom, T. W. Hänsch, and I. Bloch. Coherent transport of neutral atoms in spin-dependent optical lattice potentials. *Physical review letters*, 91(1):010407, 2003.

[51] M. Chiofalo and M. Tosi. Coherent and dissipative transport of a Bose-Einstein condensate inside an optical lattice. *Journal of Physics B: Atomic, Molecular and Optical Physics*, 34(23):4551, 2001.

[52] J. R. Anglin and W. Ketterle. Bose–Einstein condensation of atomic gases. *Nature*, 416(6877):211–218, 2002.

[53] I. Bloch. Quantum gases in optical lattices. *Physics World*, 17(25):125, 2004.

[54] O. Morsch and M. Oberthaler. Dynamics of Bose-Einstein condensates in optical lattices. *Reviews of modern physics*, 78(1):179, 2006.

[55] I. Bloch, J. Dalibard, and W. Zwerger. Many-body physics with ultracold gases. *Reviews of Modern Physics*, 80(3):885, 2008.

[56] D. Haycock, P. Alsing, I. Deutsch, J. Grondalski, and P. Jessen. Mesoscopic quantum coherence in an optical lattice. *Physical review letters*, 85(16):3365, 2000.

[57] M. Sato, S. Yasui, M. Kimura, T. Hikihara, and A. Sievers. Management of localized energy in discrete nonlinear transmission lines. *EPL (Europhysics Letters)*, 80(3):30002, 2007.

[58] M. Sato, B. Hubbard, and A. Sievers. Colloquium: Nonlinear energy localization and its manipulation in micromechanical oscillator arrays. *Reviews of modern physics*, 78(1):137, 2006.

[59] S. Lepri and G. Casati. Asymmetric Wave Propagation in Nonlinear Systems. *Phys. Rev. Lett.*, 106(16):164101, 2011.

[60] B. Rumpf and A. C. Newell. Coherent structures and entropy in constrained, modulationally unstable, nonintegrable systems. *Physical Review Letters*, 87(5), 2001.

[61] B. Rumpf and A. C. Newell. Localization and coherence in nonintegrable systems. *Physica D: Nonlinear Phenomena*, 184(1):162–191, 2003.

[62] S. Borlenghi, W. Wang, H. Fangohr, L. Bergqvist, and A. Delin. Towards a magnonic thermal diode. *arXiv preprint arXiv:1306.5924*, 2013.

[63] K. Uchida, S. Takahashi, K. Harii, J. Ieda, W. Koshibae, K. Ando, S. Maekawa, and E. Saitoh. Observation of the spin Seebeck effect. *Nature*, 455(7214):778–781, 2008.

[64] P. W. Anderson. Absence of diffusion in certain random lattices. *Physical review*, 109(5):1492, 1958.

[65] G. Kopidakis and S. Aubry. Intraband discrete breathers in disordered nonlinear systems. I. Delocalization. *Physica D: Nonlinear Phenomena*, 130(3):155–186, 1999.

[66] G. Kopidakis and S. Aubry. Discrete breathers and delocalization in nonlinear disordered systems. *Physical review letters*, 84(15):3236, 2000.

[67] G. Kopidakis and S. Aubry. Intraband discrete breathers in disordered nonlinear systems. II. Localization. *Physica D: Nonlinear Phenomena*, 139(3):247–275, 2000.

[68] G. Kopidakis, S. Komineas, S. Flach, and S. Aubry. Absence of Wave Packet Diffusion in Disordered Nonlinear Systems. *Phys. Rev. Lett.*, 100(8):084103, 2008.

[69] A. S. Pikovsky and D. L. Shepelyansky. Destruction of Anderson Localization by a Weak Nonlinearity. *Phys. Rev. Lett.*, 100(9):094101, 2008.

[70] J. Gomez-Gardenes, L. Floria, M. Peyrard, and A. Bishop. Nonintegrable Schrödinger discrete breathers. *Chaos: An Interdisciplinary Journal of Nonlinear Science*, 14:1130, 2004.

[71] G. James. Centre manifold reduction for quasilinear discrete systems. *Journal of Nonlinear Science*, 13(1):27–63, 2008.

[72] A. Sievers and S. Takeno. Intrinsic localized modes in anharmonic crystals. *Physical Review Letters*, 61(8):970–973, 1988.

[73] I. Daumont, T. Dauxois, and M. Peyrard. Modulational instability: first step towards energy localization in nonlinear lattices. *Nonlinearity*, 10(3):617–630, 1997.

[74] K. Rasmussen, S. Aubry, A. Bishop, and G. Tsironis. Discrete nonlinear Schrödinger breathers in a phonon bath. *Eur. Phys. J. B*, 15:169–175, 2000.

[75] G. Tsironis and S. Aubry. Slow relaxation phenomena induced by breathers in nonlinear lattices. *Physical review letters*, 77(26):5225, 1996.

[76] F. Piazza, S. Lepri, and R. Livi. Slow energy relaxation and localization in 1D lattices. *Journal of Physics A: Mathematical and General*, 34(46):9803, 2001.

[77] F. Piazza, S. Lepri, and R. Livi. Cooling nonlinear lattices toward energy localization. *Chaos: An Interdisciplinary Journal of Nonlinear Science*, 13:637, 2003.

[78] R. Livi, R. Franzosi, and G.-L. Oppo. Self-localization of Bose-Einstein condensates in optical lattices via boundary dissipation. *Physical review letters*, 97(6):060401–060401, 2006.

[79] B. Rumpf. Growth and erosion of a discrete breather interacting with Rayleigh-Jeans distributed phonons. *EPL (Europhysics Letters)*, 78(2):26001, 2007.

[80] B. Rumpf. Transition behavior of the discrete nonlinear Schrödinger equation. *Physical Review E*, 77(3):036606, 2008.

[81] B. Rumpf. Stable and metastable states and the formation and destruction of breathers in the discrete nonlinear Schrödinger equation. *Physica D: Nonlinear Phenomena*, 238(20):2067–2077, 2009.

[82] M. Peyrard. The pathway to energy localization in nonlinear lattices. *Physica D: Nonlinear Phenomena*, 119(1):184–199, 1998.

[83] R. Franzosi, R. Livi, and G.-L. Oppo. Probing the dynamics of Bose–Einstein condensates via boundary dissipation. *Journal of Physics B: Atomic, Molecular and Optical Physics*, 40(6):1195, 2007.

[84] L. Onsager. Statistical hydrodynamics. *Il Nuovo Cimento (1943-1954)*, 6:279–287, 1949.

[85] N. F. Ramsey. Thermodynamics and statistical mechanics at negative absolute temperatures. *Physical Review*, 103(1):20, 1956.

[86] M. Johansson and K. Ø. Rasmussen. Statistical mechanics of general discrete nonlinear Schrödinger models: Localization transition and its relevance for Klein-Gordon lattices. *Physical Review E*, 70(6):066610, 2004.

[87] R. Franzosi. Microcanonical Entropy and Dynamical Measure of Temperature for Systems with Two First Integrals. *J. Stat. Phys.*, 143:824–830, 2011.

[88] G. Casati, C. Mejía-Monasterio, and T. Prosen. Increasing Thermoelectric Efficiency: A Dynamical Systems Approach. *Phys. Rev. Lett.*, 101(1):016601, 2008.

[89] Z. Rieder, J. L. Lebowitz, and E. Lieb. Properties of a harmonic crystal in a stationary nonequilibrium state. *J. Math. Phys.*, 8:1073, 1967.

[90] P. Sheng. *Introduction to wave scattering, localization, and mesoscopic phenomena*, volume 88. Springer, 2006.

[91] A. Dhar and D. Roy. Heat Transport in Harmonic Lattices. *J. Stat. Phys.*, 125:805, 2006.

[92] S. Iubini, S. Lepri, and A. Politi. Nonequilibrium discrete nonlinear Schrödinger equation. *Physical Review E*, 86(1):011108, 2012.

[93] P. L. Christiansen, Y. B. Gaididei, M. Johansson, and K. Ø. Rasmussen. Breatherlike excitations in discrete lattices with noise and nonlinear damping. *Physical Review B*, 55(9):5759, 1997.

[94] C. Kipnis, C. Marchioro, and E. Presutti. Heat flow in an exactly solvable model. *J. Stat. Phys.*, 27:65, 1982.

[95] R. Zwanzig. *Nonequilibrium statistical mechanics*. Oxford University Press, 2001.

[96] A. Dhar and D. Roy. Heat transport in harmonic lattices. *Journal of Statistical Physics*, 125(4):801–820, 2006.

[97] F. Mandl and G. Shaw. *Quantum field theory, A Wiley-Interscience publication*. John Wiley and Sons Ltd, 1984.

[98] C. Giardina', R. Livi, A. Politi, and M. Vassalli. Finite thermal conductivity in 1D lattices. *Phys. Rev. Lett.*, 84(10):2144–2147, MAR 6 2000.

[99] O. Gendelman and A. Savin. Normal heat conductivity of the one-dimensional lattice with periodic potential of nearest-neighbor interaction. *Physical review letters*, 84(11):2381, 2000.

[100] L. Yang and B. Hu. Comment on "Normal Heat Conductivity of the One-Dimensional Lattice with Periodic Potential of Nearest-Neighbor Interaction". *Phys. Rev. Lett.*, 94:219404, Jun 2005.

[101] D. Escande, H. Kantz, R. Livi, and S. Ruffo. Self-consistent check of the validity of Gibbs calculus using dynamical variables. *Journal of statistical physics*, 76(1-2):605–626, 1994.

[102] A. Trombettoni, A. Smerzi, and P. Sodano. Observable signature of the Berezinskii–Kosterlitz–Thouless transition in a planar lattice of Bose–Einstein condensates. *New Journal of Physics*, 7(1):57, 2005.

[103] A. Smerzi, A. Trombettoni, P. Kevrekidis, and A. Bishop. Dynamical superfluid-insulator transition in a chain of weakly coupled Bose-Einstein condensates. *Physical review letters*, 89(17):170402, 2002.

[104] A. Iacobucci, F. Legoll, S. Olla, and G. Stoltz. Negative thermal conductivity of chains of rotors with mechanical forcing. *Physical Review E*, 84(6):061108, 2011.

[105] M. Eleftheriou, S. Lepri, R. Livi, and F. Piazza. Stretched-exponential relaxation in arrays of coupled rotators. *Physica D: Nonlinear Phenomena*, 204(3):230–239, 2005.

[106] X. Leoncini, A. D. Verga, and S. Ruffo. Hamiltonian dynamics and the phase transition of the XY model. *Physical Review E*, 57(6):6377, 1998.

[107] L. Delfini, S. Lepri, and R. Livi. A simulation study of energy transport in the Hamiltonian XY model. *Journal of Statistical Mechanics: Theory and Experiment*, 2005(05):P05006, 2005.

[108] S. Iubini, S. Lepri, R. Livi, and A. Politi. Off-equilibrium Langevin dynamics of the discrete nonlinear Schrödinger chain. *Journal of Statistical Mechanics: Theory and Experiment*, 2013(08):P08017, 2013.

[109] A. Mosk. Atomic gases at negative kinetic temperature. *Physical review letters*, 95(4):040403, 2005.

[110] A. Rapp, S. Mandt, and A. Rosch. Equilibration rates and negative absolute temperatures for ultracold atoms in optical lattices. *Physical review letters*, 105(22):220405, 2010.

[111] H. Yoshida. Construction of higher order symplectic integrators. *Physics Letters A*, 150(5):262–268, 1990.

[112] J. Boreux, T. Carletti, and C. Hubaux. High order explicit symplectic integrators for the Discrete Non Linear Schrödinger equation. *arXiv preprint arXiv:1012.3242*, 2010.

[113] S. Braun, J. P. Ronzheimer, M. Schreiber, S. S. Hodgman, T. Rom, I. Bloch, and U. Schneider. Negative absolute temperature for motional degrees of freedom. *Science*, 339(6115):52–55, 2013.

[114] J. Dunningham. Phase measurement of Bose-Einstein condensates in lattices. *PHYSICAL REVIEW-SERIES A-*, 66(4):041601–R, 2002.

[115] A. Martin and L. Allen. Measuring the phase of a Bose-Einstein condensate. *Physical Review A*, 76(5):053606, 2007.

[116] F. Lederer, G. I. Stegeman, D. N. Christodoulides, G. Assanto, M. Segev, and Y. Silberberg. Discrete solitons in optics. *Physics Reports*, 463(1):1–126, 2008.

[117] M. Ivanchenko, O. Kanakov, V. Shalfeev, and S. Flach. Discrete breathers in transient processes and thermal equilibrium. *Physica D: Nonlinear Phenomena*, 198(1):120–135, 2004.

[118] K. Kirkpatrick. Solitons and Gibbs measures for nonlinear Schroedinger equations. *Mathematical Modelling of Natural Phenomena*, 7(02):95–112, 2012.

[119] S. Iubini, R. Franzosi, R. Livi, G.-L. Oppo, and A. Politi. Discrete breathers and negative-temperature states. *New Journal of Physics*, 15(2):023032, 2013.

[120] A. Bray. Theory of phase-ordering kinetics. *Advances in Physics*, 43(3):357–459, 1994.

[121] P. Politi and C. Misbah. Nonlinear dynamics in one dimension: A criterion for coarsening and its temporal law. *Phys. Rev. E*, 73:036133, Mar 2006.

[122] P. C. Hohenberg and B. I. Halperin. Theory of dynamic critical phenomena. *Rev. Mod. Phys.*, 49:435–479, Jul 1977.

[123] M. R. Evans and T. Hanney. Nonequilibrium statistical mechanics of the zero-range process and related models. *Journal of Physics A: Mathematical and General*, 38(19):R195, 2005.

[124] S. Redner. *A guide to first-passage processes*. Cambridge University Press, 2001.

[125] S. J. Cornell, K. Kaski, and R. B. Stinchcombe. Domain scaling and glassy dynamics in a one-dimensional Kawasaki Ising model. *Phys. Rev. B*, 44:12263–12274, Dec 1991.

[126] C. Godrèche. Dynamics of condensation in zero-range processes. *Journal of Physics A: Mathematical and General*, 36(23):6313, 2003.

[127] S. Iubini, A. Politi, and P. Politi. Coarsening dynamics in a simplified DNLS model. *Journal of Statistical Physics, DOI:10.1007/s10955-013-0896-4*, 2013.

[128] M. Cencini, F. Cecconi, and A. Vulpiani. *Chaos: from simple models to complex systems*, volume 17. World Scientific Publishing Company, 2010.

[129] A. Pikovsky, M. Rosenblum, and J. Kurths. *Synchronization: a universal concept in nonlinear sciences*, volume 12. Cambridge university press, 2003.

[130] S. Iubini, S. Lepri, R. Livi, and A. Politi. Unpublished.

[131] K. Binder and A. P. Young. Spin glasses: Experimental facts, theoretical concepts, and open questions. *Reviews of Modern physics*, 58(4):801, 1986.

[132] R. Palmer. Broken ergodicity. *Advances in Physics*, 31(6):669–735, 1982.

[133] S. Iubini, S. Lepri, R. Livi, G.-L. Oppo, and A. Politi. In preparation.

[134] R. Burden and G. Hedstrom. The distribution of the eigenvalues of the discrete Laplacian. *BIT Numerical Mathematics*, 12(4):475–488, 1972.